NASA Technical Memorandum 101083

Experimental Aerodynamic Characteristics of a Joined-Wing Research Aircraft Configuration

Stephen C. Smith and Ronald K. Stonum

April 1989

National Aeronautics and Space Administration

NASA Technical Memorandum 101083

Experimental Aerodynamic Characteristics of a Joined-Wing Research Aircraft Configuration

Stephen C. Smith, Ames Research Center, Moffett Field, California
Ronald K. Stonum, Air Force Systems Command Liaison Office, U. S. Air Force, Ames Research Center, Moffett Field, California

April 1989

NASA

National Aeronautics and Space Administration

Ames Research Center
Moffett Field, California 94035

NOMENCLATURE

b	wing span
c	chord
c/4	25% chord line
℄	centerline
C_D	coefficient of drag
C_L	coefficient of lift
C_l	coefficient of lift of airfoil section
C_ℓ	coefficient of rolling moment
C_m	coefficient of pitching moment
C_n	coefficient of yawing moment
C_y	coefficient of side force
C_{ℓ_β}	lateral stability—change in rolling moment with sideslip
$C_{\ell_{\delta_a}}$	roll control power—change in rolling moment with aileron deflection
C_{ℓ_p}	roll damping—change in rolling moment with roll rate
$\partial C_m/\partial C_L$	longitudinal stability—change in pitching moment with lift
C_{n_β}	directional stability—change in yawing moment with sideslip
FI	forward wing inboard control surface
FM	forward wing midspan control surface
FO	forward wing outboard control surface
L/D	lift to drag ratio
L.E.	leading edge
RI	rear wing inboard control surface
RO	rear wing outboard control surface
S	wing area
U_∞	aircraft flight speed
V_u	minimum nosewheel-raising speed
V_s	power-off stall speed
$X_{l.g.}$	distance from center of gravity to main landing gear

Greek Symbols

α	angle of attack, deg
β	angle of sideslip, deg
δ	control surface deflection, deg
ϕ	angle of roll, deg
$\dot{\phi}$	roll rate, rad/sec

Subscripts

a	aileron
c.g.	center of gravity
max	maximum
r	rudder
ref	reference

SUMMARY

A wind-tunnel test was conducted at Ames Research Center to measure the aerodynamic characteristics of a joined-wing research aircraft (JWRA). This aircraft was designed to utilize the fuselage and engines of the existing NASA AD-1 aircraft. The JWRA was designed to have removable outer wing panels to represent three different configurations with the interwing joint at different fractions of the wing span. A one-sixth-scale wind-tunnel model of all three configurations of the JWRA was tested in the Ames 12-foot low-speed wind tunnel to measure aerodynamic performance, stability, and control characteristics.

This report presents the results of these tests. Longitudinal and lateral–directional characteristics were measured over an angle of attack range of $-7°$ to $14°$ and over an angle of sideslip range of $-5°$ to $+2.5°$ at a Mach number of 0.35 and a Reynolds number of 2.2×10^6/ft. Various combinations of deflected control surfaces were tested to measure the effectiveness and impact on stability of several control surface arrangements. In addition, the effects on stall and post-stall aerodynamic characteristics from small leading-edge devices called vortilons were measured.

The results of these tests indicate that the JWRA had very good aerodynamic performance and acceptable stability and control throughout its flight envelope. The vortilons produced a profound improvement in the stall and post-stall characteristics with no measurable effects on cruise performance.

INTRODUCTION

The joined wing research aircraft (JWRA) was designed jointly by NASA Ames Research Center and ACA Industries, Inc. of Torrance, CA as part of a Small Business Innovation Research (SBIR) program. The purpose of this program was to build a joined-wing proof-of-concept and research aircraft by modifying the existing NASA AD-1 oblique wing aircraft. The AD-1 aircraft, shown in figure 1, is described in reference 1. A new wing system which was representative of a joined-wing, transonic commercial transport aircraft was designed to fit onto the fuselage of the AD-1, using the existing undercarriage and fuselage-mounted engines. The design of the JWRA is described in references 2 and 3.

A one-sixth-scale wind-tunnel model of the JWRA was built using the fuselage of the AD-1 wind-tunnel model. This model was tested in the Ames 12-Foot Pressure Wind Tunnel to measure aerodynamic performance, stability, and control characteristics. This report presents the results of these wind tunnel tests.

TEST FACILITY

The tests were conducted in the Ames 12-Foot Pressure Wind Tunnel. Figure 2 shows the JWRA model installed in the wind tunnel test section. The model was supported on a swept blade-type strut mounted on a bipod support system. The blade was swept back $50°$ from the normal axis of the model and was contoured with a 15%-thick low speed airfoil. Figure 3 shows the strut geometry.

MODEL DESCRIPTION

A one-sixth-scale model of the JWRA was built based on the one-sixth scale AD-1 wind tunnel model. The model had removable outer wing panels to represent three different wing configurations. With the full-sized outer wing-panels installed, the interwing joint was located at 60% of the semispan.

A three-view drawing of this configuration, called the JW-1, is shown in figure 4. The JW-2 configuration had shorter outer panels so that the joint was located at 80% of the semispan. A three-view drawing of the JW-2 is shown in figure 5. The JW-3 configuration had the outer panels removed so that the interwing joint was located at 100% of the semispan. The JW-3 configuration is shown in figure 6. Detailed dimensional data on all three configurations ares given in table 1.

The design of the airfoils for the JWRA is discussed in reference 2. The wing geometry was produced by locating each airfoil perpendicular to the 25% chord-line and lofting straight lines between these defining sections. The coordinates of the airfoils are given in table 2.

The JWRA wings were fitted with five control surfaces on each side, representing various arrangements of flaps, elevators, and ailerons. The nomenclature for the various control surfaces on the wings is shown in figure 7. The vertical tail was fitted with a conventional rudder. The control surface deflections available for the model are given in table 3. The sign convention for control surface deflections was chosen to be trailing-edge down as positive for all the wing surfaces and trailing-edge right as positive for the rudder.

The JWRA wings were designed so that small undersurface leading-edge fences called vortilons could be mounted at three span stations. A detail of the vortilon geometry and the three mounting stations is shown in figure 8.

The engine pylons were designed so that speedbrakes could be installed between the fuselage and nacelles. A detail of the speedbrake geometry and installation is shown in figure 9. The model had simple flowthrough nacelles without instrumentation for measuring internal duct losses.

TEST CONDITIONS AND PROCEDURES

At the time these tests were conducted, the 12-Foot Pressure Wind Tunnel could not be pressurized. Therefore, the tests were conducted with the wind-tunnel total pressure equal to the ambient atmospheric pressure. Model strength limitations established a maximum dynamic pressure of 170 psf. Almost all the data from these tests were taken at these conditions, which produced a test Mach number of 0.35, a test Reynolds number of approximately 2.2×10^6/ft, and a chord Reynolds number of approximately 1.0×10^6. It was found that some of the deflected aileron configurations would have exceeded the rolling-moment capacity of the force balance, so it was necessary to reduce the dynamic pressure to 120 psf for some tests, and in a few cases, to 90 psf.

The angle of attack was varied from $-7°$ to $14°$ and the angle of sideslip was varied from $-5°$ to $+2.5°$. The angle of attack was measured by an electronic inclinometer installed in the model directly below the force balance. The angle of sideslip was mea-

sured from the turntable portion of the wind-tunnel model-support system. The measured sideslip angle was corrected for model support and balance deflection.

A 2.0 in. internal six-component strain-gage force balance was used to measure aerodynamic forces and moments. The moment reference center was located at the assumed c.g. location for each configuration, which was based on a static stability margin of $0.35c_{ref}$. The reference area for computing aerodynamic coefficients was the projected plan area of the forward wing. The moment reference center and reference area for each configuration are given in table 1. The axis system and sign conventions for aerodynamic data in this report are shown in figure 10. Lift and drag coefficient data are presented in the wind axis system. All other aerodynamic coefficients are presented in the body axis system.

The data presented in this report have been adjusted for wall effects and blockage effects. The wall corrections were determined by the method described in reference 4, and the blockage corrections were determined by the method described in reference 5. No adjustments were made to remove internal drag from the nacelles or the small cavity in the fuselage where the blade support attached to the balance.

RESULTS AND DISCUSSION

Experimental aerodynamic data for the JWRA are shown in figures 11 through 84. The results for the JW-1 configuration are shown in figures 11 through 41. The JW-2 results are shown in figures 42 through 58. The JW-3 results are shown in figures 59 through 75. Results for the JW-1 wing–body (rear wing removed) are shown in figures 76 through 79, and results for the body only are shown in figures 80 through 84.

JW-1 Configuration

Longitudinal characteristics (zero control deflections)- The longitudinal characteristics of the JW-1 are shown in figures 11 through 14. Figures 11 through 13 show the variation of lift, drag, and pitching moment with angle of attack. The variation of longitudinal stability, $(\partial C_m/\partial C_L)$, with angle of attack is shown in figure 14. A maximum lift coefficient $(C_{L_{max}})$ of 1.20 was obtained at a 6° angle of attack. This is a satisfactory value for a wing with 30°of sweep and maximum section lift coefficent $(C_{l_{max}})$ of 1.5. The apparently low angle of attack for stall is the result of the large wing incidence relative to the body axis (see table 1) which was necessitated by the short landing gear of the AD-1, as discussed in reference 2. The cruise lift-coefficent of 0.45 was achieved at a $-3°$ angle of attack.

There was a reduction in lift curve slope between $2\frac{1}{2}°$ and 6° angle of attack which indicated a growing region of flow separation on the wing. Figures 13 and 14 show a loss of stability associated with this separation region. The JW-1 exhibited classical swept-wing stall characteristics where the aircraft was unstable at the stall angle, and became stable again at a high, post-stall angle of attack of, in this case, about 12°. However, as shown in figure 13, this unstable stall was not severe, since a nose-down pitching moment still existed with neutral elevator control and nose-down elevator control would easily reduce the angle of attack below stall. Figure 14 shows that the JW-1 had a static stability margin of 0.30 to 0.36 over the normal flight envelope (C_L=0.3–1.0) for this moment reference location.

Lateral-directional characteristics- The lateral-directional characteristics of the baseline JW-1 are shown in figures 15 through 19. Figures 15 through 17 show variations in side-force, yawing-moment, and rolling-moment coefficients with angle of attack for various angles of sideslip, $\beta = 0.0°, \pm 2.5°,$ and $-5.0°$. There were abrupt changes in the lateral-directional characteristics above the angle of attack where the wing stalled. These changes are usually associated with asymmetric separations due to minor geometric asymmetries in the model. The untrimmed rolling moment, yawing moment, and side-force diminish at higher angles of attack, so no unusual or violent departure characteristics are expected. Figures 18 and 19 show variations in lateral stability, C_{ℓ_β}, and directional stability, C_{n_β}, with angle of attack. Figure 18 shows an unusual loss of lateral stability at high angles of attack. It appears that the positive dihedral contribution from the forward wing was reduced as the wing stalled and the negative dihedral of the rear wing began to dominate. Although the reduction of lateral stability at high angles of attack would have some effect on the post-stall flying qualities, it is not expected that this would be serious, especially considering the available lateral control, as described below.

Forced transition- The model Reynolds number for these tests was about one-third of the flight-vehicle Reynolds number. Transition strips were installed on the model to study the effects of forced transition on the JWRA model. The primary concern was that the low chord Reynolds number might lead to areas of premature laminar separation on the model that would not occur on the full scale aircraft. This would not only affect the drag data, but also the lift and pitching moment data.

Transition strips consisting of a random distribution of 0.009- to 0.010-in. glass spheres were installed on the model. The particle size was selected based on the method of reference 6. Two fixed transition locations were studied; figures 20 through 22 show the results of this study. First, transition was fixed at 35% chord on all the wing and tail surfaces and on the fuselage just ahead of the crest of the canopy. This was where natural laminar transition was expected to occur on the full scale aircraft. As shown in figures 20 through 22, use of this transition location caused some increase in the drag and also affected the lift and pitching moment characteristics slightly. If a premature laminar separation was causing loss of stability, the transition strip would be expected to help the problem by delaying separation and increasing $C_{l_{max}}$. However, the use of the transition strip seemed to aggravate the problem of stability loss rather than lessen it. To verify that no laminar separation was occurring forward of the transition strip, a second test was done with the transition strip installed at 10% chord on the wing and tail surfaces. Figure 20 shows no further increase in the drag from fixing transition at 10% chord. Based on these results, it was believed that the drag increase was caused by the drag of the transition strip itself and a reduction of the laminar run on the fuselage.

The transition strip at 10% chord was left in place for all the other testing of the JW-1 configuration.

Vortilons- The baseline JW-1 configuration showed undesirable loss of stability resulting from outer wing-panel stall. This is typical of high aspect-ratio swept wings with moderate taper: the lift distribution becomes more heavily loaded near the tips as the angle of attack is increased, and the wing chord is reduced at the tips because of taper, so

the higher lift loading results in very high lift coefficients on the outer wing panels. The outer wing-panels frequently stall first, which shifts the center of lift inboard and forward, producing undesirable pitchup at stall.

One device which has been used to reduce this unstable stall characteristic is a small undersurface leading-edge fence called a vortilon. The use of vortilons for improving stall and post-stall flying qualities is discussed in reference 7. The JW-1 was tested with vortilons installed at three different span locations, and combinations of these. Figures 23 and 24 show the effect of each of the three vortilon locations on the lift and pitching-moment characteristics. Each of the three vortilon locations had some influence on the prestall separation, and the post-stall lift and moment characteristics.

The inboard vortilon configuration had the most significant effect on the post-stall pitching moment. Figures 25 and 26 show more clearly than figures 23 and 24 the impact of the inboard vortilon installation on the longitudinal characteristics of the JW-1. The $C_{L_{max}}$ of the JW-1 was increased from 1.20 to 1.22 and the character of the stall break changed to a much more gentle stall. As shown in figure 26, the unstable pitchup was eliminated and the JW-1 with inboard vortilons had nearly constant pitching moment above stall for this moment reference location. A small forward shift in the c.g. location would make the stall characteristics completely stable. Figure 27 shows that there is no cruise-drag penalty for the installation of the vortilons. Figures 28 and 29 show the effect of the vortilons on the rolling moment and yawing moment. The vortilons delayed the sudden change in lateral–directional characteristics until well above the stall angle.

Figures 30 and 31 show the effect of two vortilons, installed at the inboard and outboard locations, compared with the effect of the inboard vortilon only and no vortilons. The two-vortilon configuration maintained more stability up to the stall, but did not have as much improvement of the post-stall pitchup as the single inboard vortilon.

Although other vortilon locations were tested, the effect of the inboard vortilons was so significant that this configuration was used as a new baseline configuration for all of the remaining testing of the JW-1, JW-2, and JW-3 configurations, except where noted.

Longitudinal control- Two different arrangements of controls were evaluated for longitudinal control effectiveness. Figure 7 shows the nomenclature used to describe the individual control surfaces. One control arrangement used both the inboard and outboard rear surfaces (RI+RO) as elevators for longitudinal control. The second arrangement used the inboard surface on the forward wing and the inboard rear surface (FI+RI) coupled to move equal amounts in opposite directions so that nose-up pitch command would cause FI to move downward as a flap and RI to move upward as an elevator. Data for the FI+RI control arrangement were determined by interpolating wind-tunnel data from configurations with $\delta_{RI} = -15°$ and $\delta_{FI} = 0°$ and 20°, since model hardware for $\delta_{FI} = 15°$ was not available. Figure 32 shows the control effectiveness of the RI+RO elevator combination and the FI+RI flap-elevator combination compared with the effectiveness of RI only. The FI+RI configuration had slightly greater control authority. As shown in figure 33, the FI+RI arrangement had the advantage of changing the lift in the proper sense for the change in pitching moment, i.e., a nose-up moment was accompanied by an increase in lift due to the coupled flap deflection. However, this arrangement had the disadvantage of substantially disturbing the designed incidence distribution of the wing at high angle of

attacks by deflecting the flap to trim the airplane.

One criterion for assessing longitudinal control authority is the minimum speed required to lift the nosewheel. The ratio of minimum nosewheel-raising speed to power-off stall speed was determined from moment equilibrium about the main wheels, neglecting thrust effects. This ratio was expressed as:

$$\frac{V_u}{V_s} = \sqrt{\frac{X_{l.g.} C_{L_{max}}}{X_{l.g.} C_{L_{\alpha=0}} + c_{ref} C_{m_{c.g.,\alpha=0}}}} \tag{1}$$

where the lift and pitching moment coefficients at $\alpha = 0$ were based on full control deflections of 15°, as shown in figures 31 and 32. This ratio was determined for the RI+RO and FI+RI configurations and the RI+RO configuration with the forward wing surfaces used as takeoff flaps ($\delta_{FI} = 20°$ and $\delta_{FM} = 15°$). Values of the minimum nosewheel-raising speed ratio for the three control configurations are given below.

	(RI+RO)	(FI+RI)	(RI+RO)+Flaps
V_u/V_s	0.97	0.89	0.84

The RI+RO+flaps configuration was the most effective, although all three control schemes were able to raise the nosewheel below the stall speed. The reader should bear in mind that these values are based on 15° control deflections and more control authority would be available from greater control deflections.

Control surface deflection also affected the post-stall stability characteristics. Both the RI+RO and FI+RI configurations appear to be completely stable well above the stall.

Trimmed characteristics- Wind-tunnel data obtained with and without the control surfaces deflected were used to derive trimmed lift and drag characteristics of each longitudinal control arrangement (neglecting thrust effects). Figure 34 shows the trimmed lift characteristics of the FI+RI configuration, and the RI+RO configuration with and without the FI and FM surfaces acting as take-off flaps.

Figure 35 shows the variation of trimmed lift-to-drag ratio (L/D) with lift coefficient for both control arrangements. The FI+RI configuration had a slightly lower L/D because of the alteration of wing twist as the controls are deflected.

Lateral-directional control- The JW-1 had a conventional aileron surface on the forward wing outboard of the interwing joint (FO). This aileron may be supplemented with either the middle forward flap (FM) or the outer surface on the rear wing (RO). Each aileron surface used differential deflection so that the right aileron was deflected −15° and the left aileron was deflected +10°. Figure 36 shows the control effectiveness of the outboard aileron alone and supplemented by each of the other two candidate ailerons. Figure 37 shows the effect of these control surfaces on yawing moment. The FM surface was considerably more effective as an additional aileron than the RO surface. The forward wing ailerons produced yaw away from the turn, whereas the rear wing aileron produced yaw into the turn. In all cases, the yaw coupling was small compared with the available directional control from the rudder, as shown in figure 38.

To assess the control authority of various aileron configurations, an estimate of the steady-state roll rate for a full-scale JW-1 was made from the measured aileron effectiveness and an estimate of the roll damping from a vortex-lattice program. The steady-state roll rate was estimated from

$$\dot{\phi} = \frac{C'_{\ell_{\delta_a}} \delta_a}{C'_{\ell_p} \frac{b}{2U_\infty}} \tag{2}$$

From figure 36, $C'_{\ell_{\delta_a}} \delta_a = 0.035$ at $\alpha = 0$ for $\delta_{FO} = -15°/+10°$. The roll damping, C'_{ℓ_p}, was estimated to be -0.6. The JW-1 span was 40 ft. and it was assumed to be flying at 150 ft/sec. The steady-state roll rate for this configuration was estimated to be 0.44 rad/sec or 25°/sec. Greater aileron deflection would, of course, lead to a greater roll-rate.

Control effectiveness at high angles of attack is also an important evaluation criterion. Figures 36 and 38 indicate that both the ailerons and rudder maintain good control authority above stall and were more than adequate to control the abrupt changes in rolling and yawing moment above the stall angle-of-attack shown in figures 28 and 29.

Speed brake- The JW-1 was tested with simple speed brakes deployed from the engine pylons as shown in figure 8. These speed brakes were designed as a means of altering the glide slope for landing, because of the high L/D of the JWRA and the high idle-thrust of the turbojet engines. Figures 39 through 41 show the lift, drag, and pitching-moment characteristics of the JW-1 with and without the speed brake deployed.

JW-2 Configuration

Longitudinal characteristics- The longitudinal characteristics of the JW-2 are shown in figures 42 through 46. The transition strips were removed from the wings for flow-visualization experiments on the JW-1 and were not reapplied. The JW-2 and JW-3 configurations were tested without forced transition. Figures 42 through 44 show the variation of lift, drag, and pitching moment with angle of attack. Figure 45 shows the variation of longitudinal stability with angle of attack. The JW-2 had a static stability of 0.30 to 0.34 over the normal flight envelope for this moment reference location. Figure 46 shows the pitching moment characteristics of the JW-2 with the vortilons removed. As with the JW-1, the longitudinal characteristics without the vortilon are less satisfactory.

Lateral-directional characteristics- The lateral-directional characteristics of the JW-2 are shown in figures 47 through 51. Figures 47 through 49 show variations in side-force, yawing-moment, and rolling-moment coefficients with angle of attack for sideslip angles of 0°, and ± 2.5°. Figures 50 and 51 show variations in lateral stability, C'_{ℓ_β}, and directional stability, C_{n_β}, with angle of attack.

Longitudinal control- Both the RI+RO and FI+RI control arrangements were evaluated on the JW-2. As with the JW-1 configuration, data for the FI+RI control arrangement were determined by interpolating wind tunnel data. The control effectiveness of both arrangements is shown in figure 52. Figure 53 shows the effect of these controls on the lift characteristics of the JW-2. The two control arrangements had nearly the same elevator effectiveness on the JW-2.

Trimmed characteristics- Wind-tunnel data with and without the control surfaces deflected were used to derive trimmed lift and drag characteristics of the JW-2 using both the RI+RO and FI+RI control configurations. Figure 54 shows the trimmed lift characteristics and figure 55 shows the variation of trimmed L/D with lift coefficient for both arrangements.

Lateral-directional control- The conventional aileron surface, FO, was shorter on the JW-2 since the outer wing-panel was smaller. Figure 56 shows the control effectiveness of the shorter FO aileron, both alone and supplemented by each of the candidate inboard ailerons. Figure 57 shows the effect of these controls on yawing moment. Figure 58 shows the directional control effectiveness of the rudder. As with the JW-1, the FM surface was more effective as a supplemental aileron than the RO surface.

JW-3 Configuration

Longitudinal characteristics- The longitudinal characteristics of the JW-3 are shown in figures 59 through 63. Figures 59 through 61 show the variation of lift, drag, and pitching moment with angle of attack. Figure 62 shows the variation of longitudinal stability with angle of attack. The JW-3 had a static stability of 0.28 to 0.38 over the normal flight envelope for this moment reference location. Figure 63 shows the pitching moment characteristics of the JW-3 with the vortilons removed. As with the JW-1 and JW-2, the longitudinal characteristics without the vortilon are less satisfactory.

Lateral-directional characteristics- The lateral-directional characteristics of the JW-3 are shown in figures 64 through 68. Figures 64 through 66 show variations in side-force, yawing-moment, and rolling-moment coefficients with angle of attack for sideslip angles of 0°and $\pm$ 2.5°. Figures 67 and 68 show variations in lateral stability, C_{ℓ_β}, and directional stability, C_{n_β}, with angle of attack.

Longitudinal control- Both the RI+RO and FI+RI control arrangements were evaluated on the JW-3. As with the JW-1 and JW-2 configurations, data for the FI+RI control arrangement were determined by interpolating wind tunnel data. The control effectiveness of both arrangements is shown in figure 69. Figure 70 shows the effect of these controls on the lift characteristics of the JW-3. The FI+RI arrangement was somewhat less effective as an elevator than the RI+RO arrangement on the JW-3. The FI+RI arrangement became less effective on the JW-2 and JW-3 configurations because the moment reference center (at the c.g.) was moved forward to achieve the same level of longitudinal stability. This shortened the moment arm of the additional lift on the forward wing caused by deflection of the FI surface.

Trimmed characteristics- Wind-tunnel data with and without the control surfaces deflected were used to derive trimmed lift and drag characteristics of the JW-3 using both the RI+RO and FI+RI control configurations. Figure 71 shows the trimmed lift characteristics and figure 72 shows the variation of trimmed L/D with lift coefficient for both arrangements.

Lateral-directional control- The outer wing-panel was removed on the JW-3, leaving

only the inboard surfaces available for roll control. The FM and RO surfaces were evaluated as ailerons. Figure 73 shows the control effectiveness of the FM and RO surfaces acting individually and together. Figure 74 shows the effect of these controls on yawing moment. The FM surface was considerably more effective as an aileron than the RO surface. As with the JW-1 and JW-2, the FM surface produced adverse yaw, whereas the RO surface produced yaw into the turn. Rudder deflection data for the JW-3 was taken only with the ailerons deflected. Figure 75 shows the rudder effectiveness with the FM aileron deflected. The yaw coupling was quite small and easily controllable with the rudder in all cases.

JW-1 Wing–Body

The JW-1 configuration was tested with the rear wing removed to obtain longitudinal aerodynamic characteristics of the wing–body only. The vertical tail and engines were left on the fuselage, and vortilons were installed at the inboard wing station. The area of the vertical tail where the rear wing attaches was faired smoothly to match the contours of the vertical tail. The JW-1 moment reference center and reference area were used. Figures 76 through 78 show the variation of lift, drag, and pitching moment with angle of attack. Figure 79 shows the variation of pitching moment with angle of attack with the vortilons removed.

Body Only

Longitudinal characteristics of the JWRA fuselage with vertical tail and engines installed are shown in figures 80 through 82. The wing-root area of the fuselage was faired over smoothly. The JW-1 moment reference center and reference area were used for computation of coefficients. Figure 83 and 84 show the directional characteristics of this configuration.

CONCLUDING REMARKS

A one-sixth-scale model of a joined-wing research aircraft (JWRA) was tested in the NASA Ames 12-Foot Pressure Wind Tunnel. The JWRA was designed to have removable outer wing panels to represent three different configurations with the interwing joint located at different fractions of the wing span. The aerodynamic characteristics of these three wing configurations, called JW-1, JW-2, and JW-3, were measured. The JWRA was found to have acceptable levels of stability and control, especially with vortilons installed. All of the control surfaces maintained sufficient effectiveness to control the JWRA well above the stall angle of attack.

Two longitudinal control configurations were evaluated for use on the JWRA. The FI−RI arrangement was found to be slightly more effective than the RI+RO arrangement on the JW-1. However, the FI+RI arrangement lost effectiveness as the moment reference center was moved forward on the JW-2 and JW-3, since the pitching-moment contribution from an increase in wing lift was reduced. On the JW-3, this arrangement was less effective than the RI+RO arrangement. The FI+RI arrangement had a slightly lower L/D than the RI+RO arrangement on all three configurations, because of the alteration of the wing-incidence distribution when the FI surface was deflected.

Two control surfaces were evaluated for roll control effectiveness to supplement the aileron on the JW-1 and JW-2 and to act as the primary aileron on the JW-3. In all cases, the FM surface was more effective as an aileron than the RO surface. None of the aileron surfaces studied created severe adverse yaw.

A small speed-brake arrangement installed on the engine pylons was found to produce a significant amount of drag, providing a convenient means of glidepath control for landing.

REFERENCES

1. Sim, A.G.; and Curry, R.E.: Flight Determined Aerodynamic Derivatives of the AD-1 Oblique-Wing Research Airplane. NASA TP-2222, Oct. 1984.

2. Smith, S.C.; Cliff, S.E.; and Kroo, I.M.: The Design of a Joined-Wing Flight Demonstrator Aircraft. AIAA Paper 87-2930, Sept. 1987.

3. Wolkovitch, J.: Joined Wing Research Airplane Feasibility Study. AIAA Paper 84-2471, Oct. 1984.

4. Sivells, J.C.; and Salmi, R.M.: Jet-Boundary Corrections for Complete and Semispan Swept Wings in Closed Circular Wind Tunnels. NACA TN-2454, Sept. 1951.

5. Herriot, J. G.: Blockage Corrections for Three-Dimensional-Flow Closed-Throat Wind Tunnels, with Consideration of the Effect of Compressibility. NACA Report 995, 1950.

6. Braslow, A.L.; and Knox, E.C.: Simplified Method for Determination of Critical Height of Distributed Roughness Particles for Boundary-Layer Transition at Mach Numbers From 0. to 5. NACA TN-4363, Sept. 1958.

7. Shevell, R.; and Schaufele, R.: Aerodynamic Design Features of the DC-9. AIAA Paper 65-738, Nov. 1965.

TABLE I.- JWRA MODEL GEOMETRIC DATA (Dimensions in feet)

Configuration	JW-1	JW-2	JW-3
Span	6.667	5.383	4.000
Length	5.597	5.597	5.597
Height	1.271	1.271	1.271
S_{ref}	3.039	2.651	2.137
c_{ref}	0.484	0.510	0.543
	Forward Wing		
Area	3.039	2.651	2.137
Sweep(c/4)	30.5°	30.5°	30.5°
Taper Ratio	0.4	0.4	0.4
Dihedral	5.0°	5.0°	5.0°
	Rear Wing		
Area	0.933	0.933	0.933
Sweep(c/4)	−32.0°	−32.0°	−32.0°
Taper Ratio	0.6	0.6	0.6
Dihedral	−20.0°	−20.0°	−20.0°
	Vertical Tail		
Area	0.475	0.475	0.475
Sweep(c/4)	32°	32°	32°
Taper Ratio	0.3	0.3	0.3
	Datums (fuselage stations)		
Nose	0.611	0.611	0.611
Fwd wing L.E. @℄	2.796	2.796	2.796
Rear wing L.E. @℄	5.661	5.661	5.661
Balance Center	3.986	3.986	3.986
Moment Reference	3.886	3.804	3.695
Main landing gear	4.122	4.122	4.122
		Airfoils	
	Forward Wing	Rear Wing	Vertical Tail
Root	JWR	JTR	JFR
Joint	JWJ		
Tip	JWT	JTT	JFT
		Incidence	
Root	7.5°	3.0°	0.0°
Joint	5.5°		
Tip	2.1°	5.0°	0.0°

Table II.- AIRFOIL COORDINATES

x/c	JWR (wing root)		JWJ (wing joint)		JWT (wing tip)	
	y/c upper	y/c lower	y/c upper	y/c lower	y/c upper	y/c lower
0.0000	0.00000	0.00000	0.00000	0.00000	0.00000	0.00000
0.0025	0.00953	-0.00776	0.01191	-0.00834	0.01215	-0.00862
0.0050	0.01350	-0.01037	0.01695	-0.01102	0.01736	-0.01130
0.0075	0.01641	-0.01228	0.02063	-0.01299	0.02115	-0.01327
0.0100	0.01883	-0.01383	0.02363	-0.01458	0.02423	-0.01485
0.0150	0.02286	-0.01615	0.02851	-0.01698	0.02919	-0.01726
0.0200	0.02624	-0.01796	0.03250	-0.01889	0.03320	-0.01918
0.0250	0.02924	-0.01951	0.03593	-0.02053	0.03663	-0.02084
0.0300	0.03196	-0.02089	0.03896	-0.02200	0.03963	-0.02233
0.0400	0.03679	-0.02336	0.04416	-0.02463	0.04472	-0.02500
0.0500	0.04100	-0.02553	0.04850	-0.02693	0.04892	-0.02734
0.0600	0.04472	-0.02747	0.05221	-0.02896	0.05246	-0.02940
0.0700	0.04808	-0.02921	0.05544	-0.03079	0.05551	-0.03126
0.0800	0.05115	-0.03082	0.05831	-0.03246	0.05820	-0.03296
0.0900	0.05399	-0.03230	0.06088	-0.03400	0.06059	-0.03453
0.1000	0.05662	-0.03369	0.06321	-0.03542	0.06275	-0.03598
0.1200	0.06136	-0.03618	0.06726	-0.03796	0.06650	-0.03856
0.1400	0.06554	-0.03836	0.07071	-0.04015	0.06969	-0.04078
0.1600	0.06926	-0.04028	0.07368	-0.04206	0.07248	-0.04271
0.1800	0.07261	-0.04198	0.07629	-0.04374	0.07496	-0.04438
0.2000	0.07562	-0.04347	0.07857	-0.04521	0.07719	-0.04583
0.2200	0.07833	-0.04478	0.08059	-0.04649	0.07921	-0.04707
0.2400	0.08076	-0.04591	0.08236	-0.04759	0.08105	-0.04813
0.2600	0.08293	-0.04688	0.08390	-0.04855	0.08270	-0.04900
0.2800	0.08485	-0.04769	0.08523	-0.04935	0.08420	-0.04971
0.3000	0.08653	-0.04834	0.08635	-0.05001	0.08552	-0.05025
0.3300	0.08860	-0.04903	0.08763	-0.05073	0.08719	-0.05076
0.3600	0.09014	-0.04938	0.08846	-0.05114	0.08846	-0.05093
0.3900	0.09113	-0.04938	0.08882	-0.05124	0.08931	-0.05073
0.4200	0.09149	-0.04894	0.08861	-0.05093	0.08962	-0.05010
0.4500	0.09116	-0.04799	0.08779	-0.05015	0.08932	-0.04897
0.4800	0.09013	-0.04654	0.08633	-0.04888	0.08839	-0.04734
0.5100	0.08838	-0.04456	0.08421	-0.04711	0.08679	-0.04519
0.5400	0.08590	-0.04205	0.08143	-0.04483	0.08450	-0.04254
0.5700	0.08277	-0.03912	0.07808	-0.04212	0.08159	-0.03947
0.6000	0.07907	-0.03585	0.07422	-0.03907	0.07815	-0.03608
0.6300	0.07489	-0.03234	0.06993	-0.03577	0.07422	-0.03248
0.6600	0.07024	-0.02863	0.06527	-0.03225	0.06985	-0.02870
0.6900	0.06518	-0.02479	0.06025	-0.02856	0.06507	-0.02482
0.7200	0.05978	-0.02090	0.05496	-0.02479	0.05993	-0.02093
0.7500	0.05408	-0.01705	0.04946	-0.02100	0.05449	-0.01711
0.7800	0.04810	-0.01326	0.04374	-0.01721	0.04875	-0.01341
0.8100	0.04189	-0.00964	0.03788	-0.01353	0.04277	-0.00992
0.8400	0.03552	-0.00628	0.03194	-0.01002	0.03659	-0.00676
0.8700	0.02904	-0.00330	0.02598	-0.00681	0.03027	-0.00403
0.9000	0.02251	-0.00085	0.02007	-0.00402	0.02387	-0.00191
0.9300	0.01602	0.00086	0.01431	-0.00185	0.01750	-0.00059
0.9600	0.00968	0.00145	0.00884	-0.00065	0.01129	-0.00041
0.9800	0.00561	0.00086	0.00547	-0.00071	0.00736	-0.00126
1.0000	0.00145	-0.00145	0.00225	-0.00225	0.00360	-0.00360

Table II.- (CONTINUED)

	JTR (tail root)		JTT (tail tip)		JFR (fin root)	JFT (fin tip)
x/c	y/c upper	y/c lower	y/c upper	y/c lower	y/c symmetric	y/c symmetric
0.0000	0.00000	0.00000	0.00000	0.00000	0.00000	0.00000
0.0025	0.00920	-0.00716	0.00914	-0.00711	0.01285	0.00871
0.0050	0.01253	-0.01026	0.01251	-0.01022	0.01808	0.01238
0.0075	0.01499	-0.01257	0.01503	-0.01258	0.02194	0.01511
0.0100	0.01703	-0.01446	0.01714	-0.01453	0.02501	0.01729
0.0150	0.02040	-0.01748	0.02067	-0.01770	0.02972	0.02053
0.0200	0.02323	-0.01991	0.02365	-0.02030	0.03338	0.02291
0.0250	0.02575	-0.02204	0.02630	-0.02257	0.03648	0.02490
0.0300	0.02807	-0.02397	0.02872	-0.02462	0.03919	0.02664
0.0400	0.03225	-0.02743	0.03309	-0.02829	0.04372	0.02950
0.0500	0.03597	-0.03048	0.03694	-0.03150	0.04739	0.03174
0.0600	0.03930	-0.03320	0.04038	-0.03435	0.05044	0.03353
0.0700	0.04233	-0.03567	0.04350	-0.03691	0.05304	0.03502
0.0800	0.04512	-0.03792	0.04635	-0.03923	0.05528	0.03627
0.0900	0.04770	-0.04000	0.04899	-0.04136	0.05723	0.03733
0.1000	0.05011	-0.04194	0.05144	-0.04333	0.05897	0.03824
0.1200	0.05448	-0.04545	0.05586	-0.04685	0.06194	0.03974
0.1400	0.05834	-0.04851	0.05973	-0.04989	0.06438	0.04092
0.1600	0.06175	-0.05120	0.06314	-0.05254	0.06645	0.04189
0.1800	0.06476	-0.05353	0.06613	-0.05480	0.06825	0.04271
0.2000	0.06742	-0.05555	0.06872	-0.05672	0.06982	0.04341
0.2200	0.06974	-0.05728	0.07097	-0.05832	0.07120	0.04403
0.2400	0.07175	-0.05874	0.07289	-0.05961	0.07242	0.04457
0.2600	0.07347	-0.05993	0.07450	-0.06063	0.07349	0.04504
0.2800	0.07489	-0.06087	0.07581	-0.06139	0.07441	0.04544
0.3000	0.07604	-0.06157	0.07681	-0.06190	0.07518	0.04578
0.3300	0.07724	-0.06216	0.07775	-0.06219	0.07604	0.04614
0.3600	0.07783	-0.06222	0.07799	-0.06194	0.07655	0.04634
0.3900	0.07781	-0.06176	0.07757	-0.06117	0.07668	0.04634
0.4200	0.07719	-0.06078	0.07654	-0.05988	0.07630	0.04609
0.4500	0.07595	-0.05928	0.07491	-0.05808	0.07534	0.04554
0.4800	0.07412	-0.05727	0.07276	-0.05584	0.07377	0.04466
0.5100	0.07174	-0.05481	0.07012	-0.05322	0.07156	0.04342
0.5400	0.06889	-0.05196	0.06704	-0.05026	0.06871	0.04182
0.5700	0.06561	-0.04878	0.06359	-0.04701	0.06532	0.03989
0.6000	0.06194	-0.04533	0.05981	-0.04350	0.06145	0.03766
0.6300	0.05795	-0.04165	0.05574	-0.03978	0.05722	0.03518
0.6600	0.05366	-0.03779	0.05141	-0.03590	0.05264	0.03249
0.6900	0.04912	-0.03379	0.04689	-0.03193	0.04777	0.02961
0.7200	0.04438	-0.02972	0.04224	-0.02794	0.04271	0.02658
0.7500	0.03947	-0.02561	0.03753	-0.02400	0.03750	0.02345
0.7800	0.03447	-0.02154	0.03281	-0.02019	0.03218	0.02022
0.8100	0.02944	-0.01757	0.02814	-0.01657	0.02683	0.01694
0.8400	0.02448	-0.01381	0.02362	-0.01325	0.02153	0.01367
0.8700	0.01967	-0.01035	0.01933	-0.01031	0.01636	0.01050
0.9000	0.01512	-0.00732	0.01535	-0.00790	0.01245	0.00755
0.9300	0.01092	-0.00486	0.01178	-0.00616	0.00845	0.00486
0.9600	0.00721	-0.00320	0.00873	-0.00527	0.00510	0.00260
0.9800	0.00512	-0.00279	0.00706	-0.00522	0.00348	0.00149
1.0000	0.00340	-0.00340	0.00570	-0.00570	0.00250	0.00080

TABLE III.- AVAILABLE CONTROL SURFACE DEFLECTIONS FOR THE JWRA MODEL

Surface	Baseline	Longitudinal	Lateral right/left
FI	0°	20°	−15°/10°
FM	0°	15°	−15°/10°
FO	0°		−15°/10°
RI	0°	10°,−5°,−15°	
RO	0°	10°,−5°,−15°	−15°/10°
RUDDER	0°,15°		

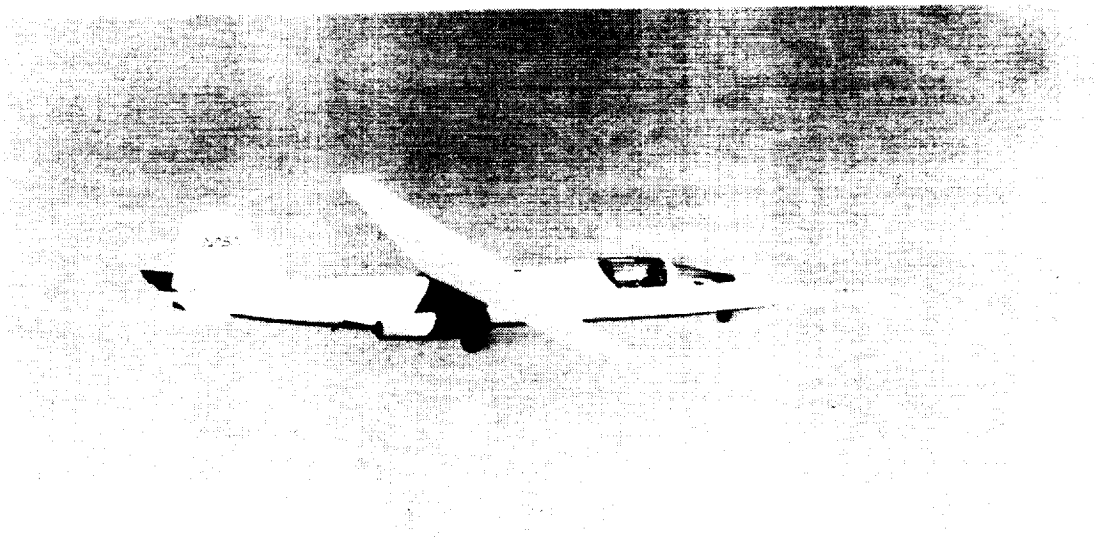

Figure 1. NASA AD-1 Oblique-Wing Aircraft.

Figure 2. One-Sixth-Scale JWRA Model Installed in the Ames 12-Foot Pressure Wind Tunnel.

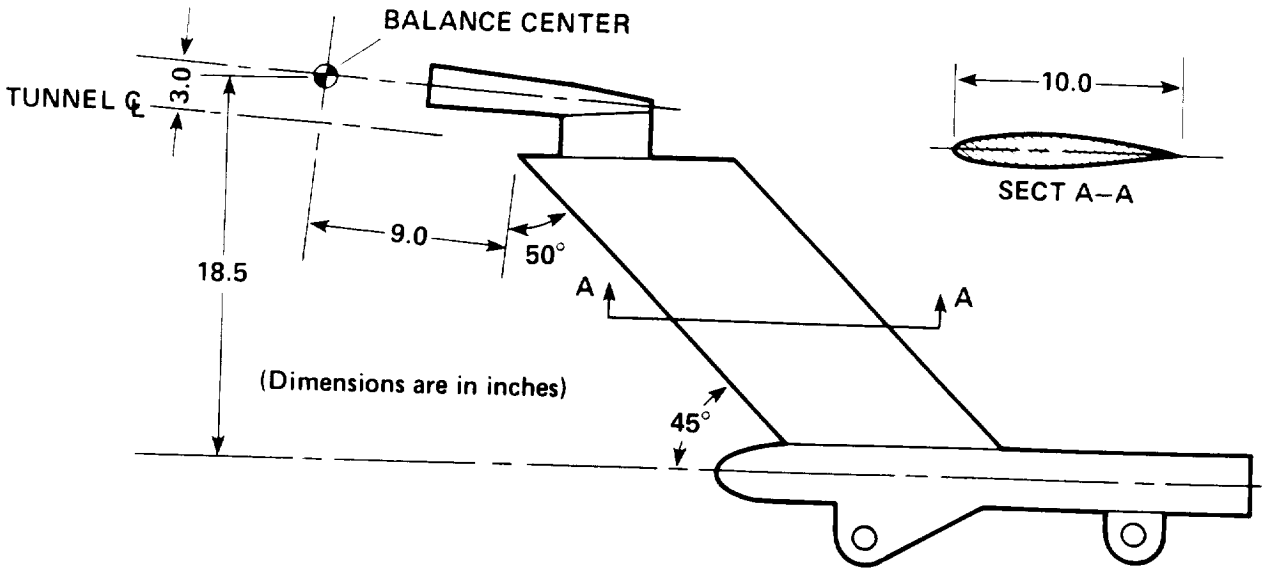

Figure 3. Model Support Strut.

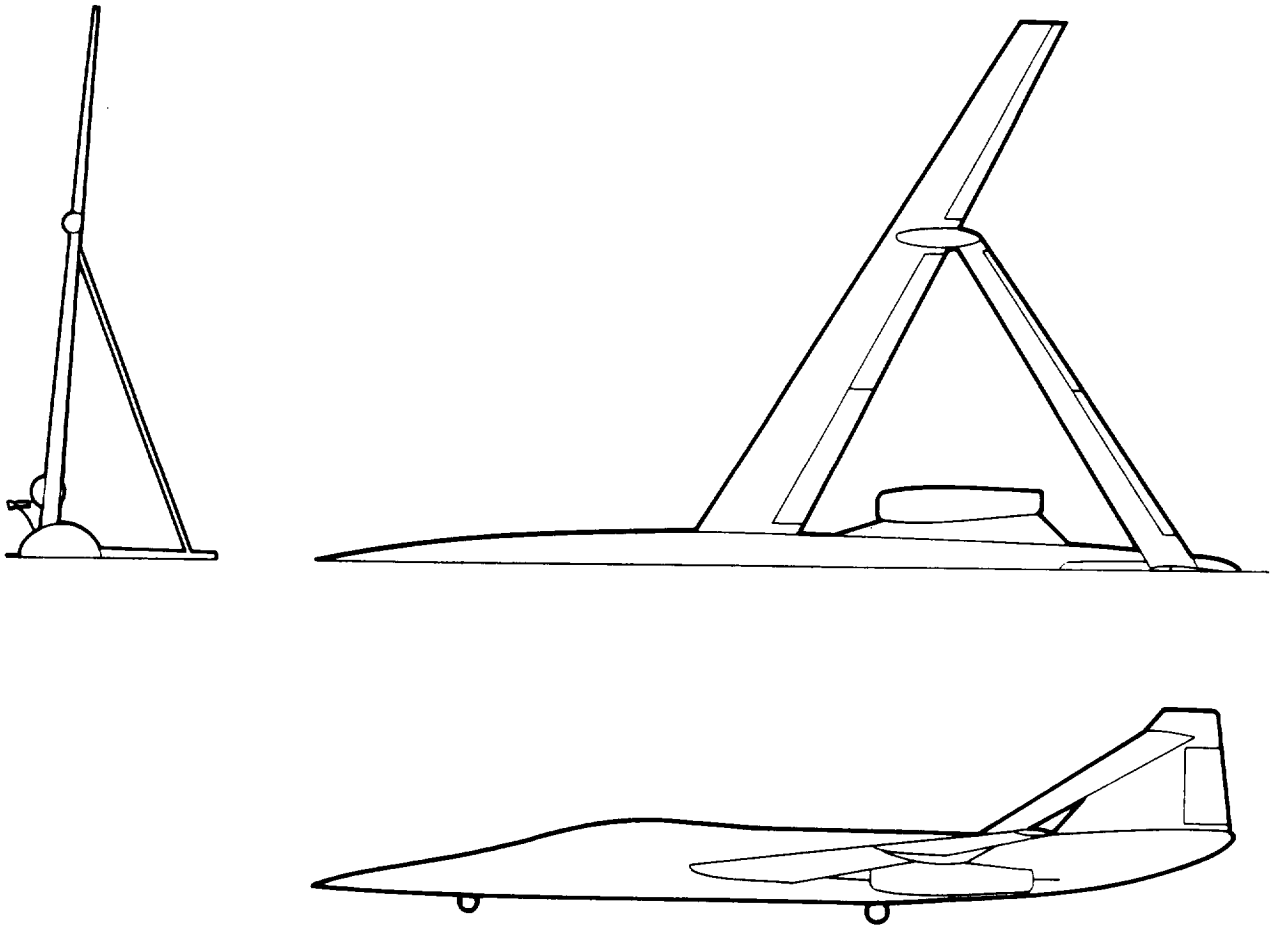

Figure 4. JW–1 Configuration.

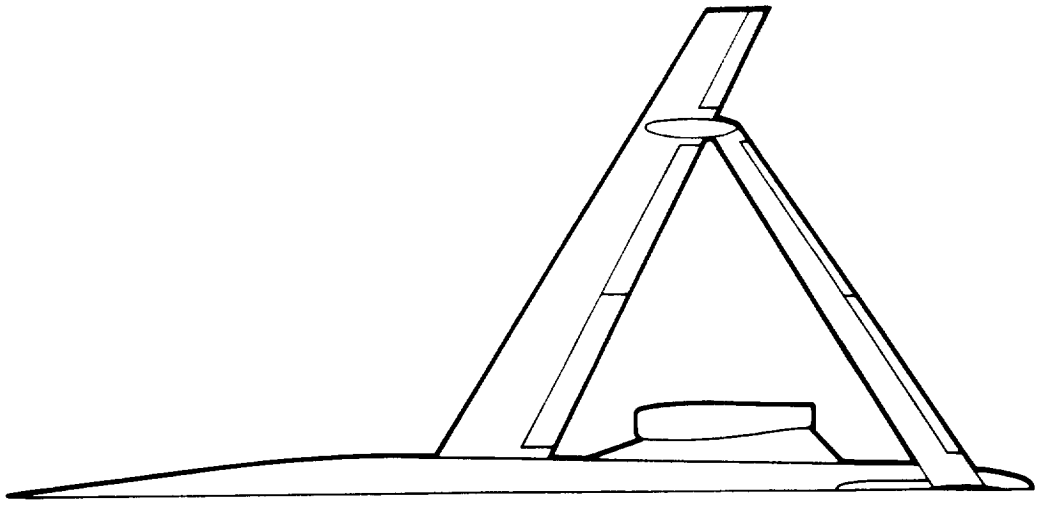

Figure 5. JW-2 Configuration.

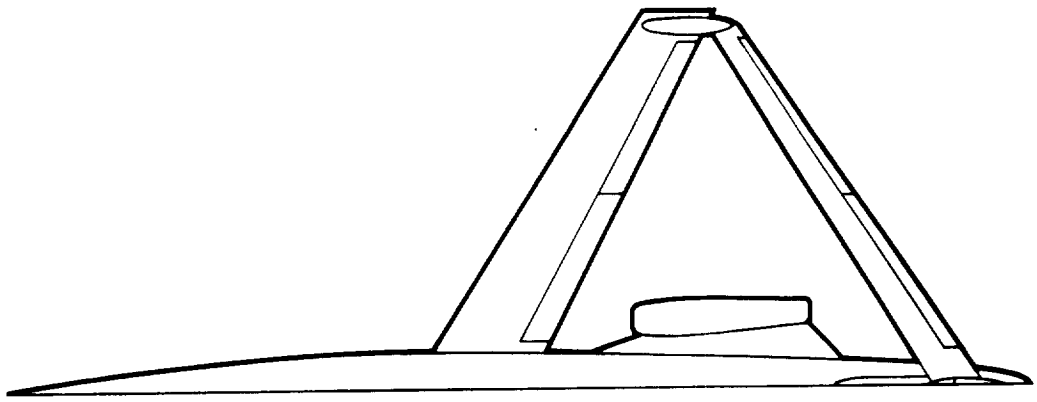

Figure 6. JW-3 Configuration.

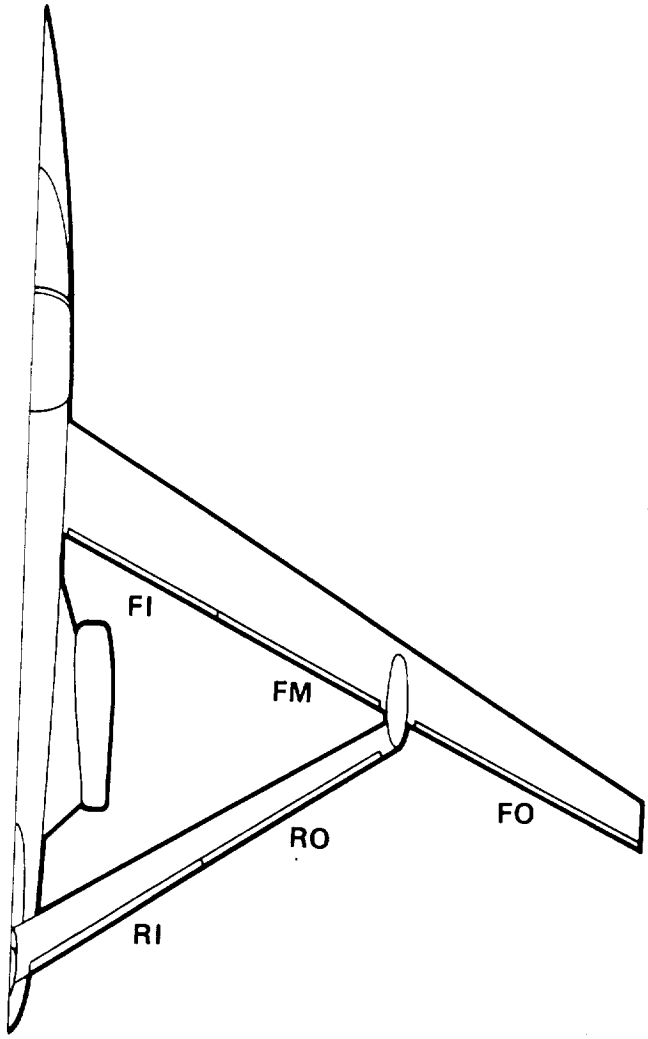

Figure 7. Control Surface Nomenclature.

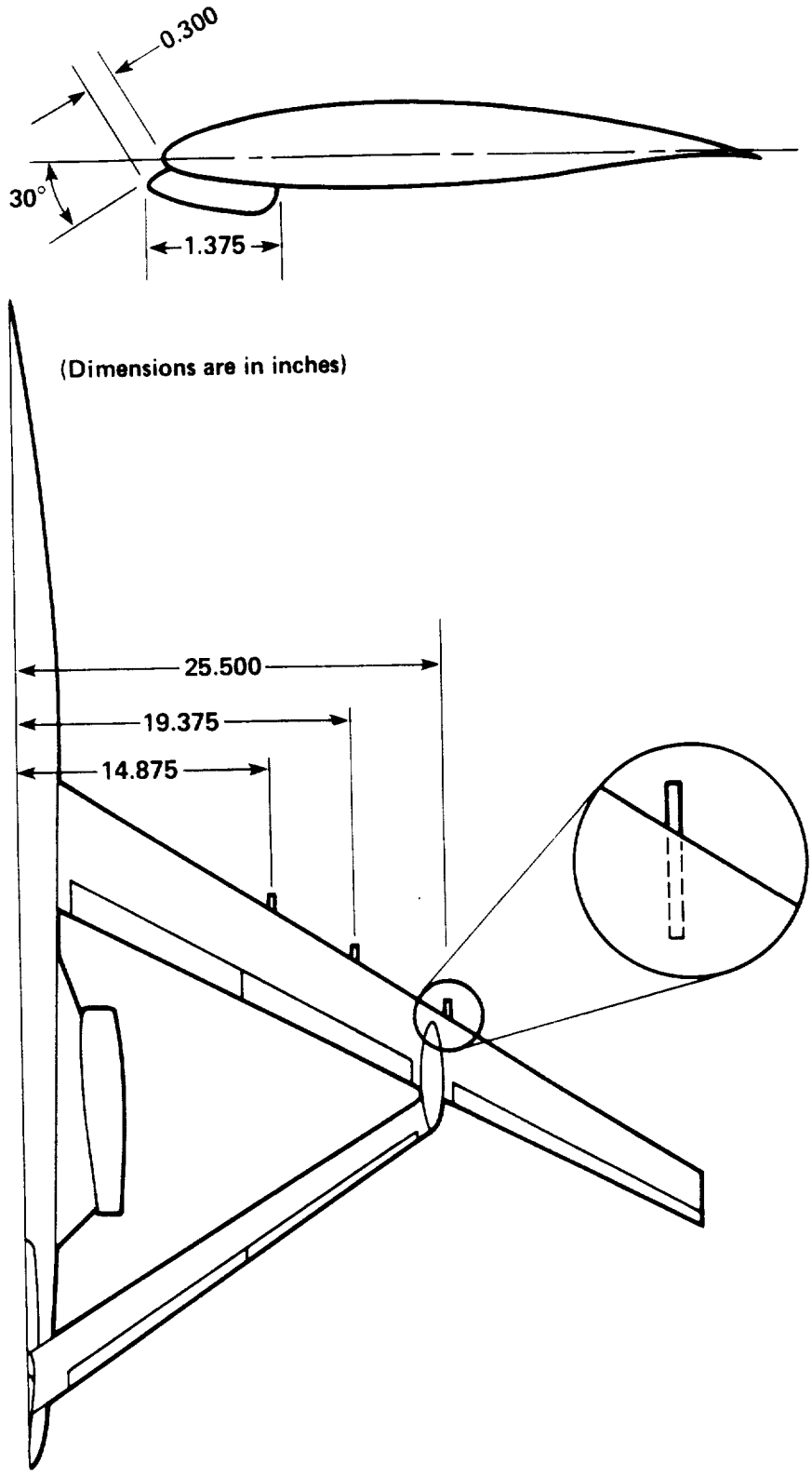

Figure 8. Vortilon Installation.

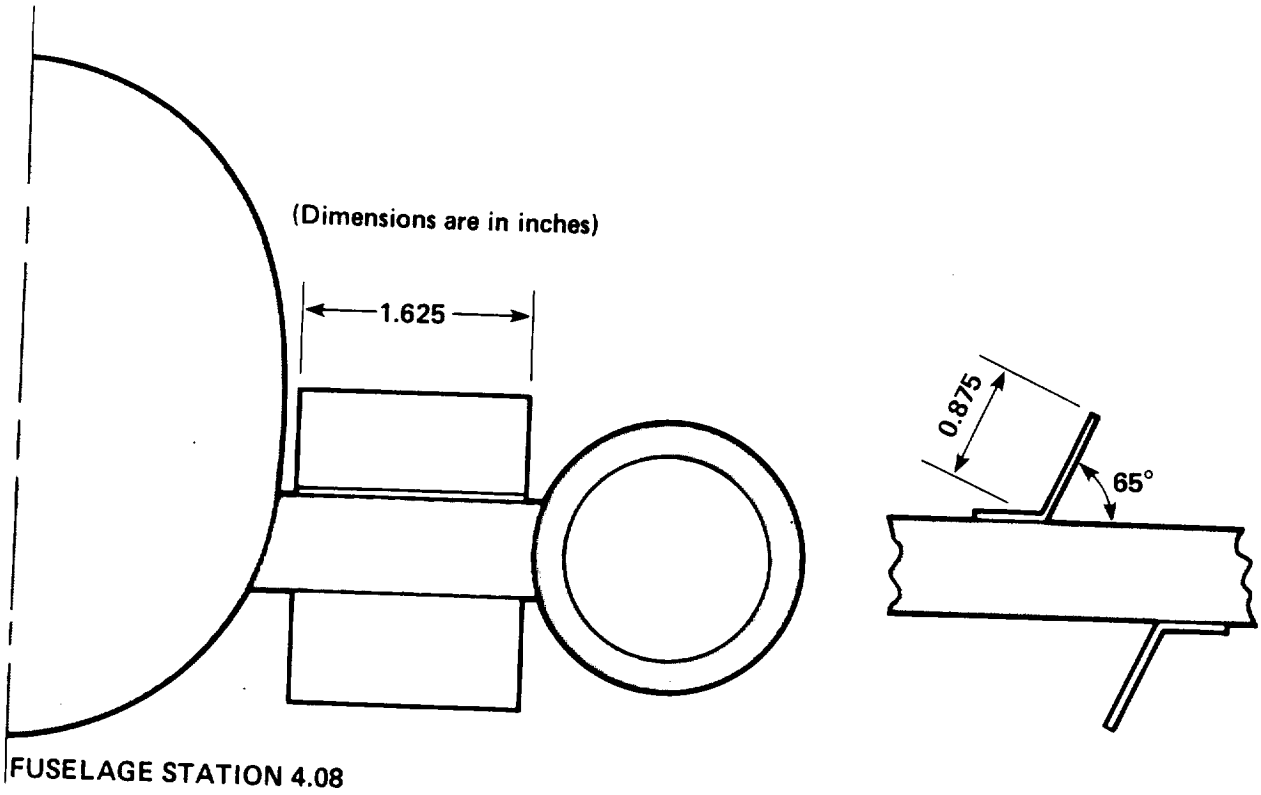

Figure 9. Speed Brake Installation on Engine Pylon.

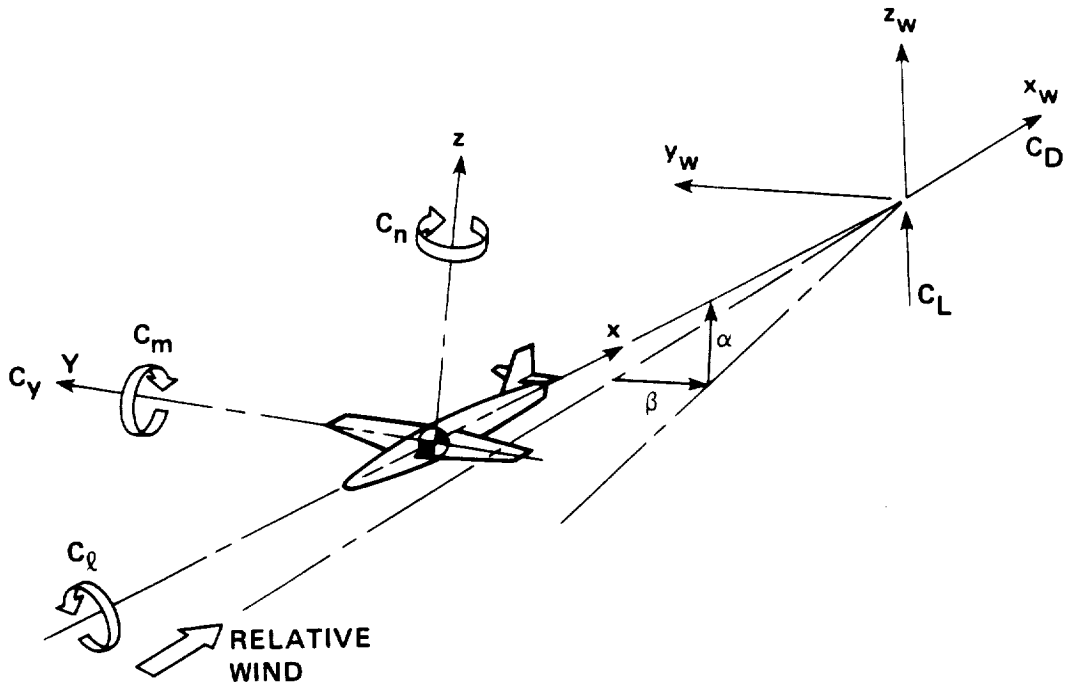

NOTES:

1. POSITIVE DIRECTIONS OF FORCE AND MOMENT COEFFICIENTS AND ANGLES ARE SHOWN BY ARROWS.
2. FOR CLARITY ORIGIN OF WIND AXES, x_w, y_w, z_w, HAVE BEEN DISPLACED FROM THE CENTER OF GRAVITY.

Figure 10. Axis Systems and Sign Conventions for Aerodynamic Data.

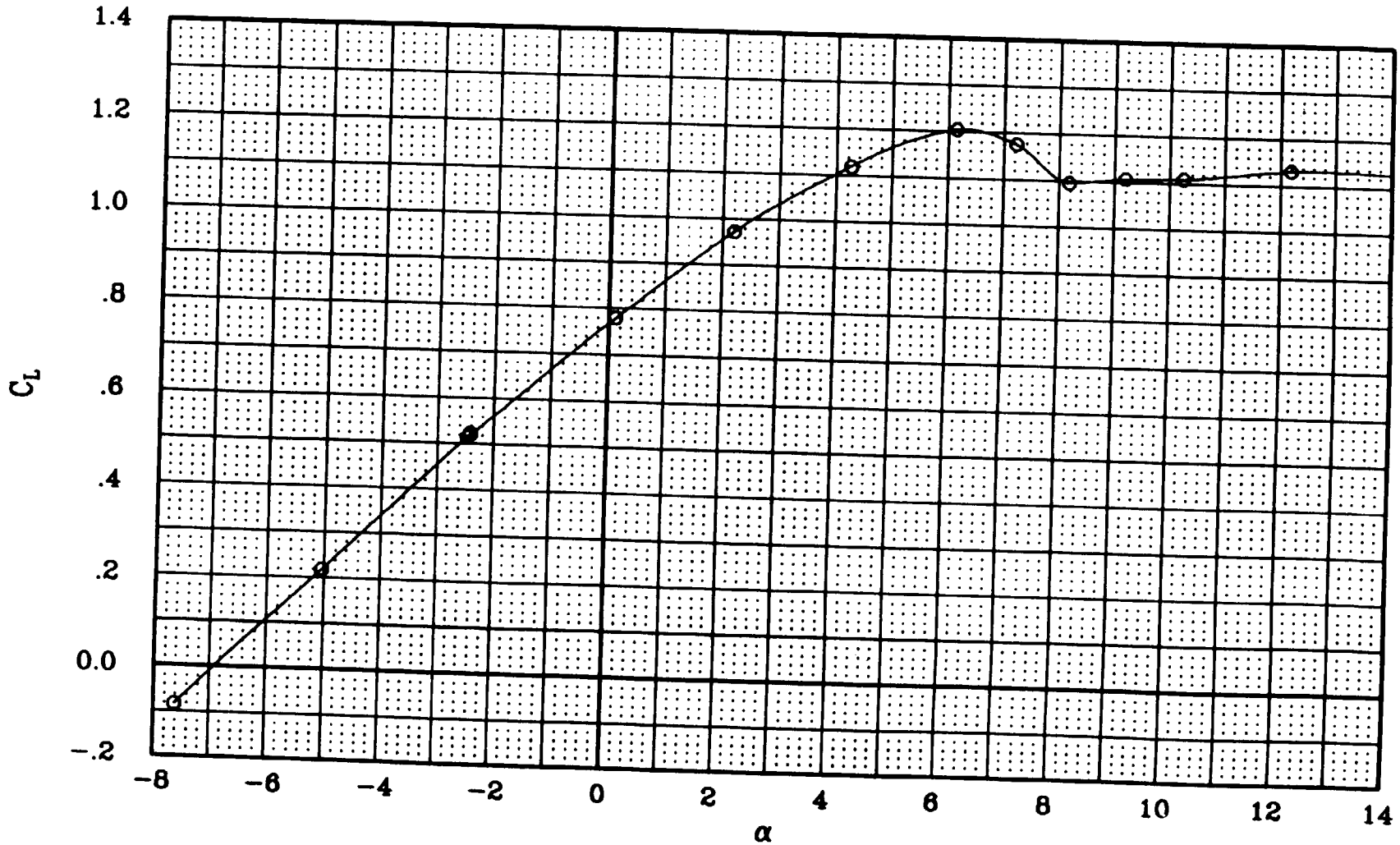

Figure 11. Longitudinal Characteristics of the JW−1 Configuration: C_L vs. α.

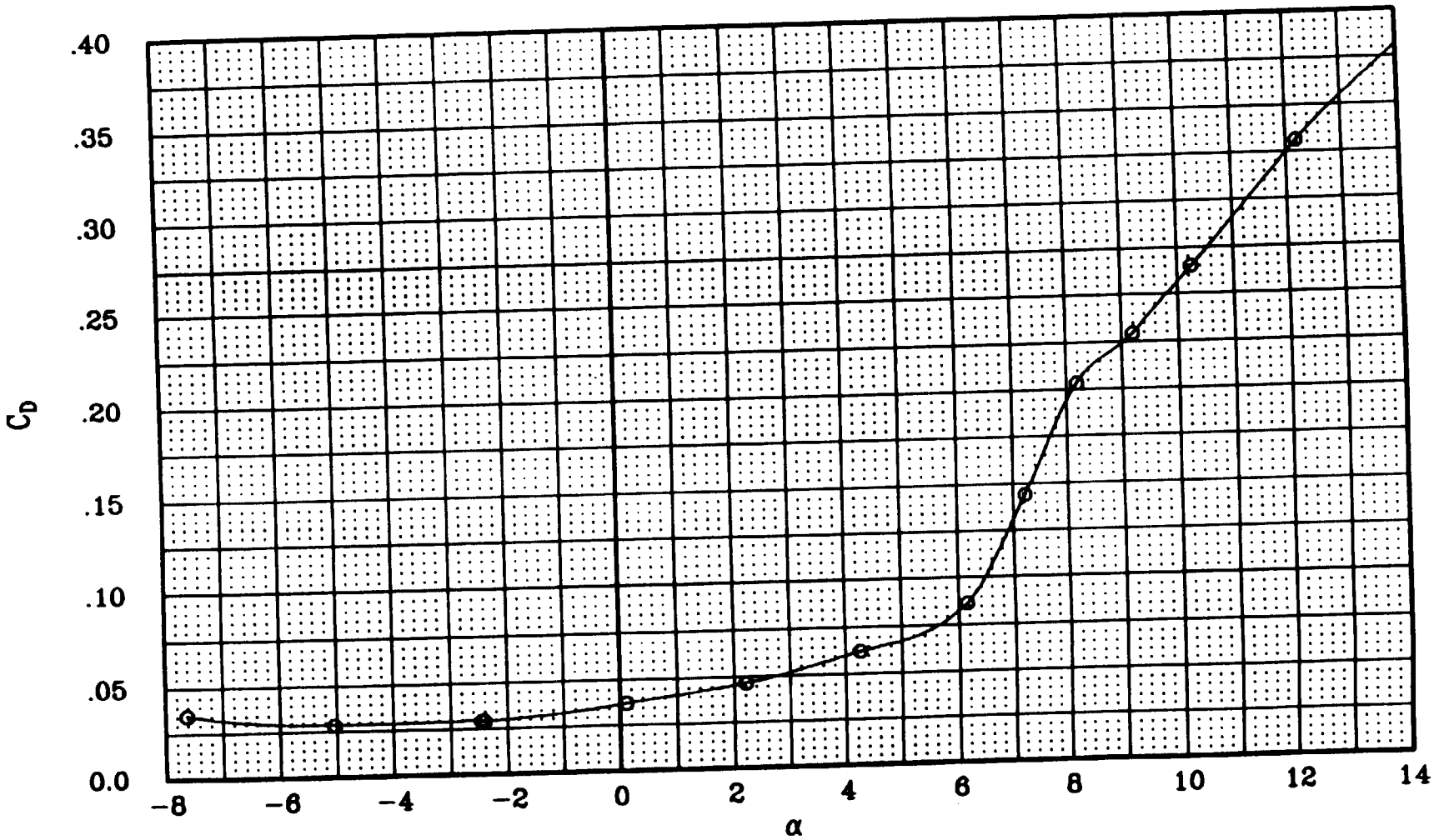

Figure 12. Longitudinal Characteristics of the JW−1 Configuration: C_D vs. α.

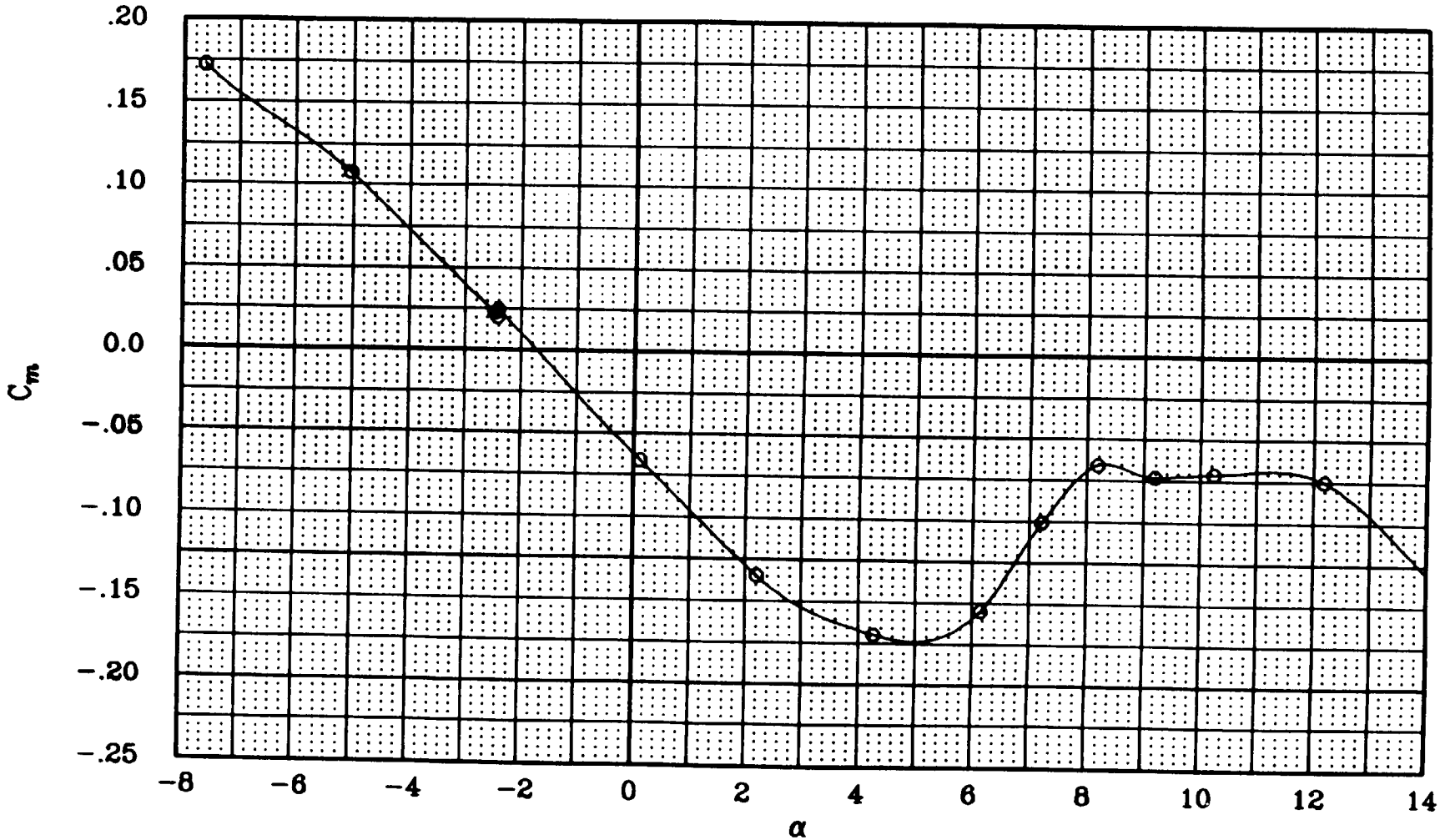

Figure 13. Longitudinal Characteristics of the JW−1 Configuration: C_m vs. α.

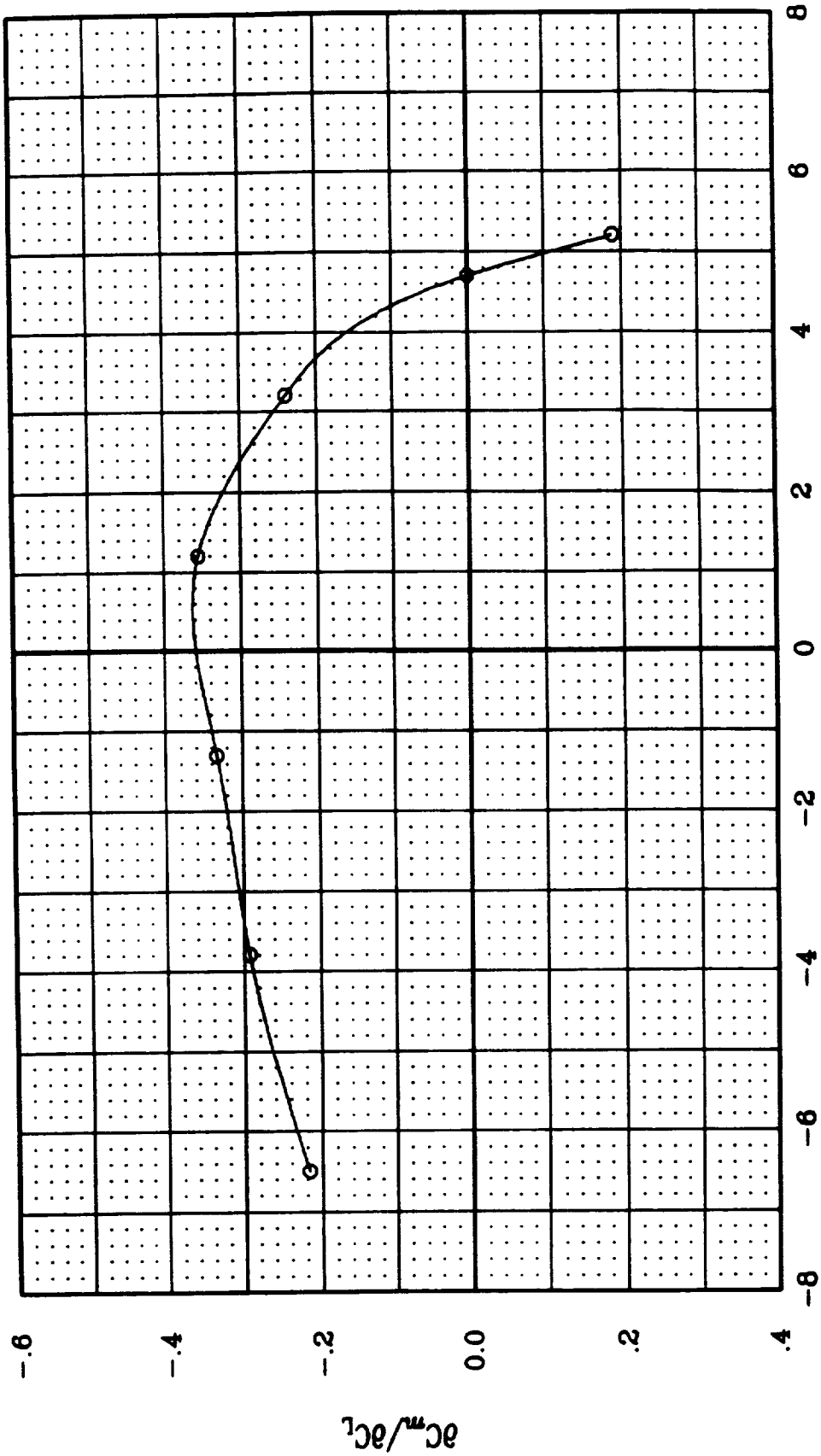

Figure 14. Longitudinal Stability, $\partial C_m/\partial C_L$, of the JW-1 Configuration.

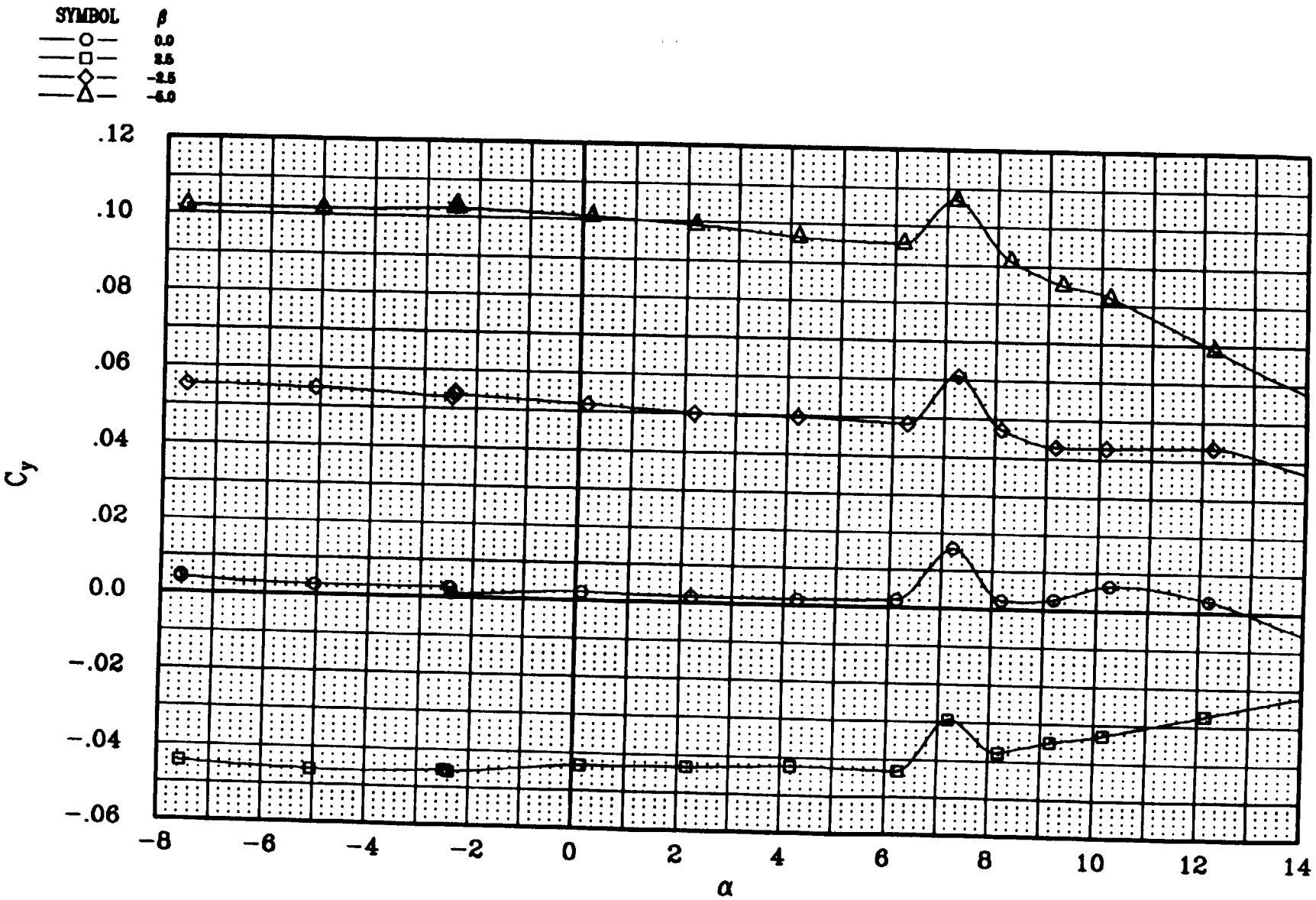

Figure 15. Lateral-Directional Characteristics of the JW-1: C_y vs, α.

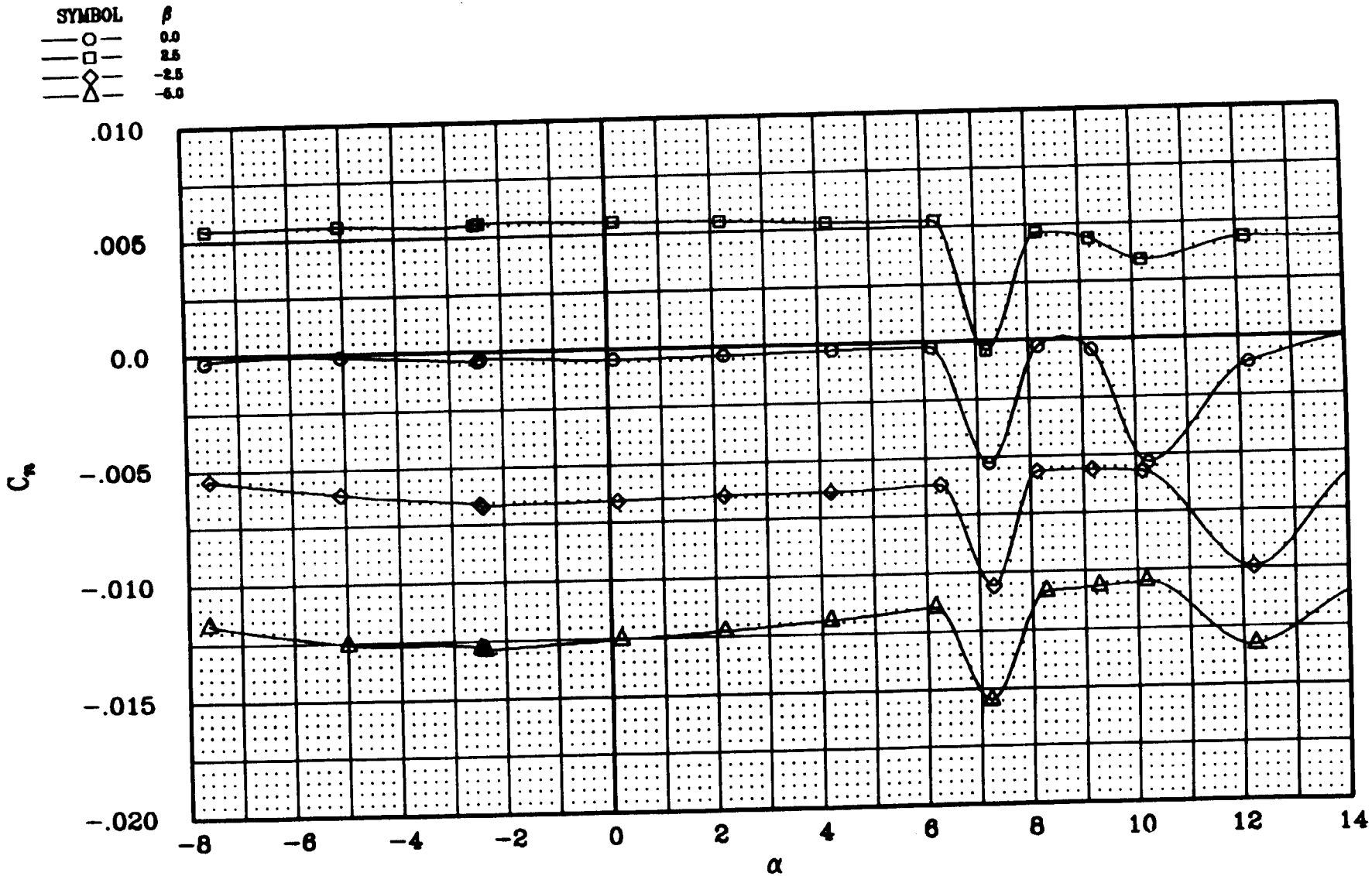

Figure 16. Lateral-Directional Characteristics of the JW-1: C_n vs. α.

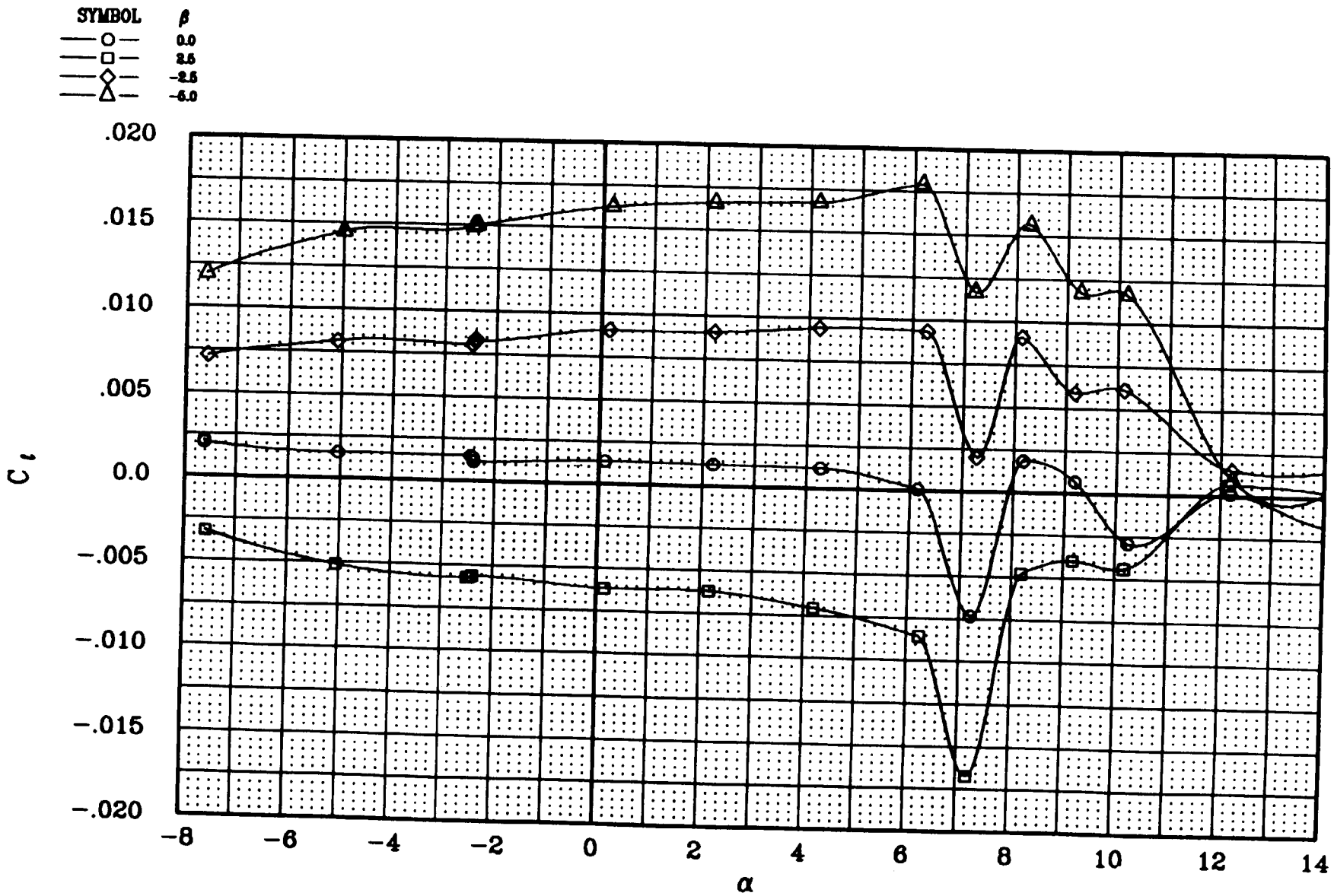

Figure 17. Lateral-Directional Characteristics of the JW-1: C_l vs. α.

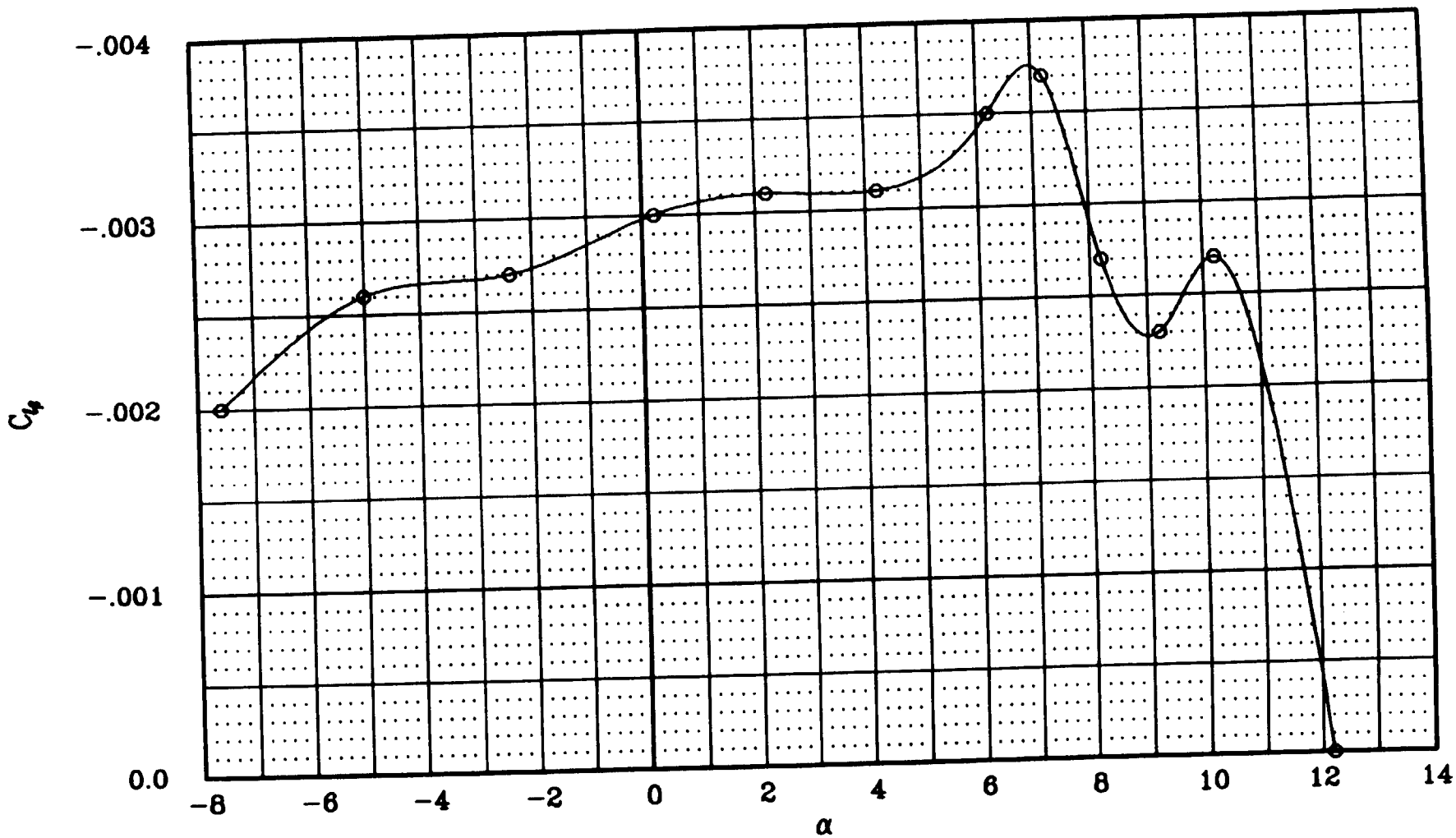

Figure 18. Lateral-Directional Stability of the JW-1 Configuration: C_{l_β} vs. α.

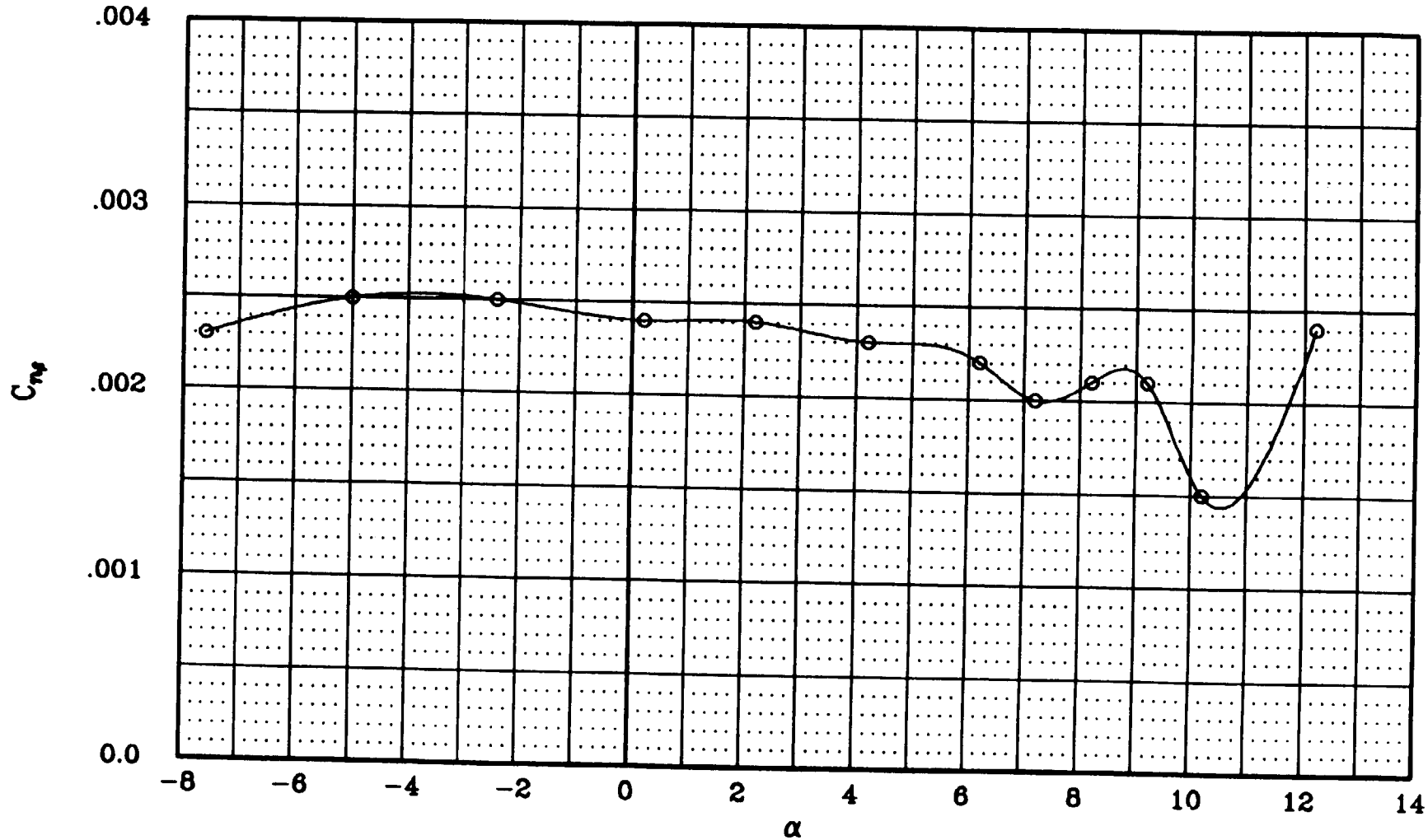

Figure 19. Lateral-Directional Stability of the JW-1 Configuration: C_{n_β} vs. α.

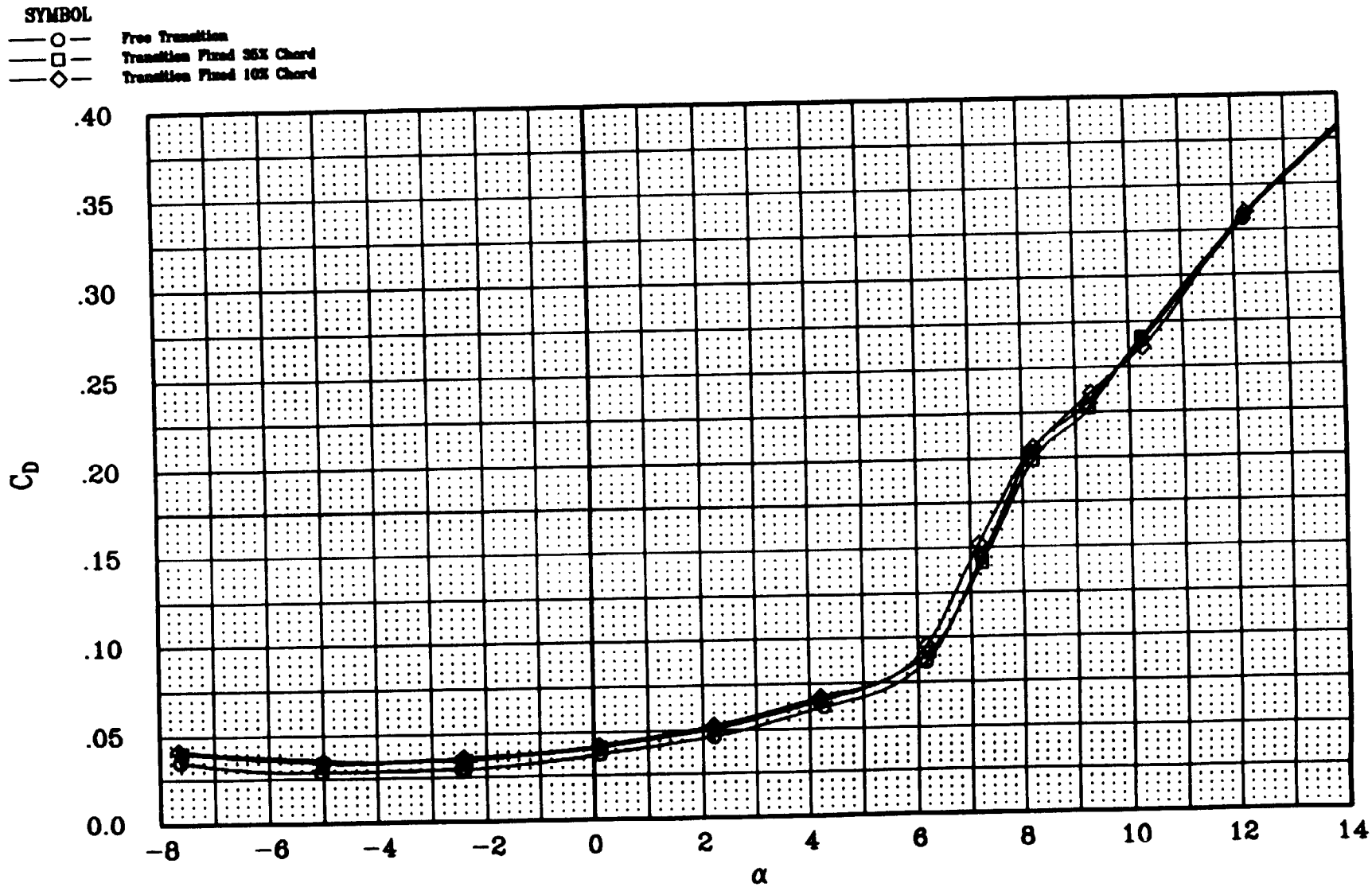

Figure 20. Effects of Transition Location on the JW-1: C_D vs. α.

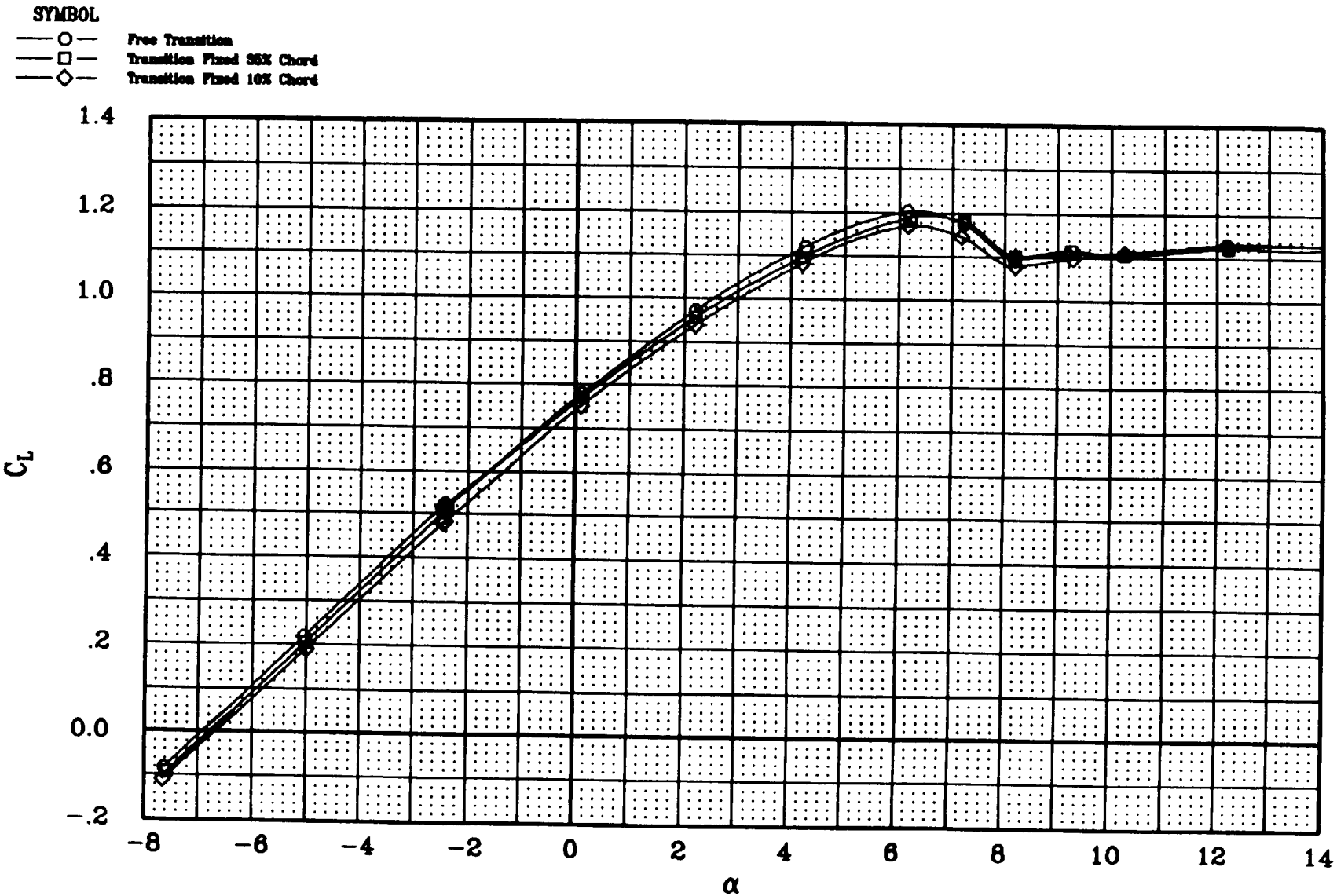

Figure 21. Effects of Transition Location on the JW-1: C_L vs. α.

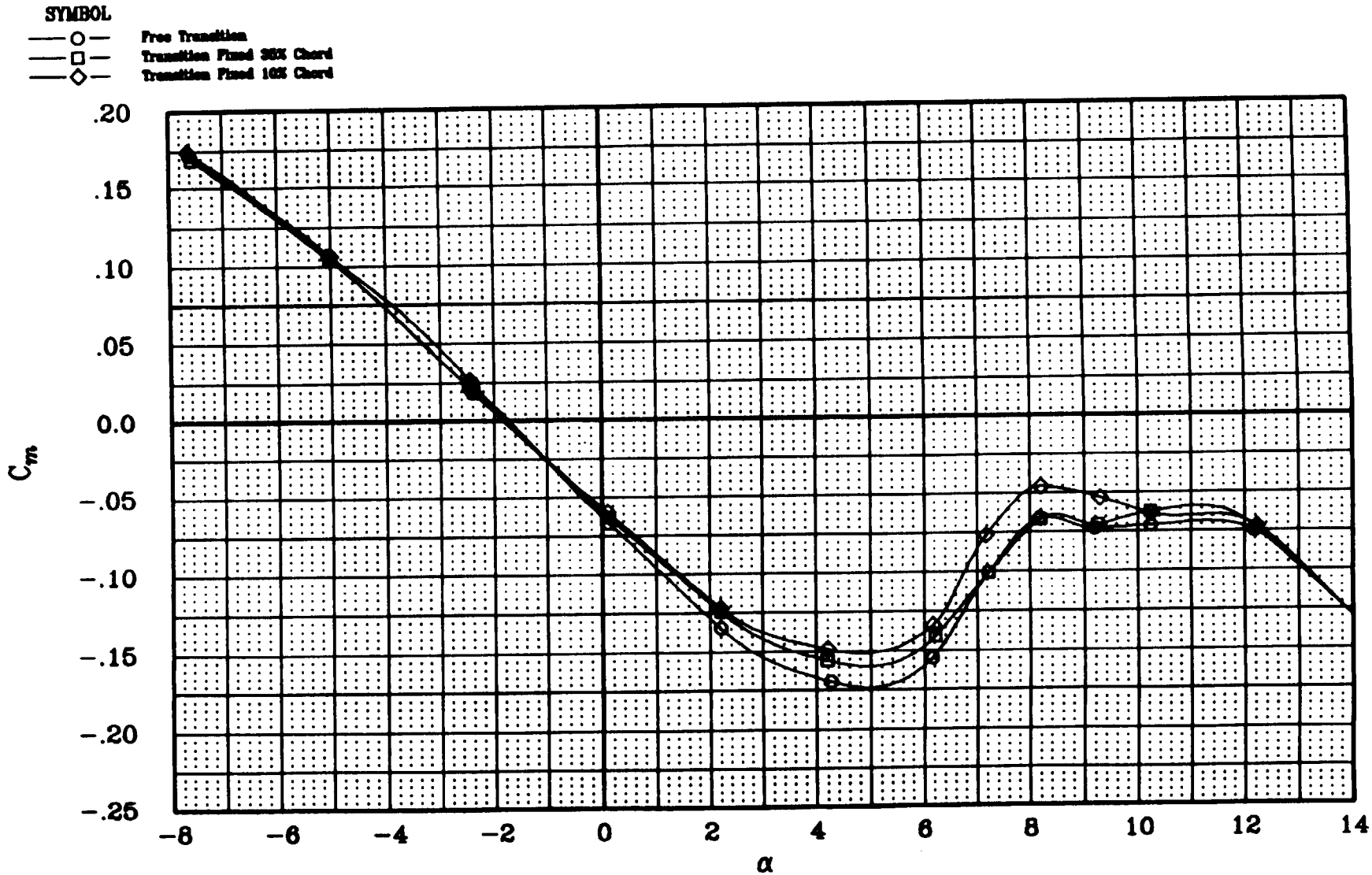

Figure 22. Effects of Transition Location on the JW−1: C_m vs. α.

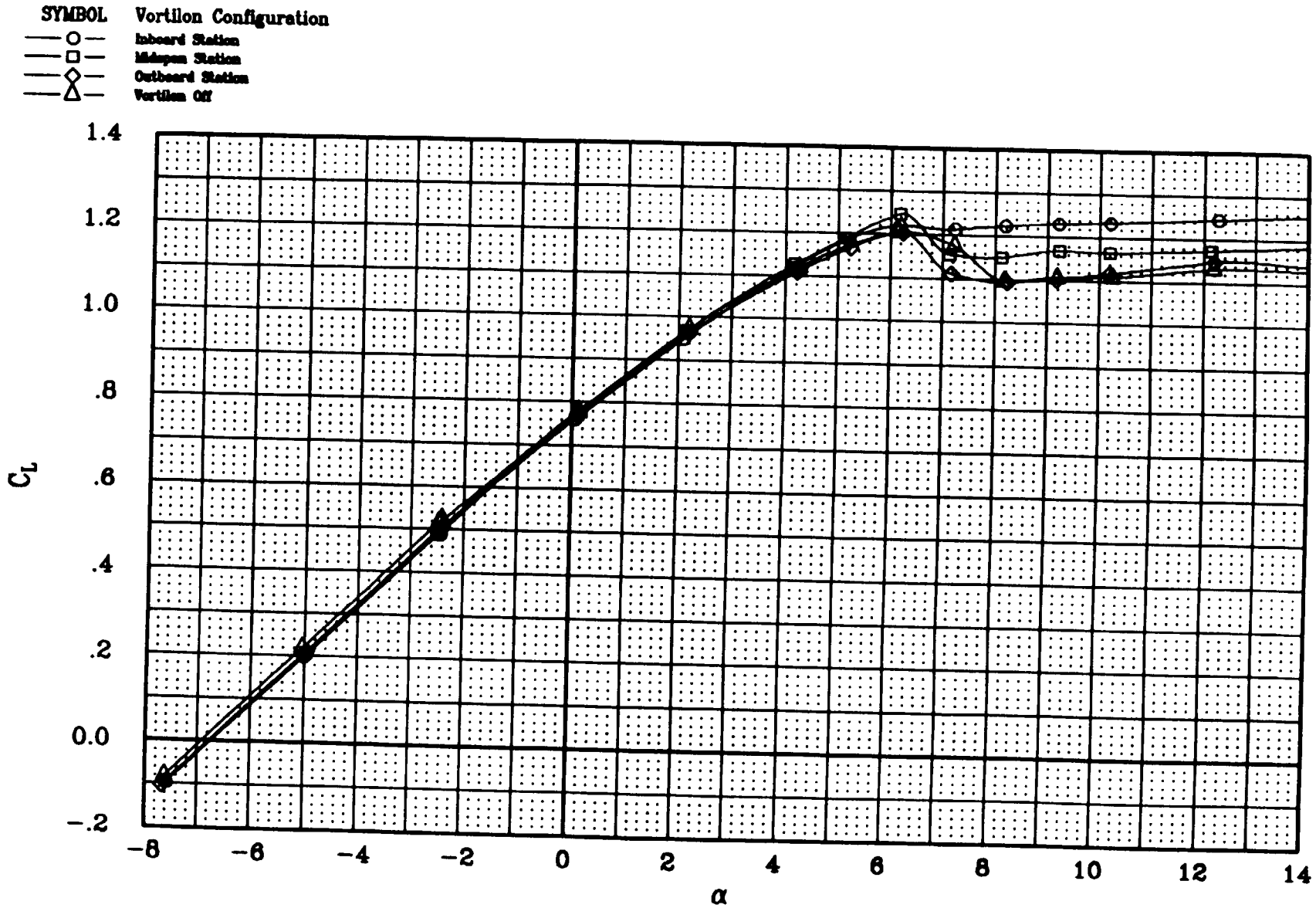

Figure 23. Effect of Vortilons On Longitudinal Characteristics of the JW-1: C_L vs. α.

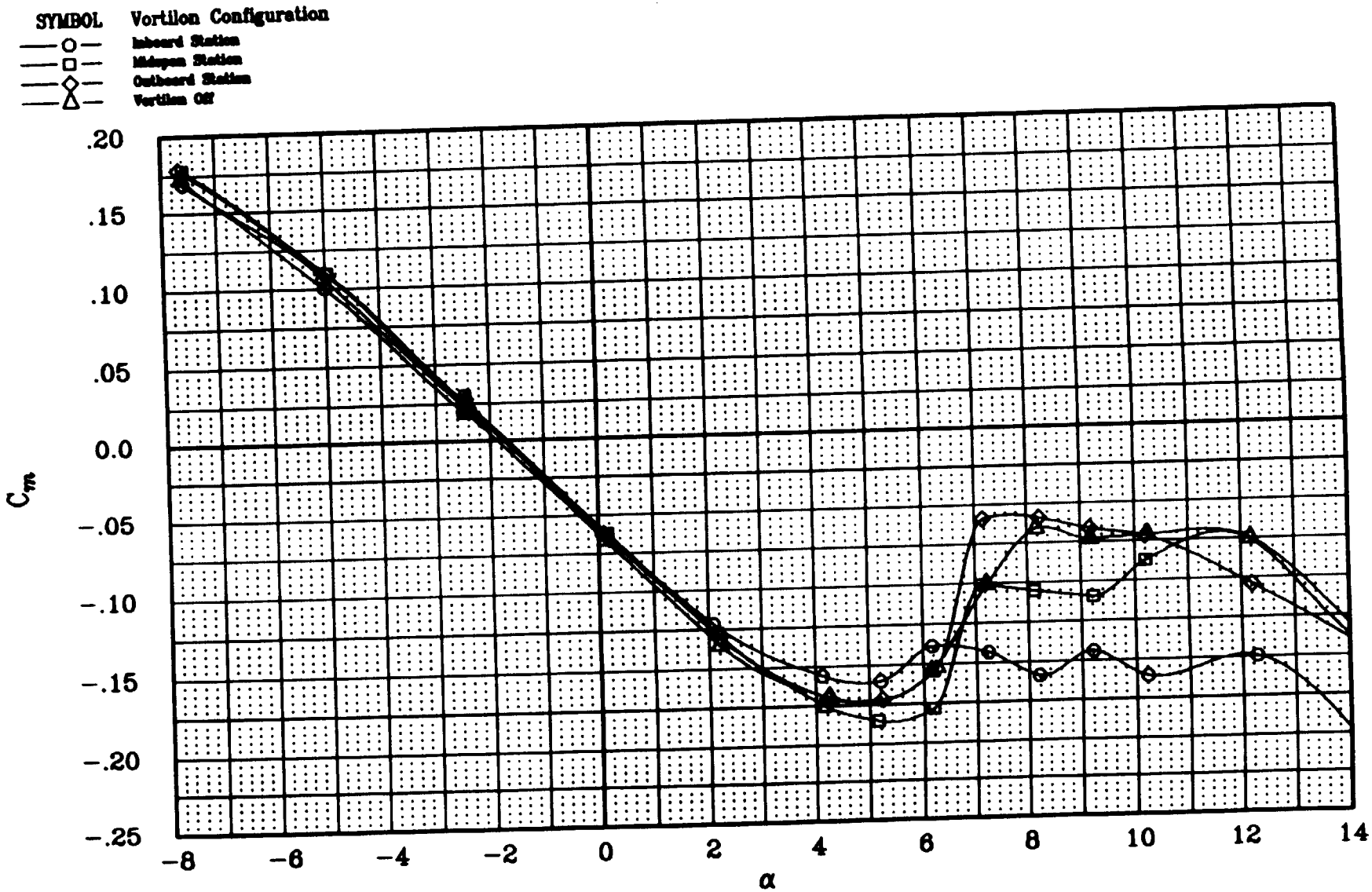

Figure 24. Effect of Vortilons On Longitudinal Characteristics of the JW−1: C_m vs. α.

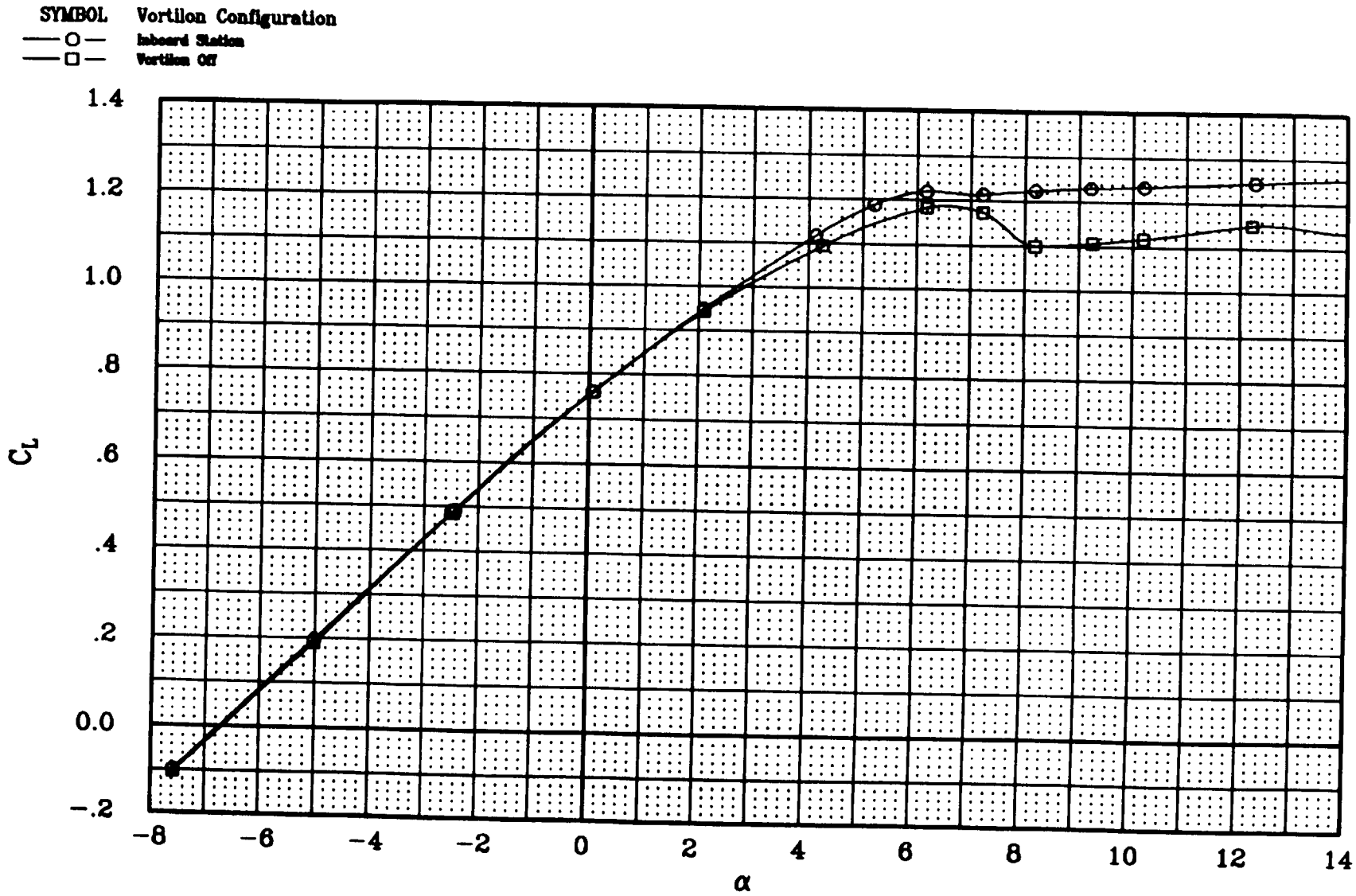

Figure 25. Effect of Inboard Vortilon On Longitudinal Characteristics of the JW-1: C_L vs. α.

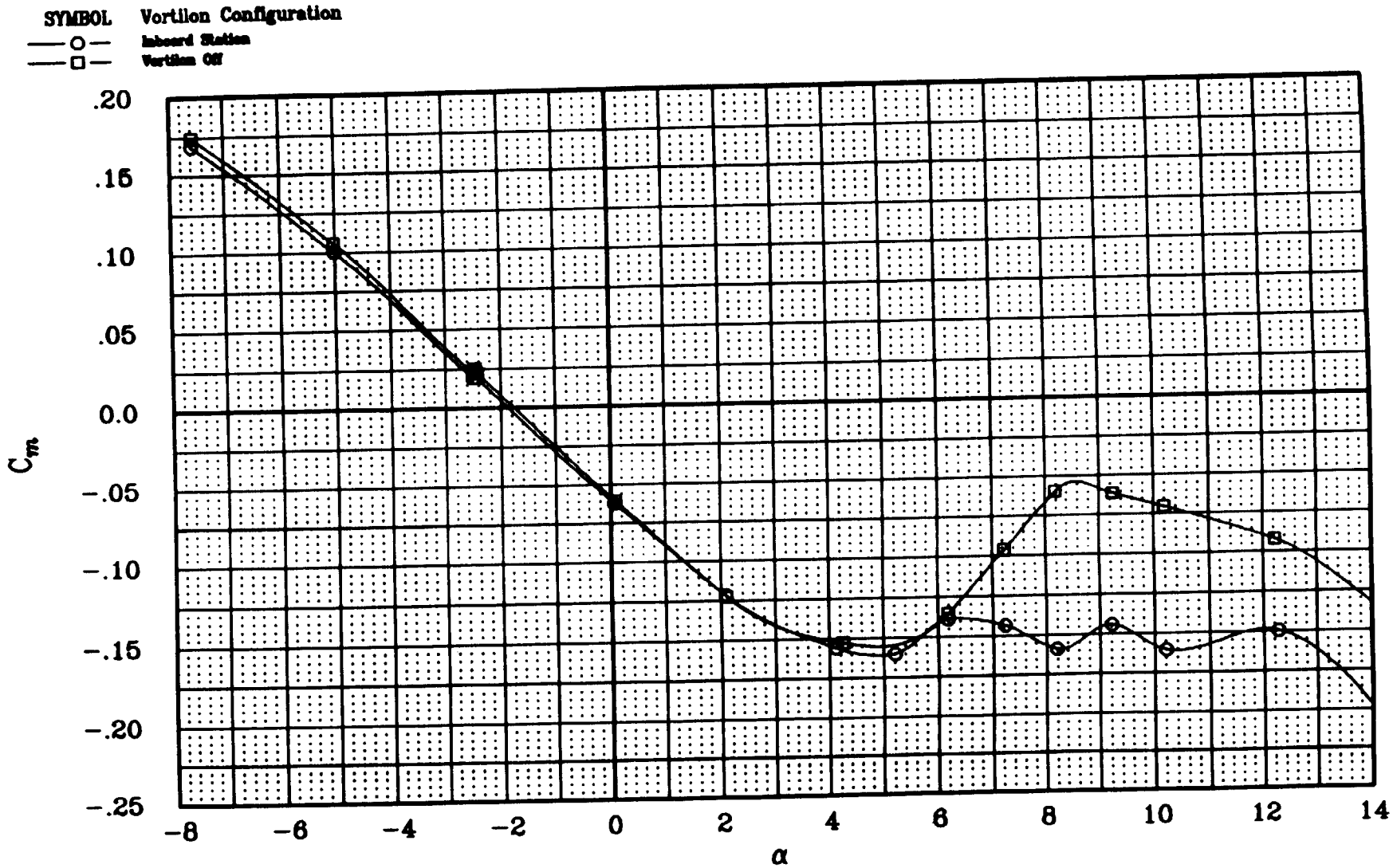

Figure 26. Effect of Inboard Vortilon On Longitudinal Characteristics of the JW−1: C_m vs. α.

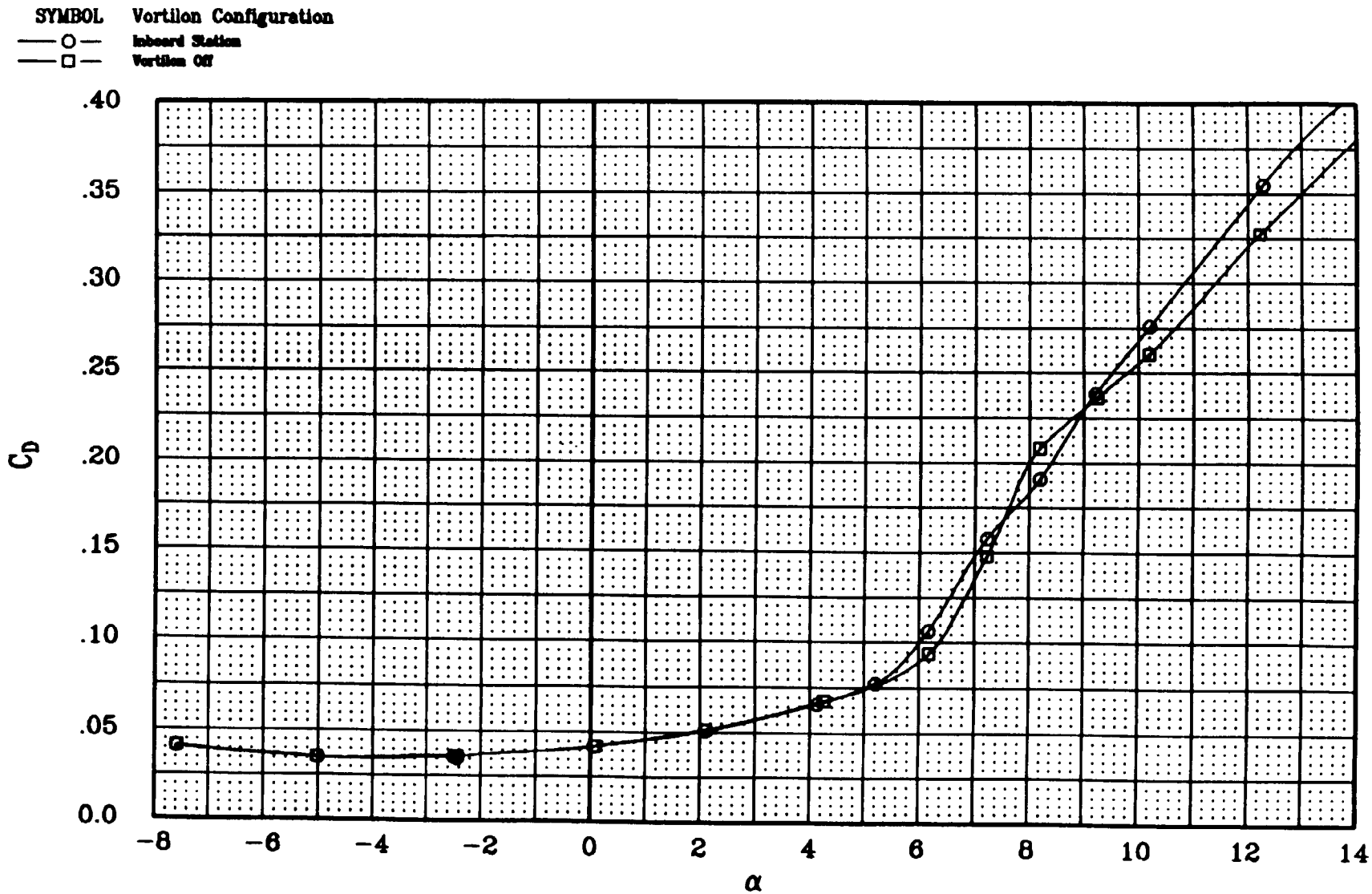

Figure 27. Effect of Inboard Vortilon On Longitudinal Characteristics of the JW−1 : C_D vs. α.

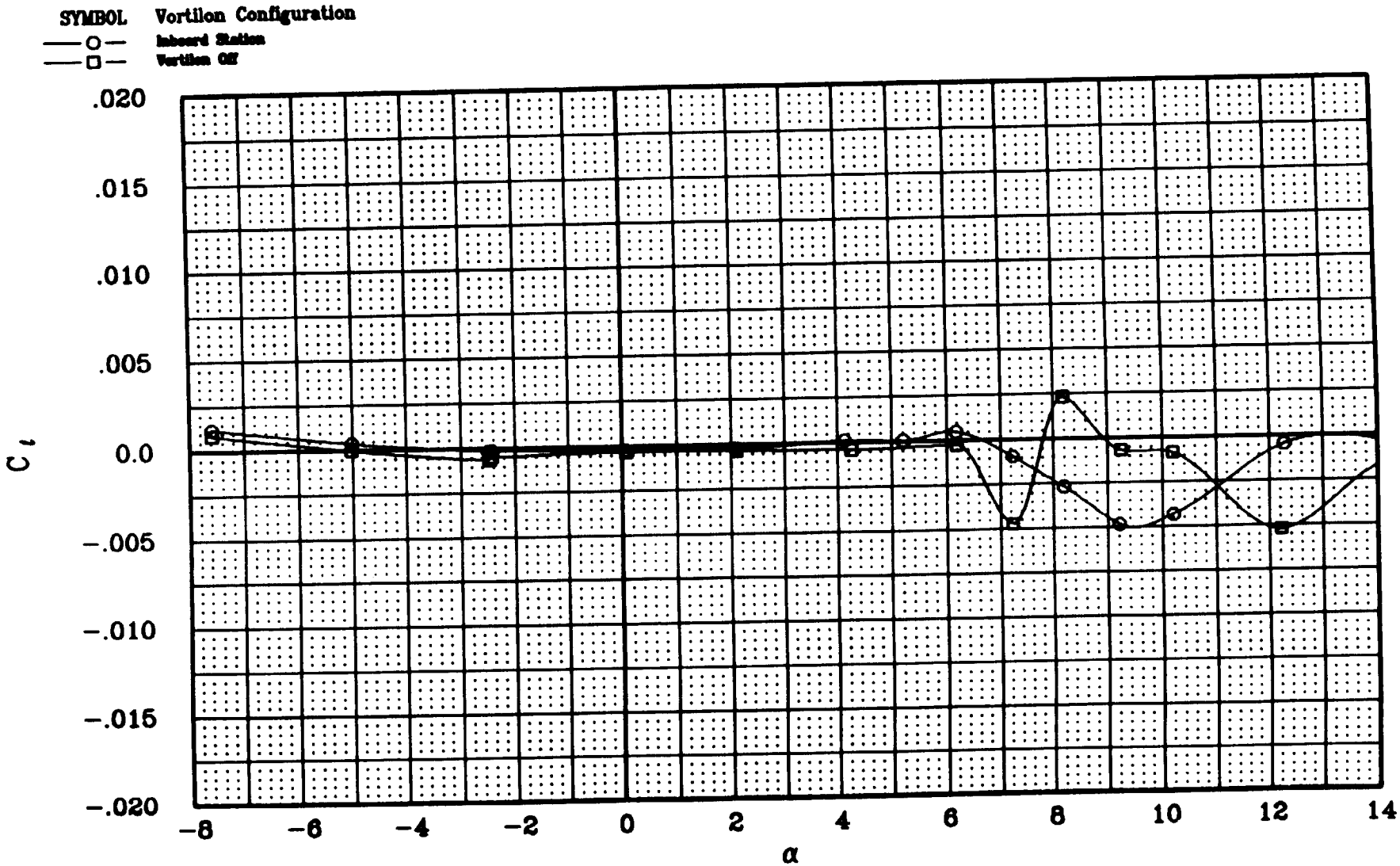

Figure 28. Effect of Inboard Vortilon On Lat.–Dir. Characteristics of the JW–1: C_l vs. α.

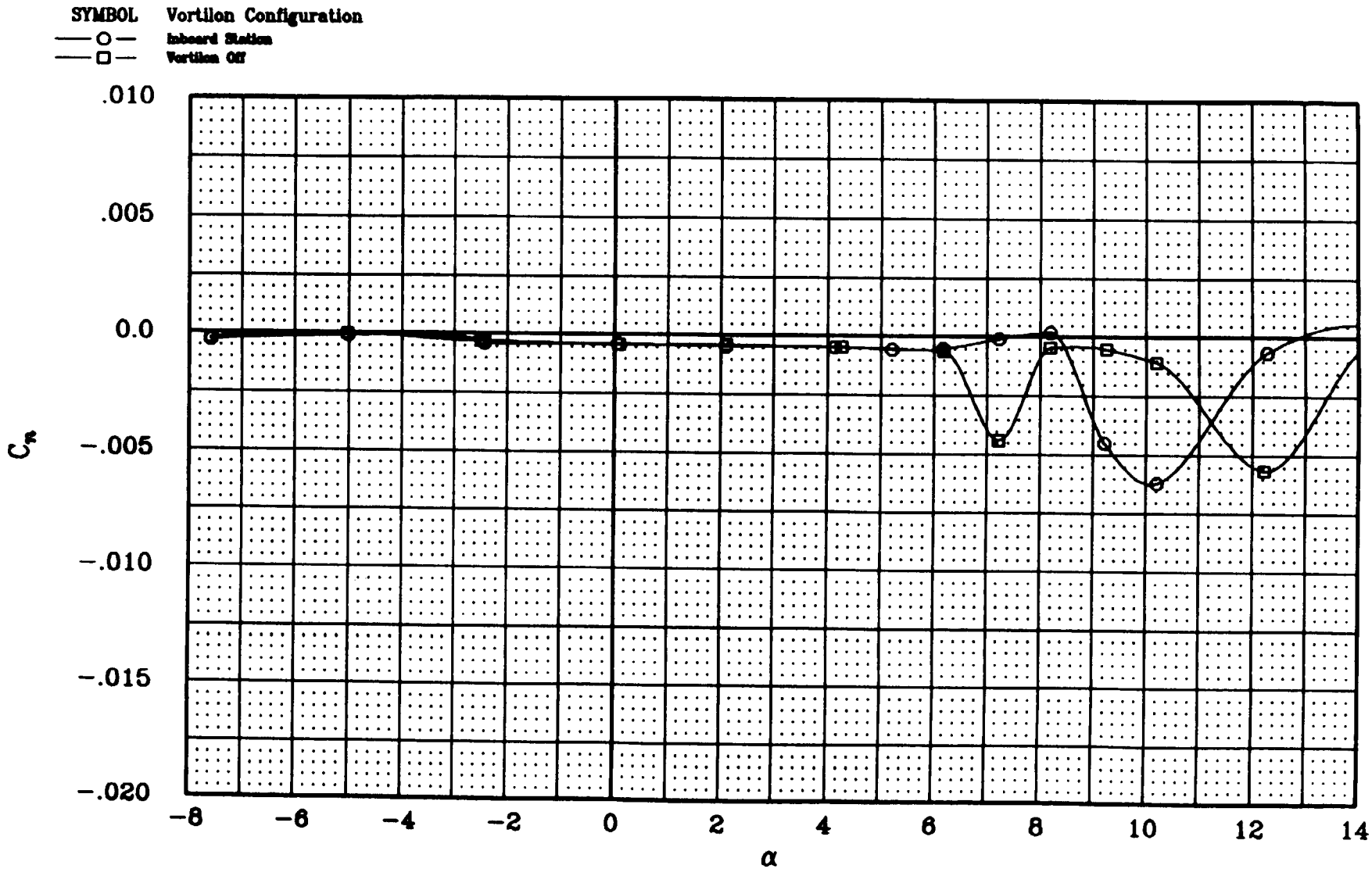

Figure 29. Effect of Inboard Vortilon On Lat.–Dir. Characteristics of the JW–1: C_n vs. α.

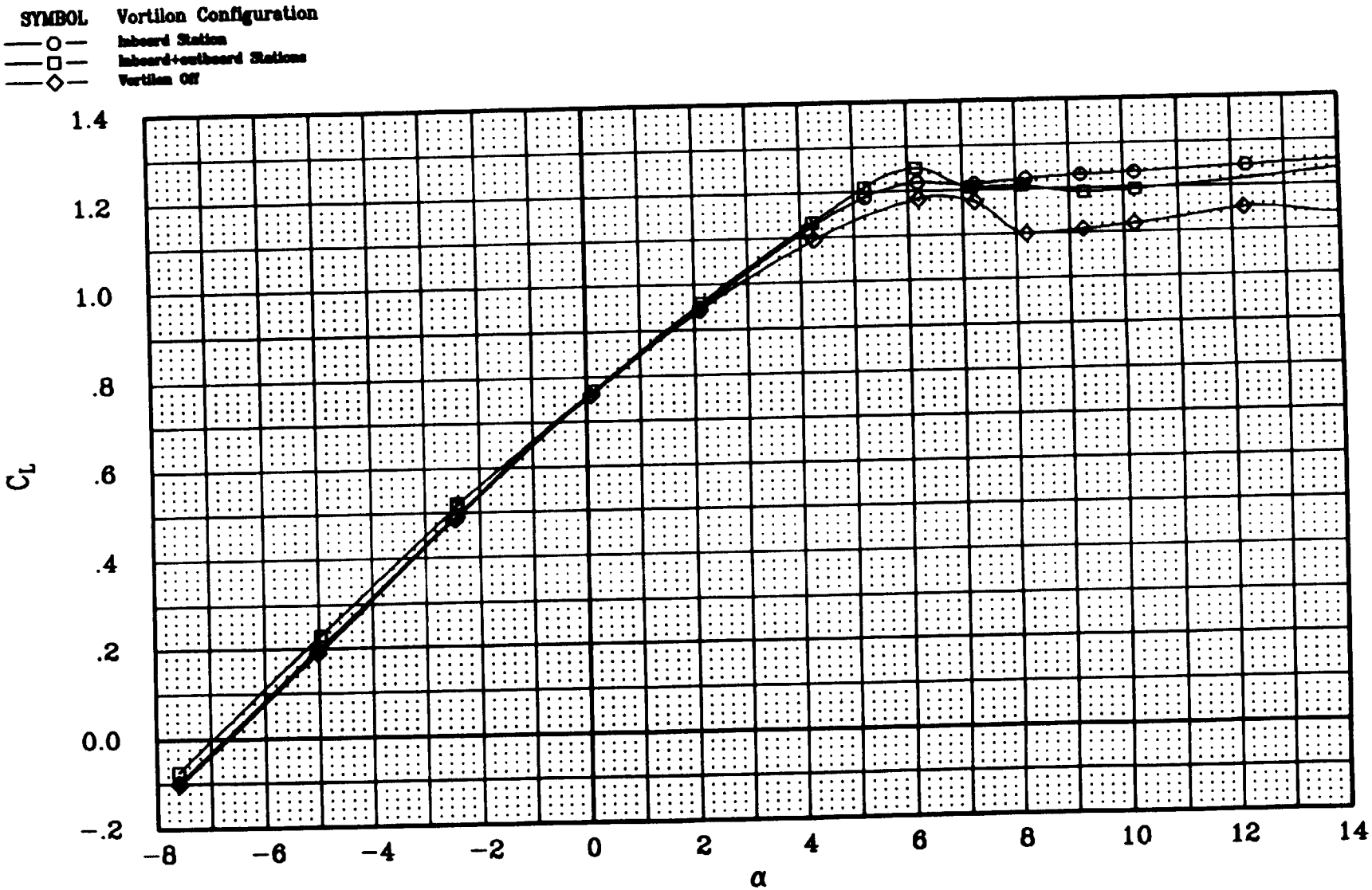

Figure 30. Effect of Vortilons On Lift Characteristics of the JW-1: Two Vortilon Configuration.

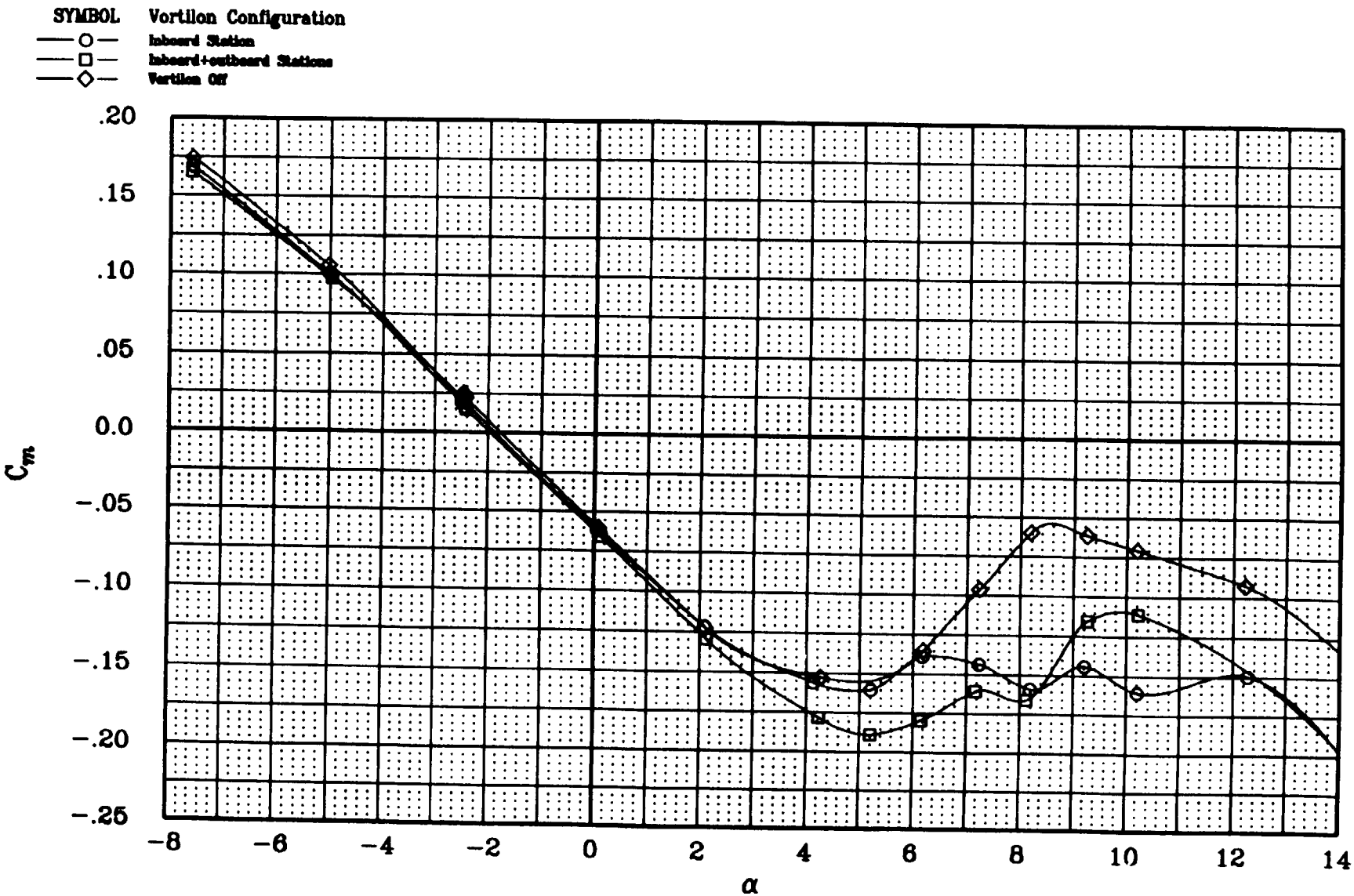

Figure 31. Effect of Vortilons On Pitching-Moment Characteristics of the JW-1: Two Vortilon Configuration.

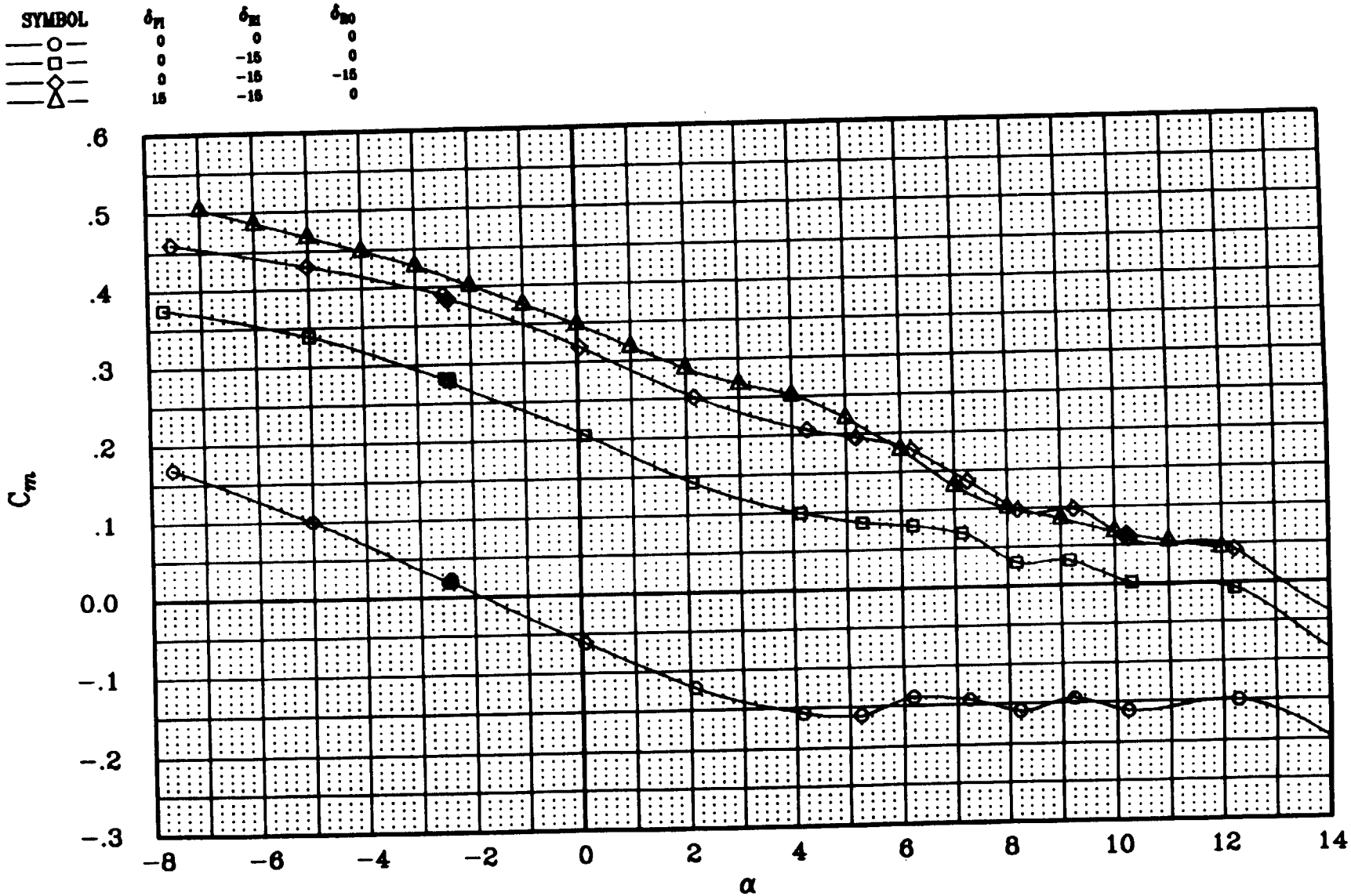

Figure 32. Effectiveness of Various Elevator Configurations on the JW-1: C_m vs. α.

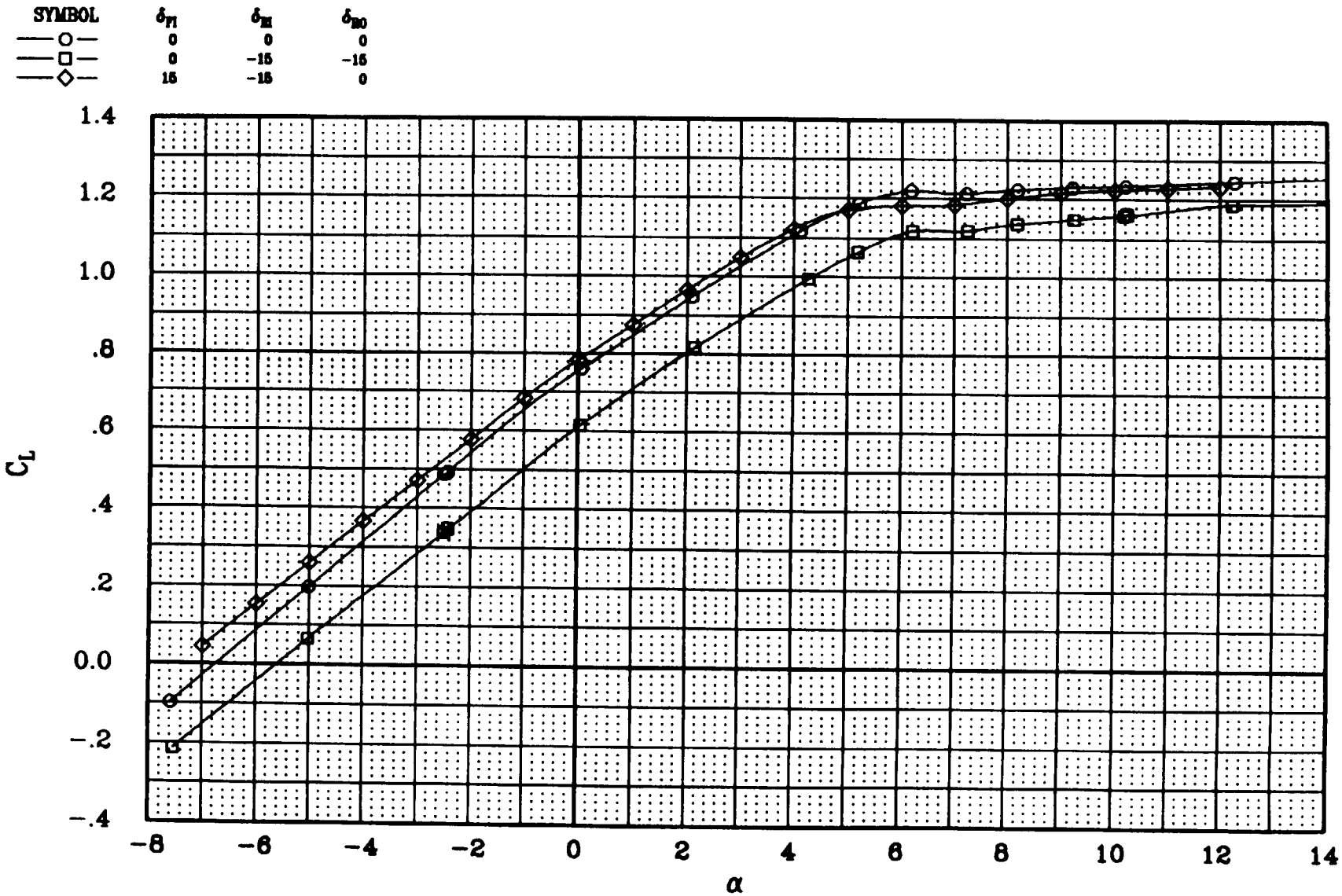

Figure 33. Effect of Various Elevator Configurations on lift on the JW-1.

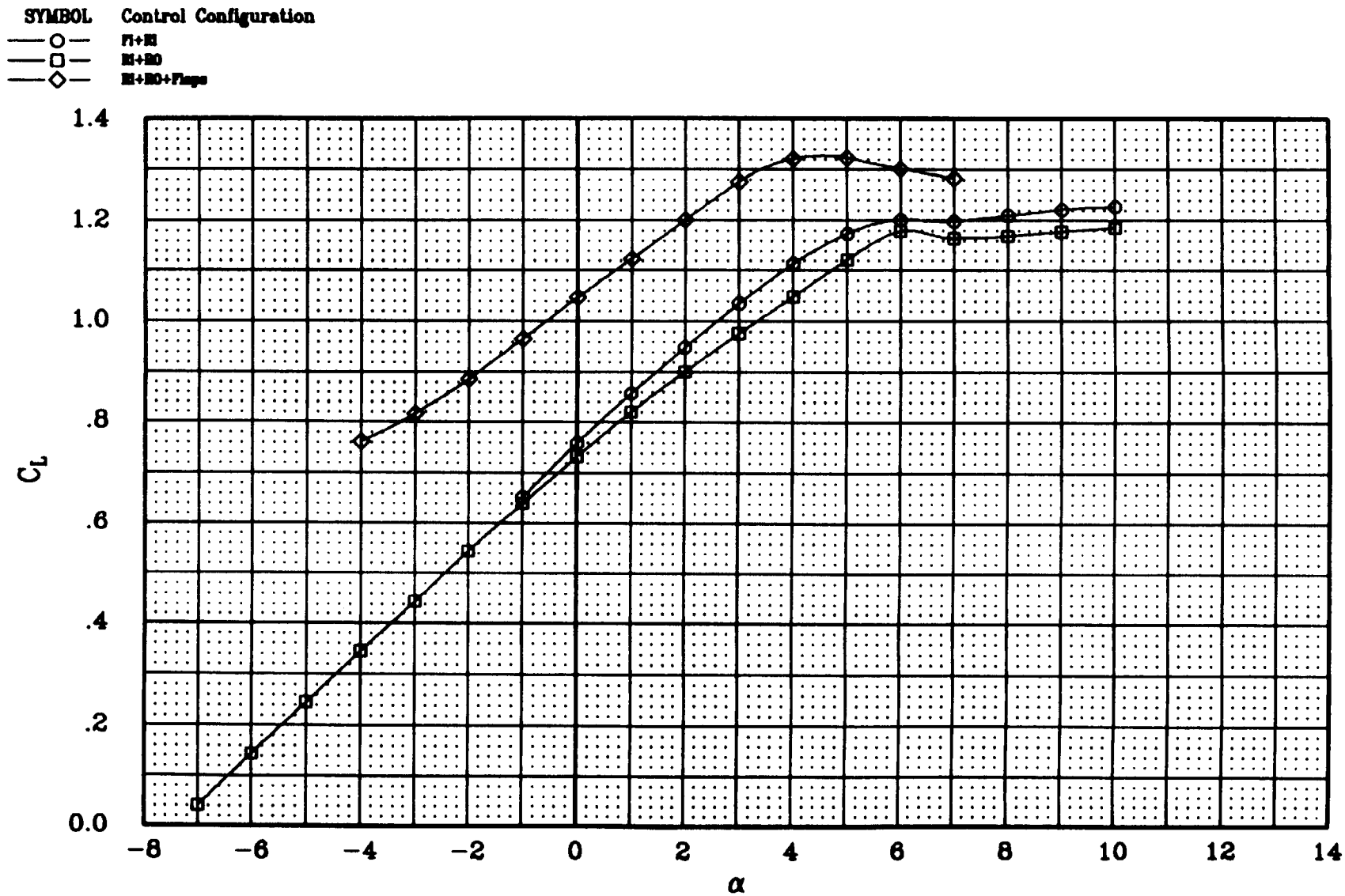

Figure 34. Trimmed Lift Characteristics of the JW−1.

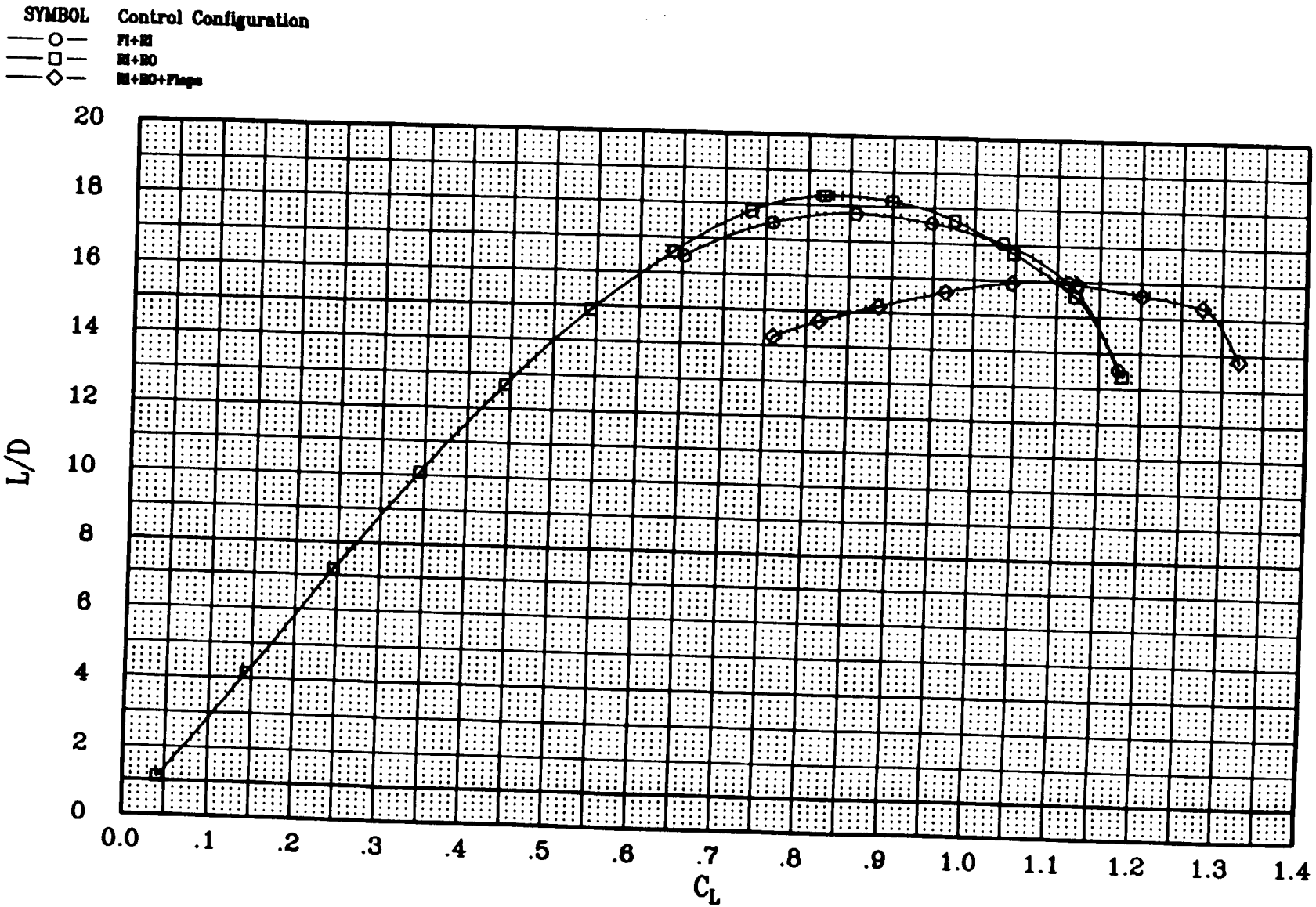

Figure 35. Trimmed Lift-to-Drag Ratio of the JW-1.

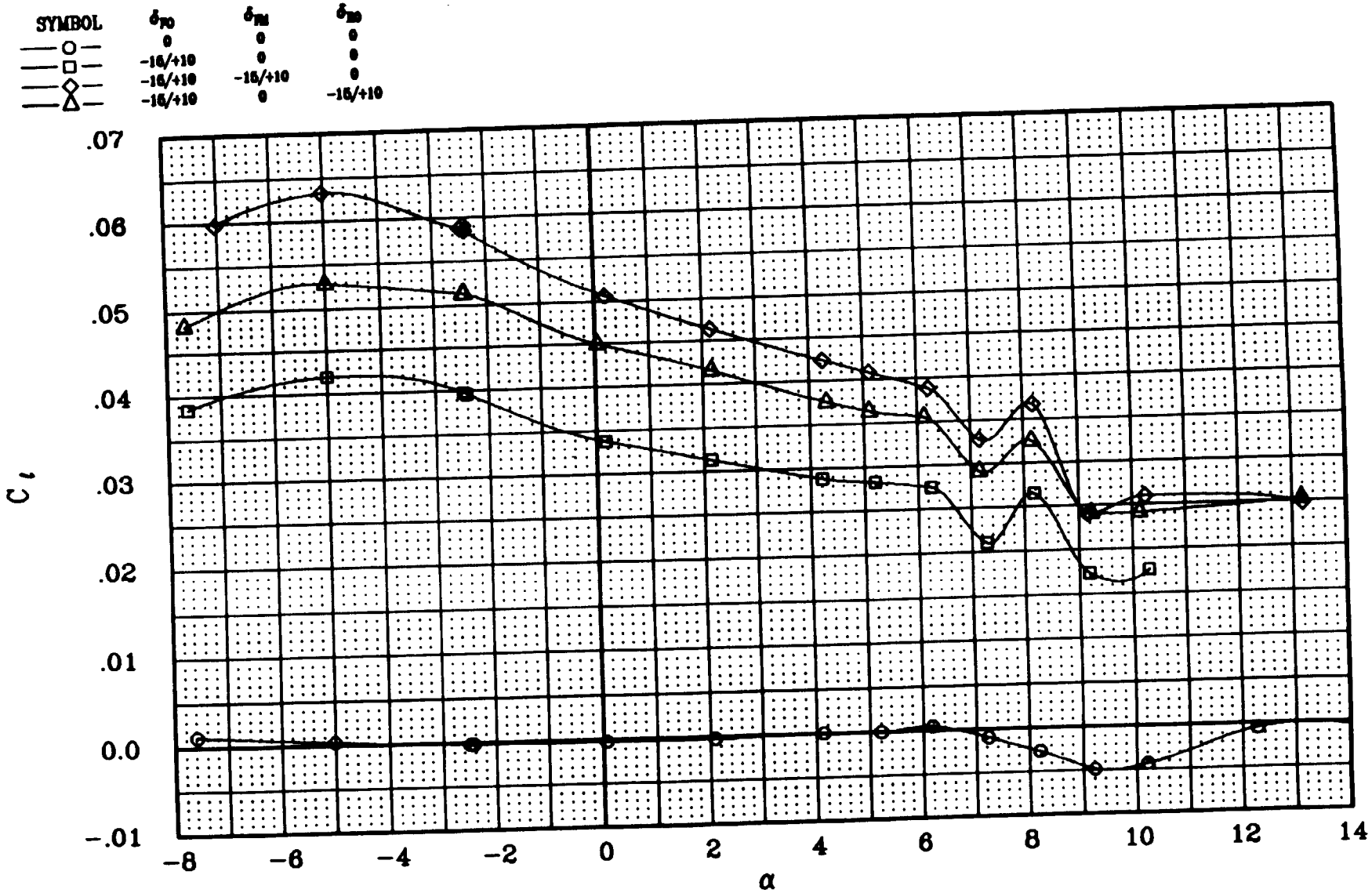

Figure 36. Effectiveness of Various Aileron Configurations on the JW-1: C_l vs. α.

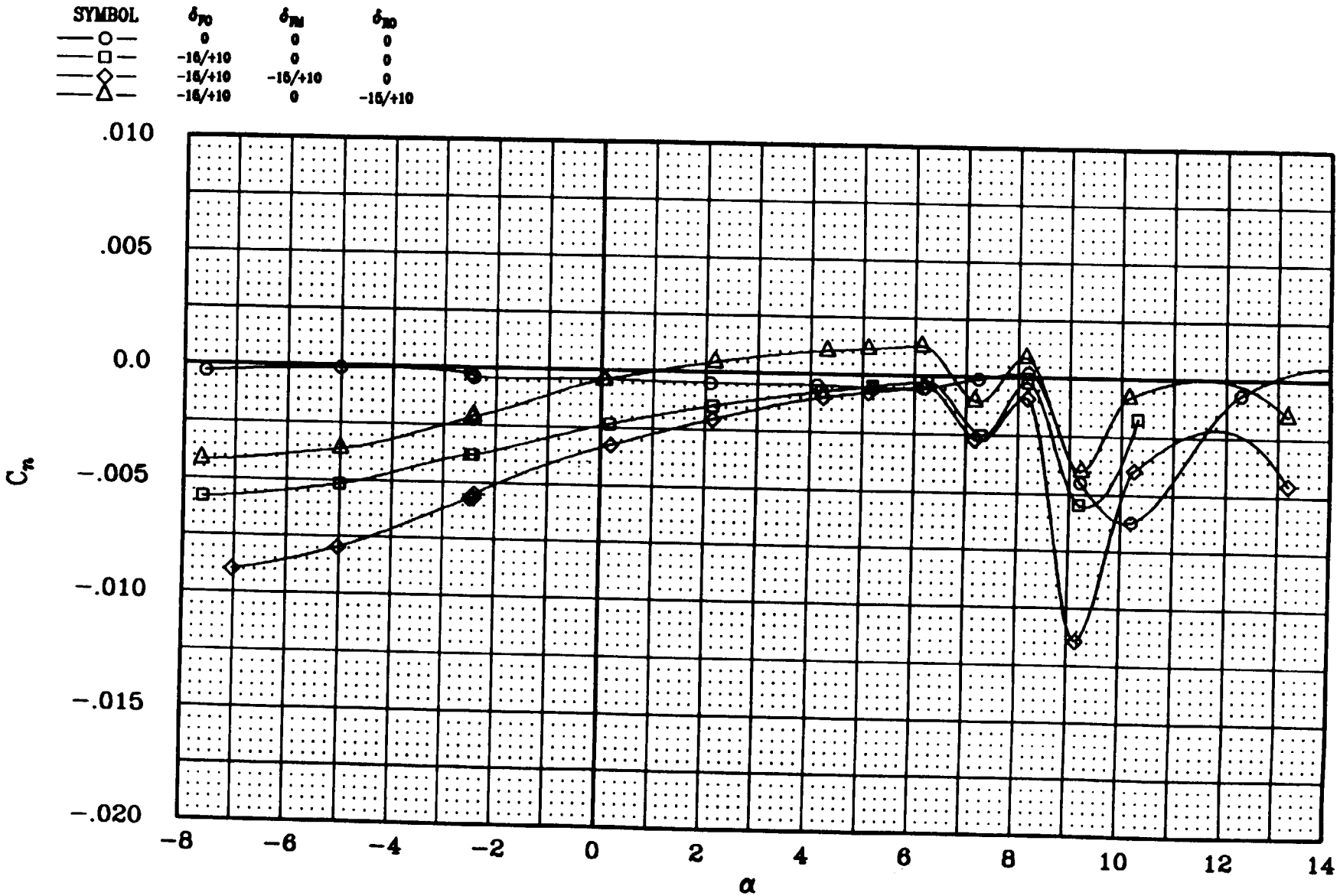

Figure 37. Yawing Moment Induced by Various Aileron Configurations on the JW−1.

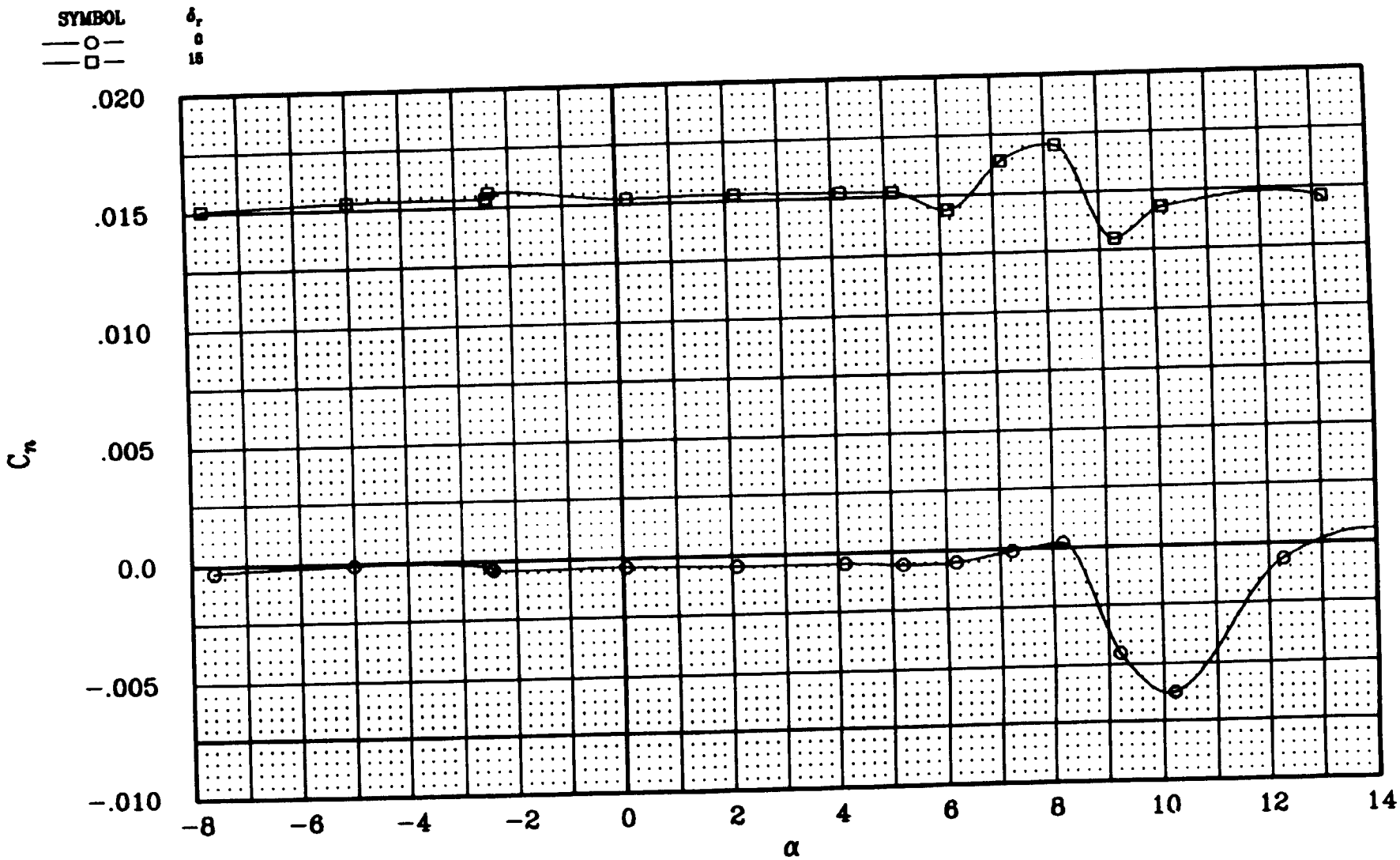

Figure 38. Rudder Effectiveness on the JW-1.

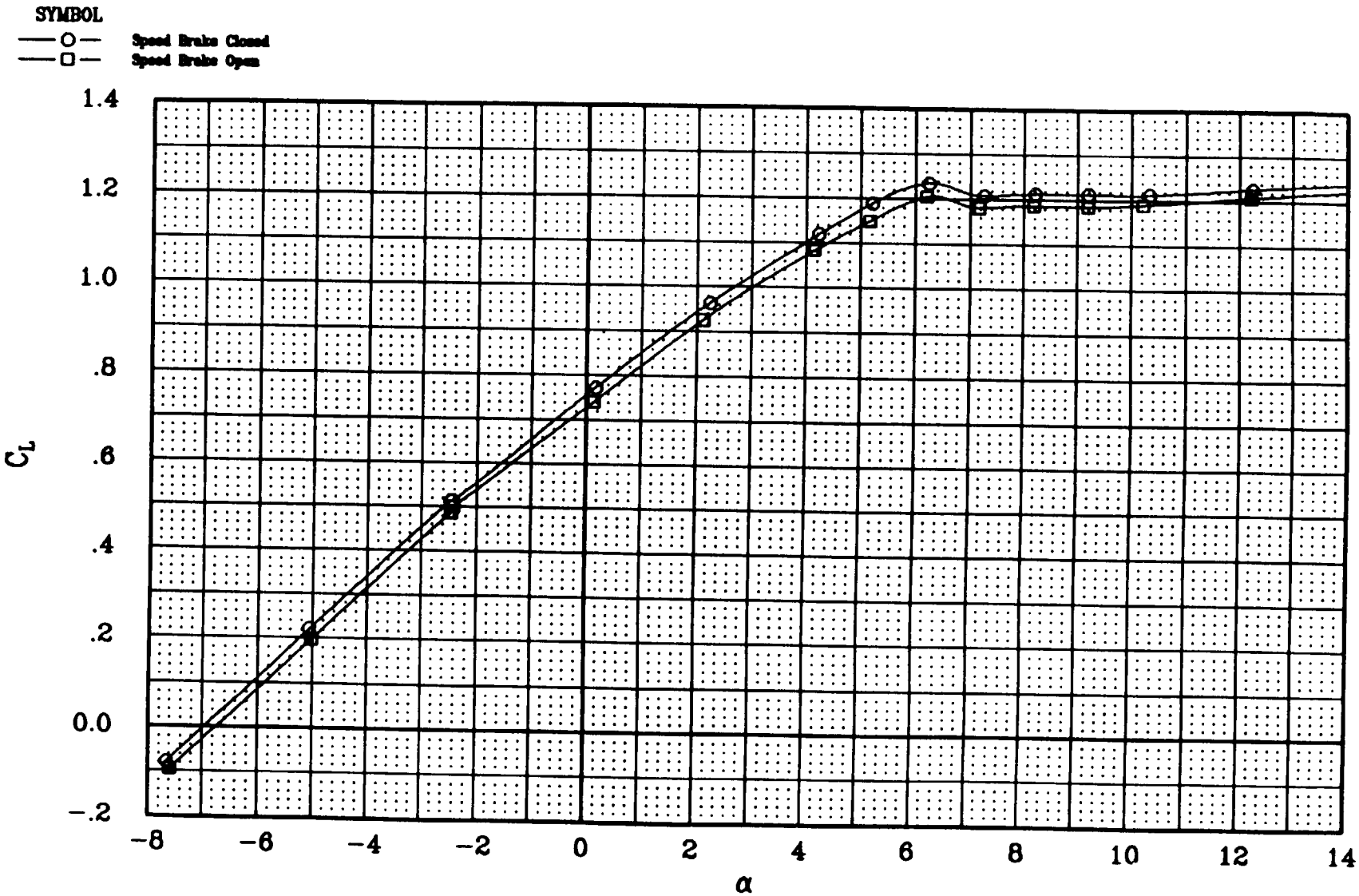

Figure 39. Effect of Speedbrake on the JW-1: C_L vs. α.

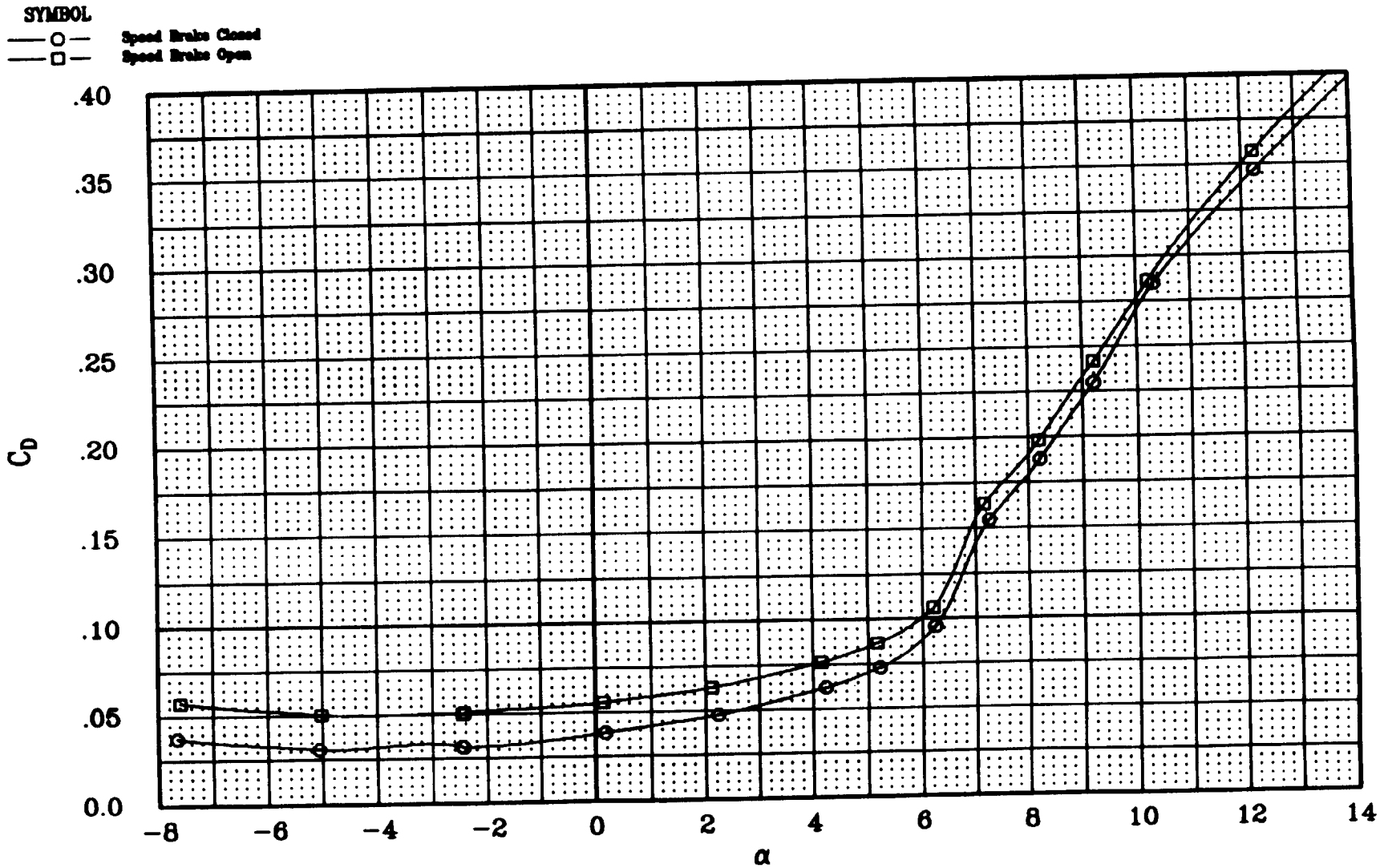

Figure 40. Effect of Speedbrake on the JW−1: C_D vs. α.

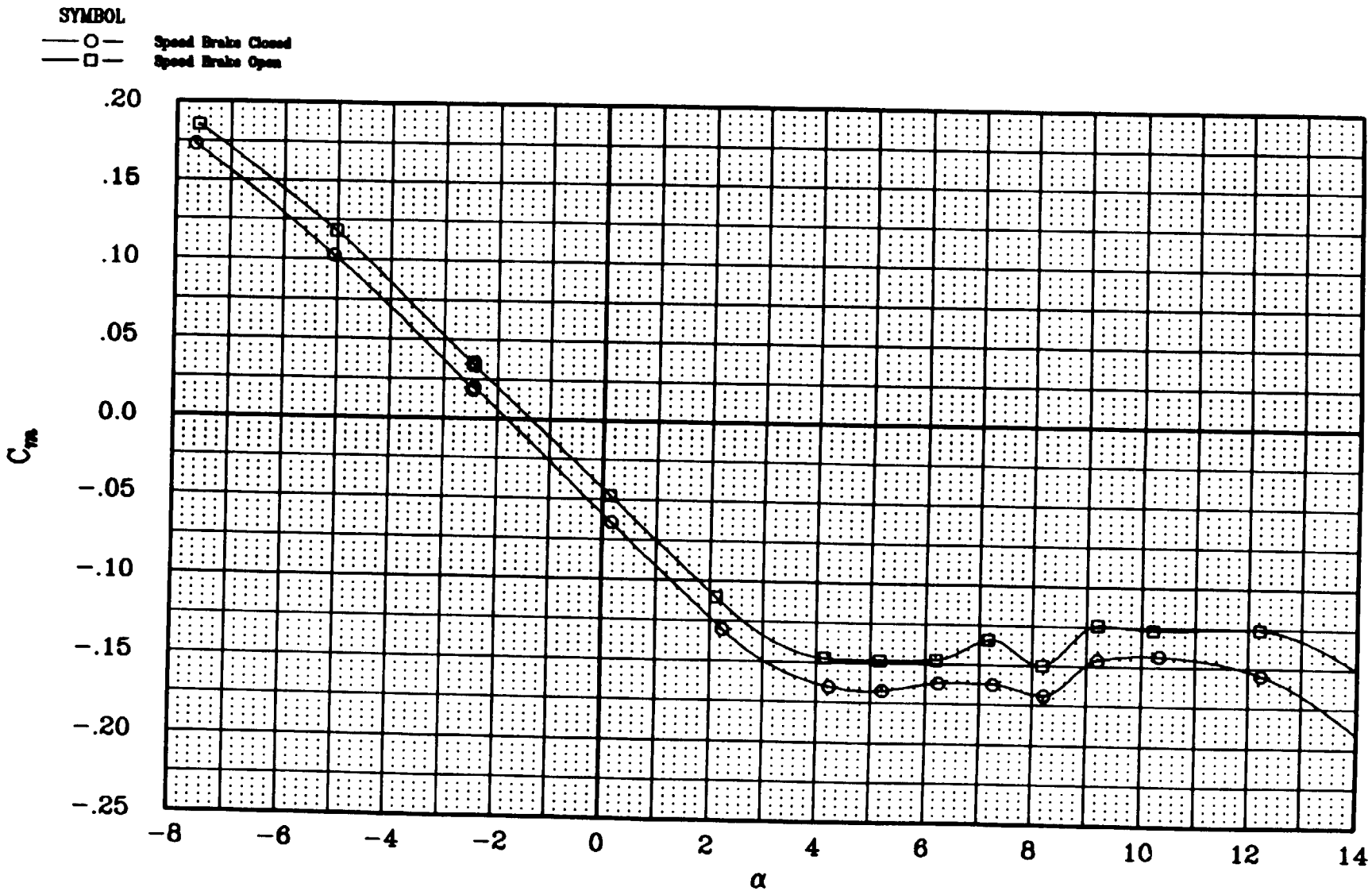

Figure 41. Effect of Speedbrake on the JW−1: C_m vs. α.

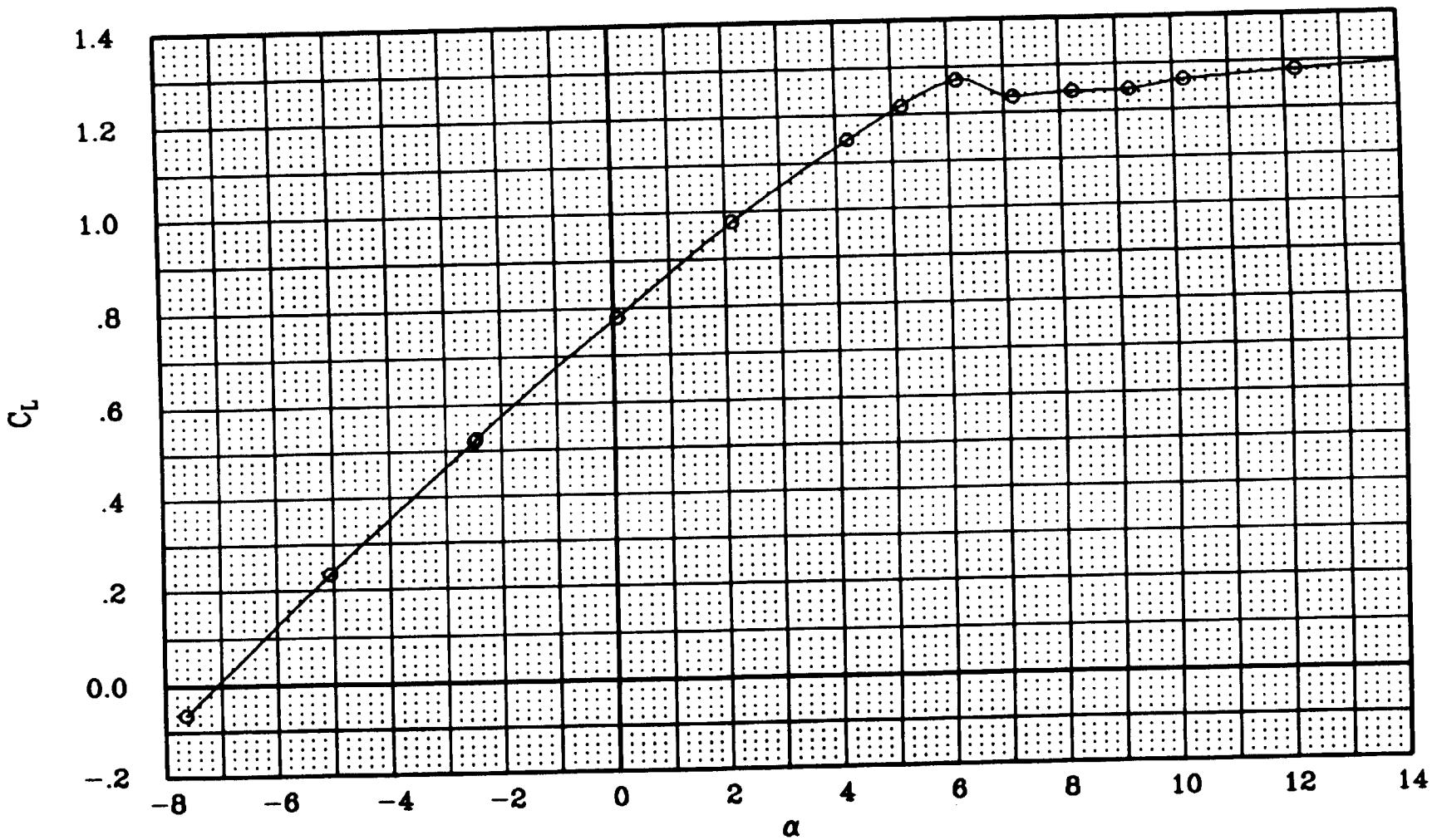

Figure 42. Longitudinal Characteristics of the JW−2 Configuration: C_L vs. α.

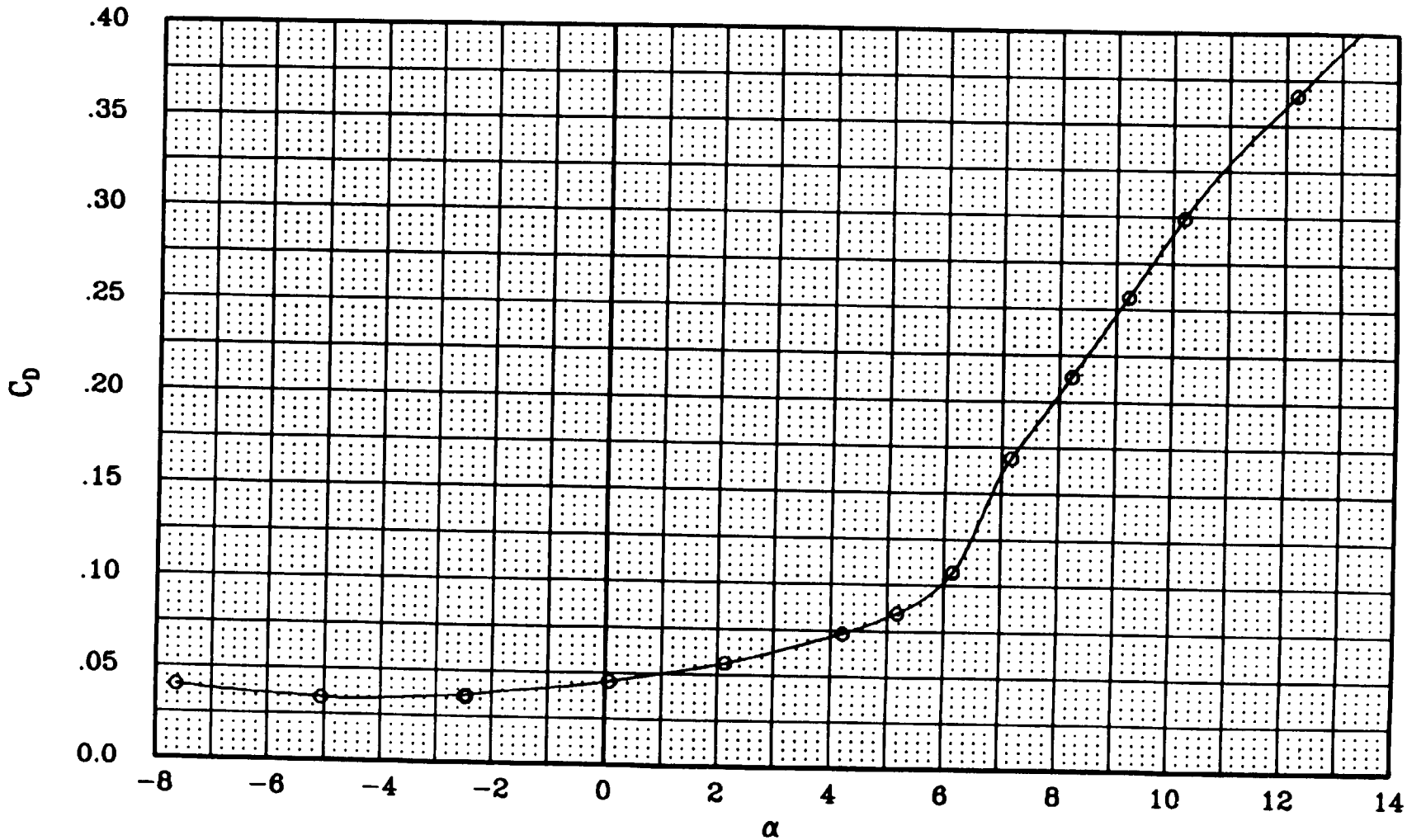

Figure 43. Longitudinal Characteristics of the JW−2 Configuration: C_D vs. α.

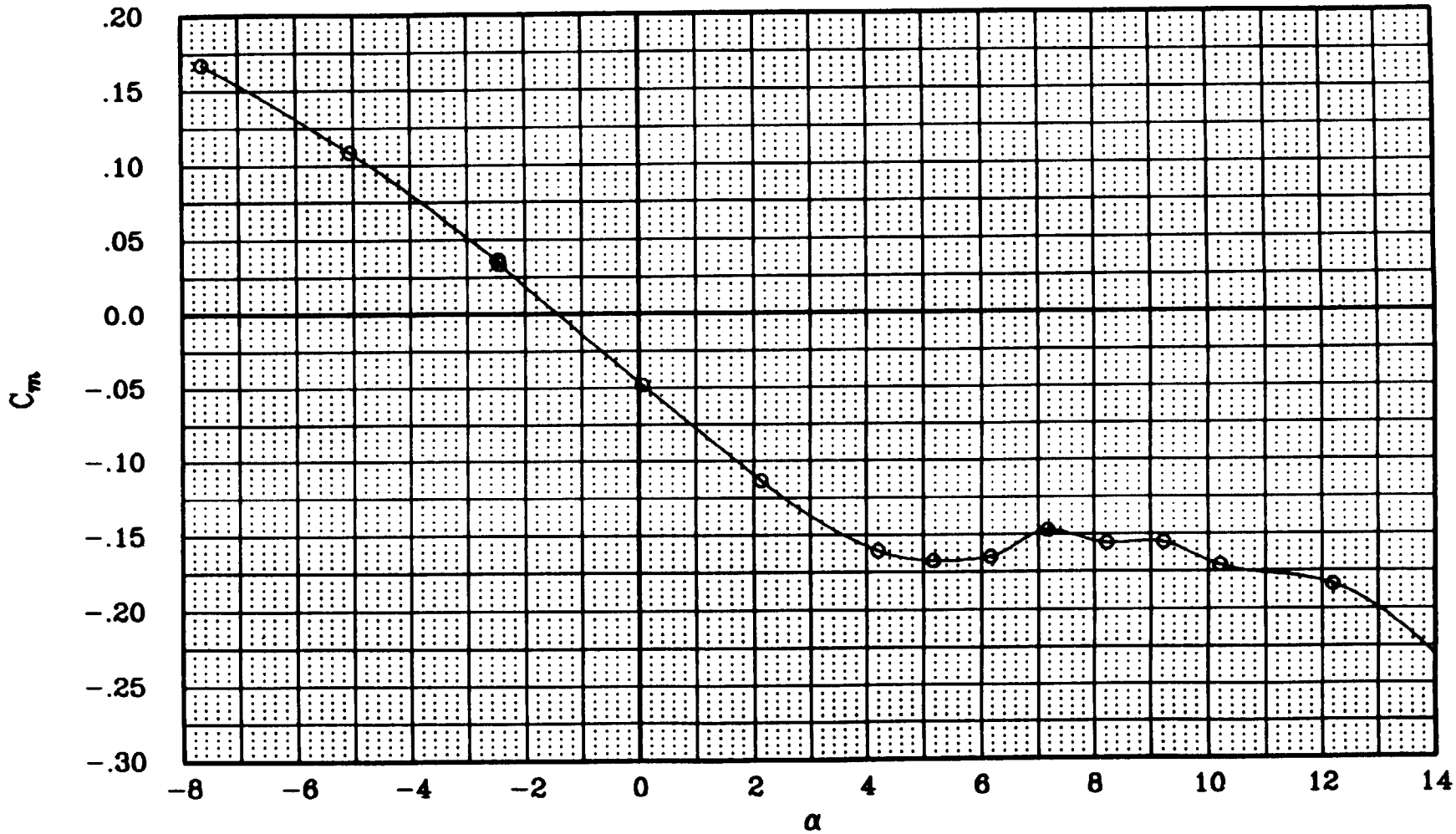

Figure 44. Longitudinal Characteristics of the JW−2 Configuration: C_m vs. α.

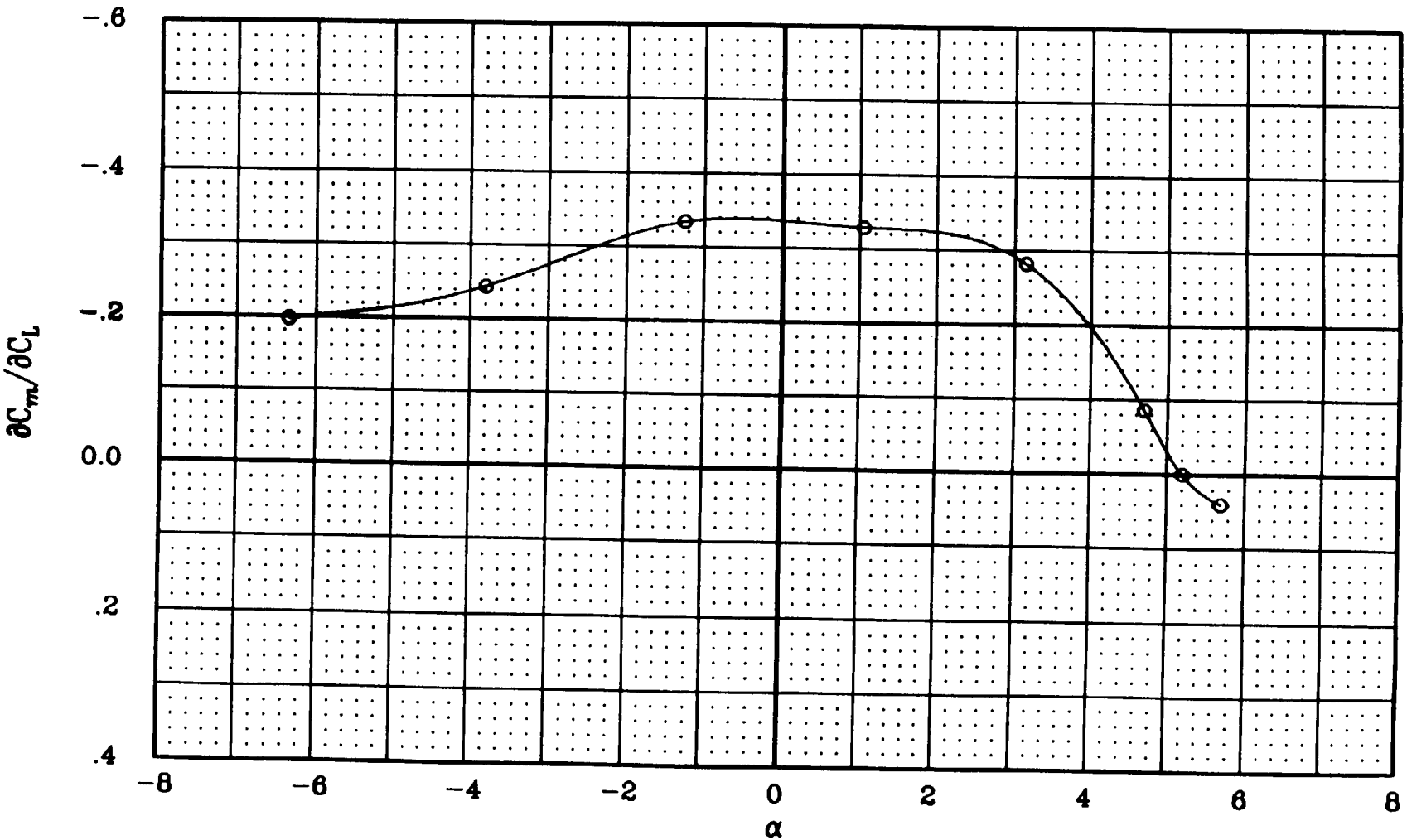

Figure 45. Longitudinal Stability, $\partial C_m/\partial C_L$, of the JW−2 Configuration.

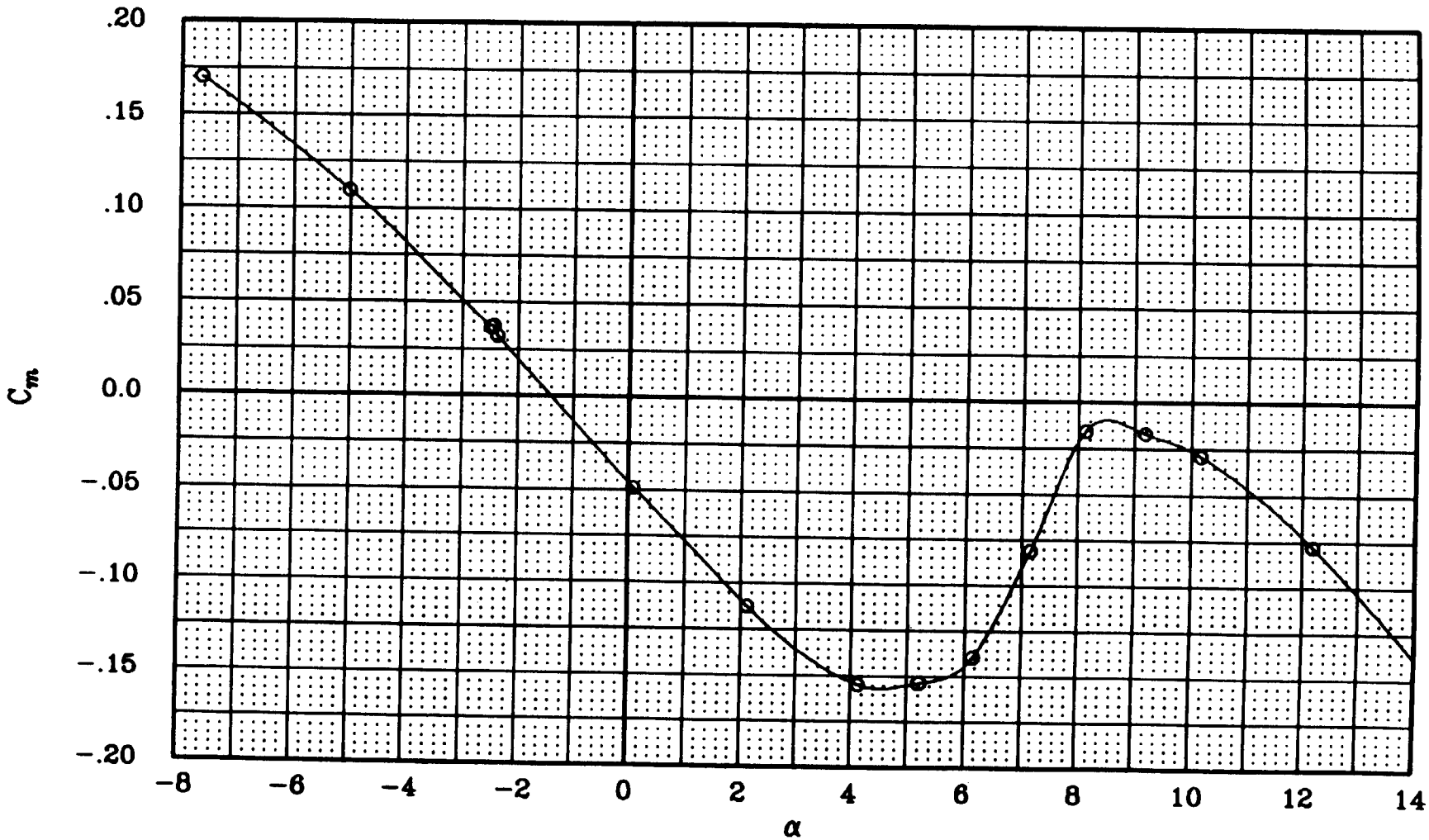

Figure 46. Longitudinal Characteristics of the JW-2 Configuration: C_m vs. α. Vortilon Removed.

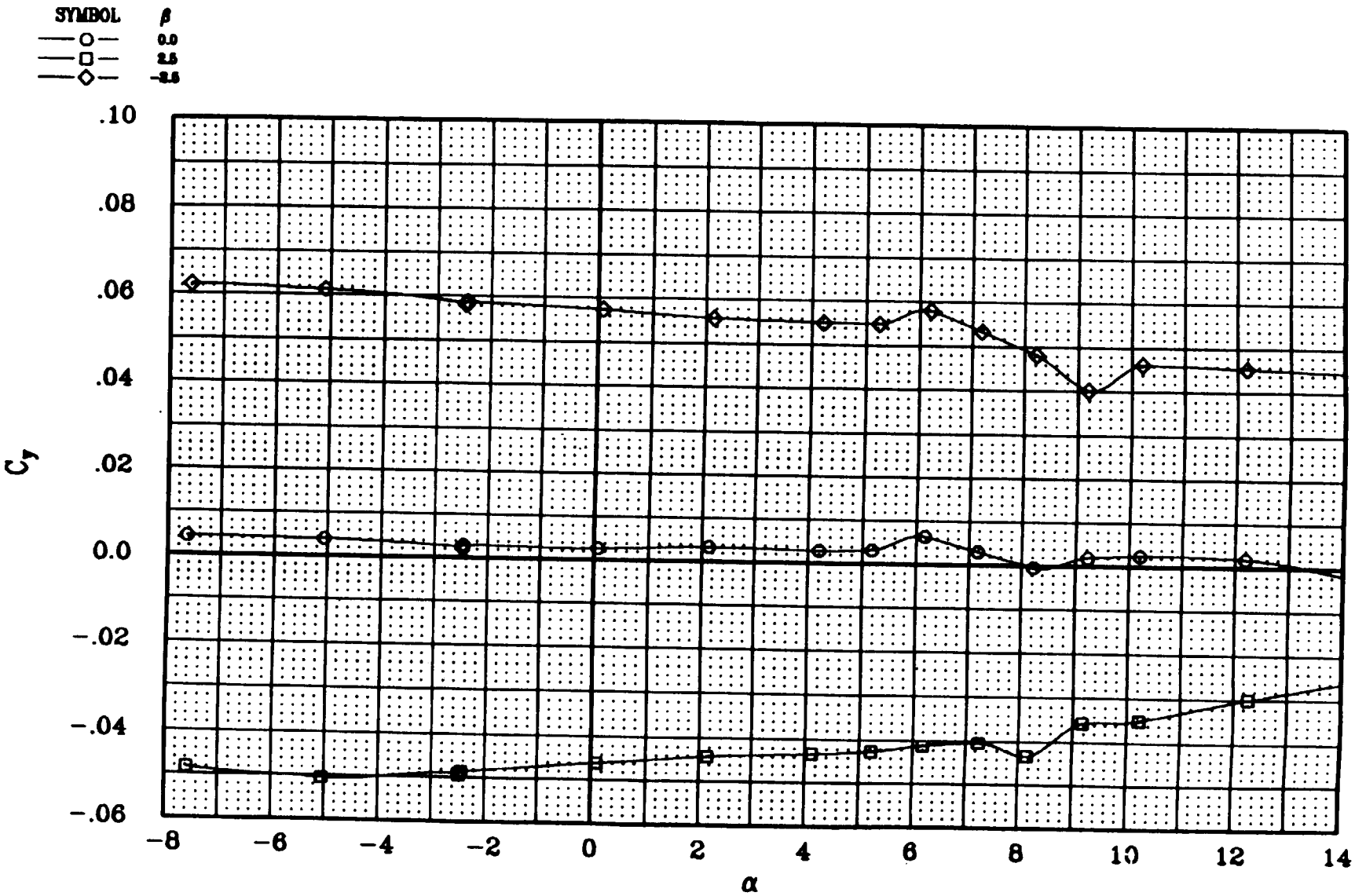

Figure 47. Lateral-Directional Characteristics of the JW-2: C_y vs. α.

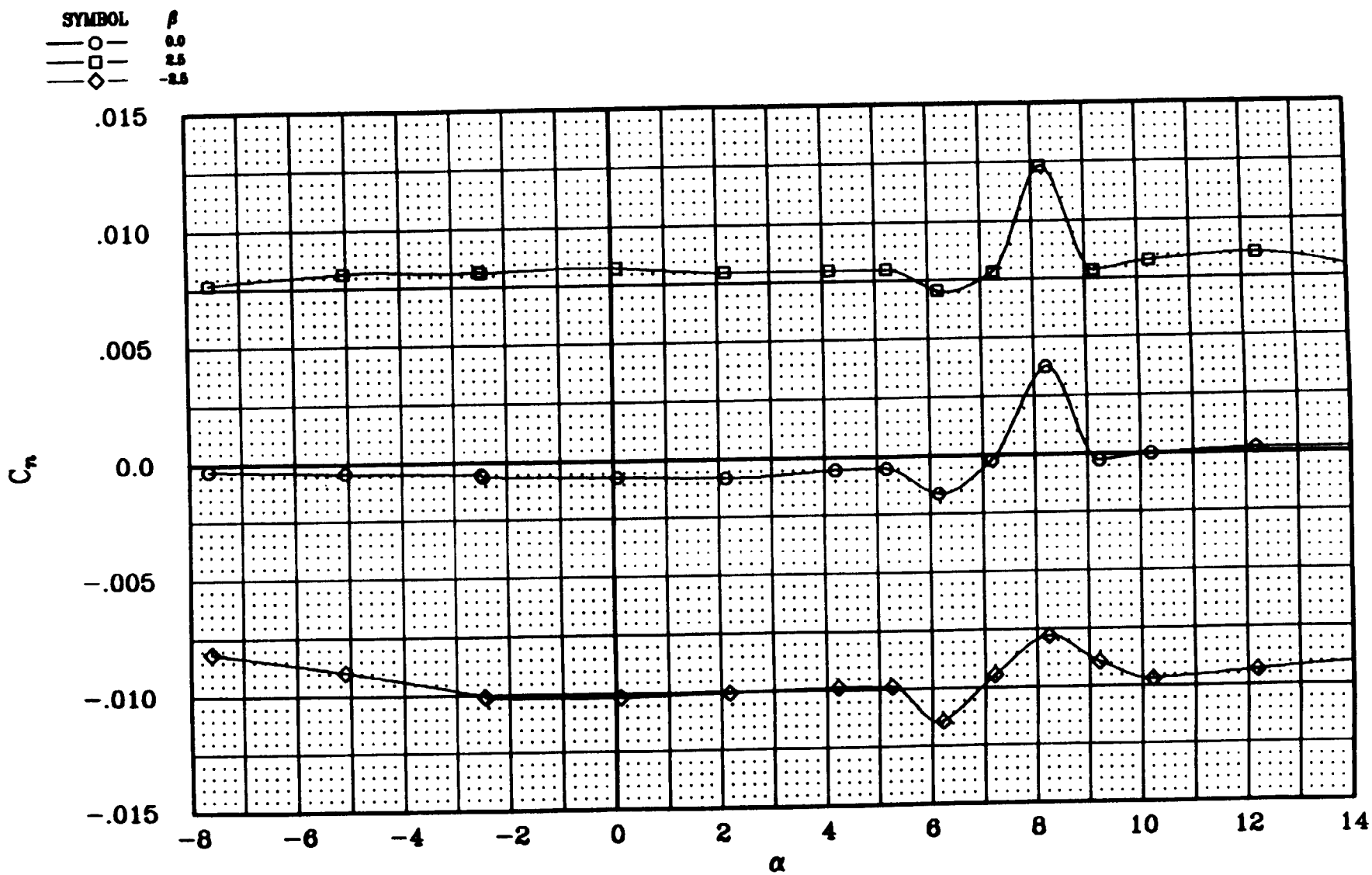

Figure 48. Lateral-Directional Characteristics of the JW-2: C_n vs. α.

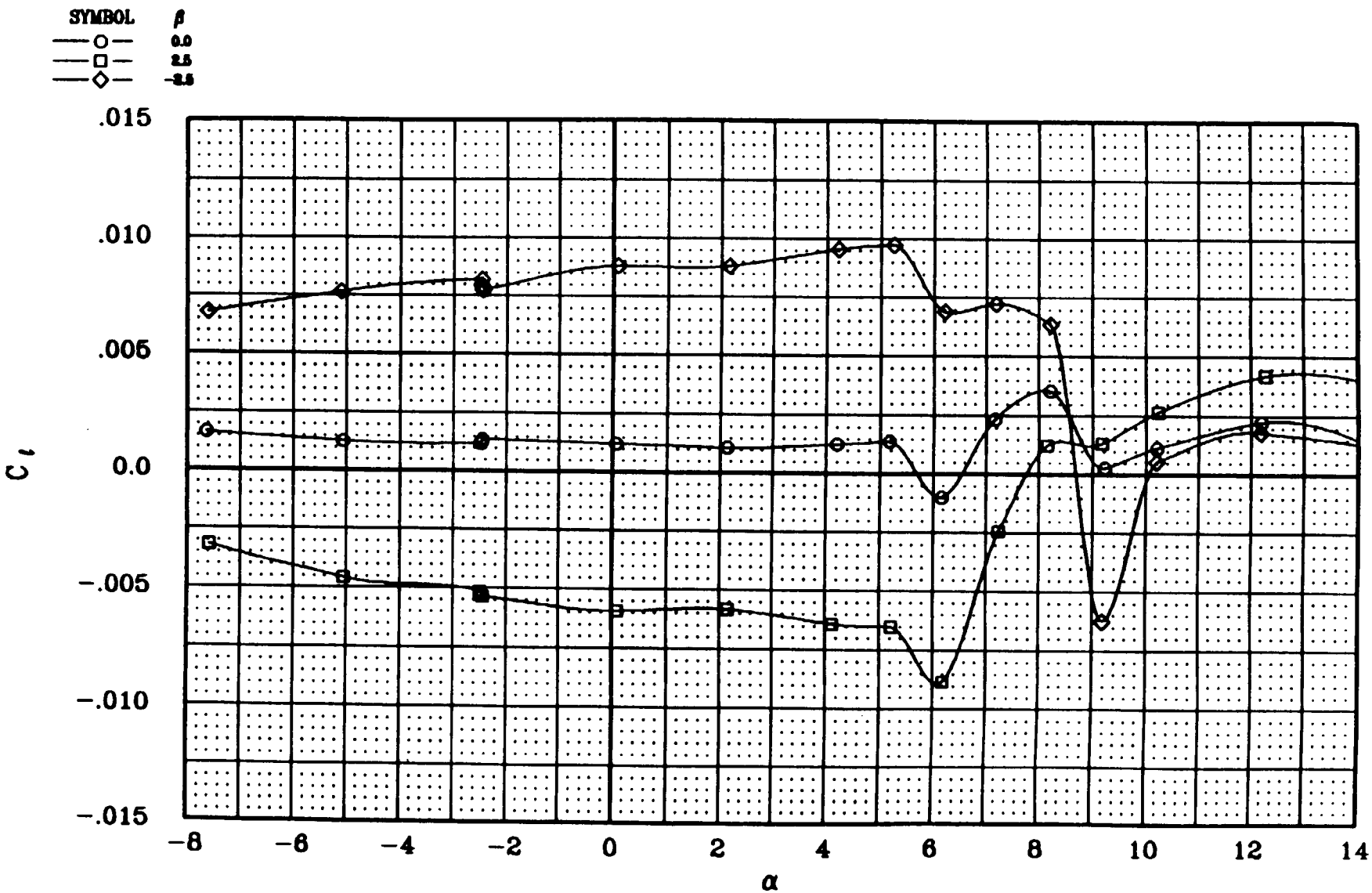

Figure 49. Lateral-Directional Characteristics of the JW-2: C_l vs. α.

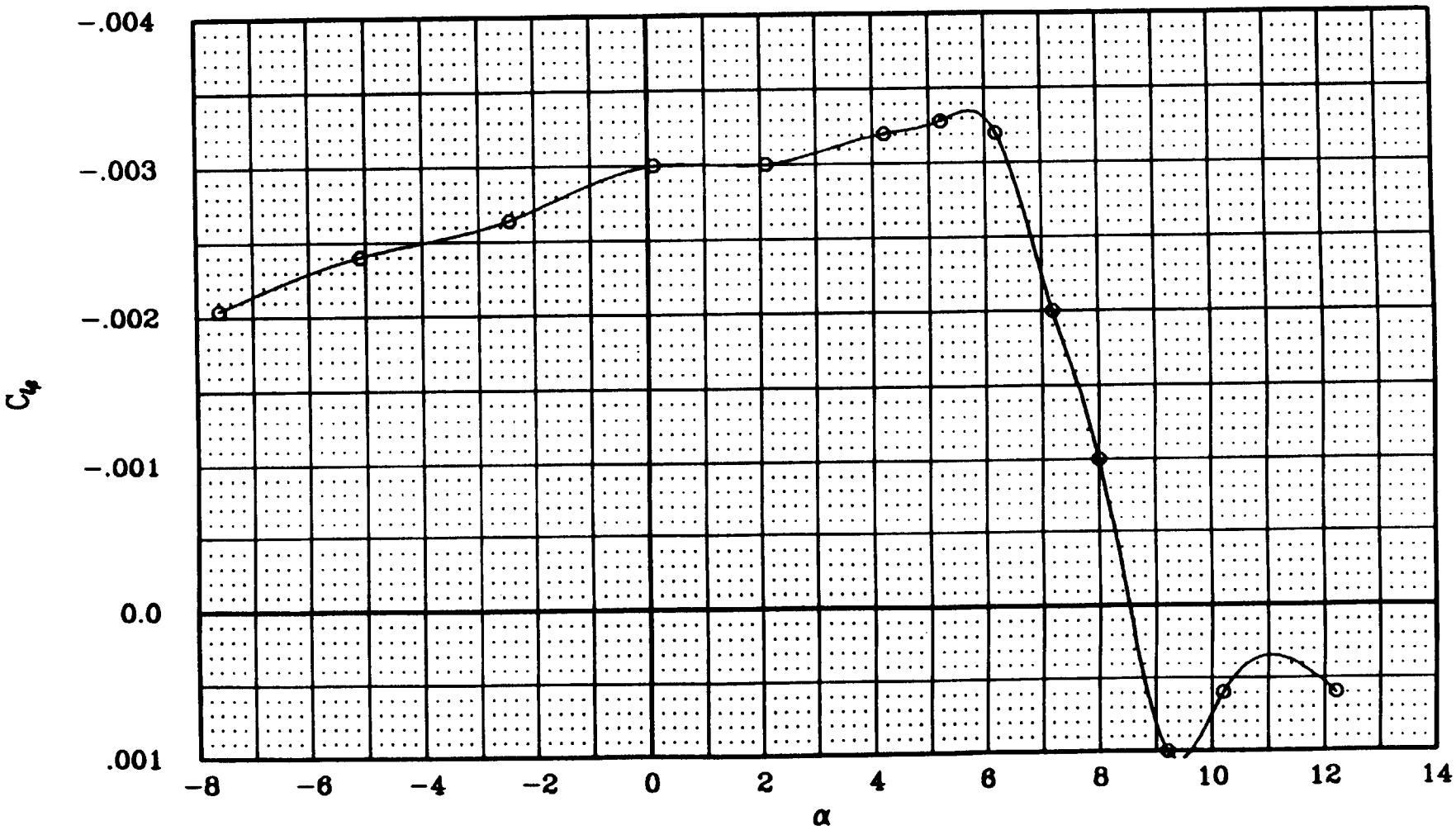

Figure 50. Lateral-Directional Stability of the JW-2 Configuration: C_{l_β} vs. α.

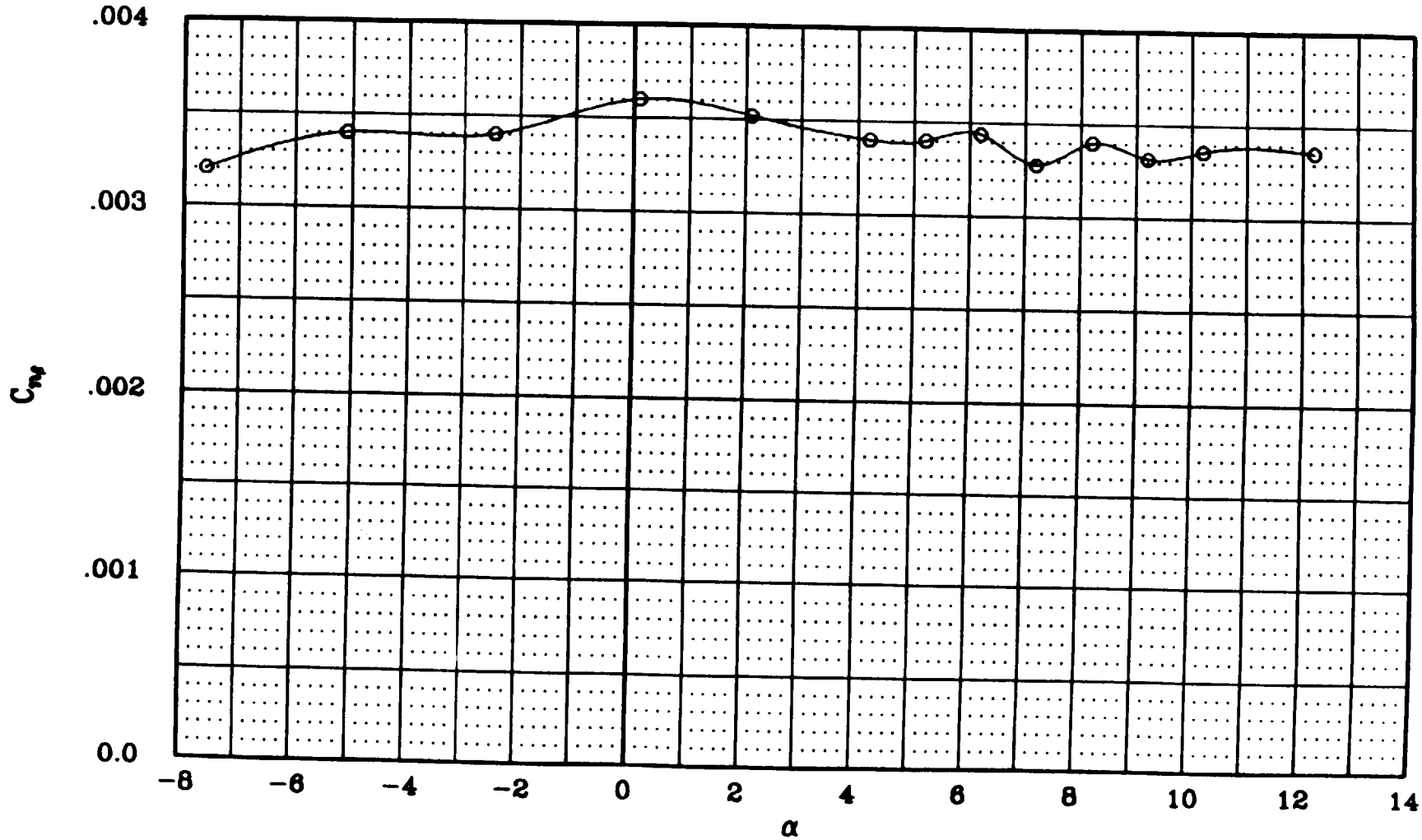

Figure 51. Lateral-Directional Stability of the JW-2 Configuration: C_{n_β} vs. α.

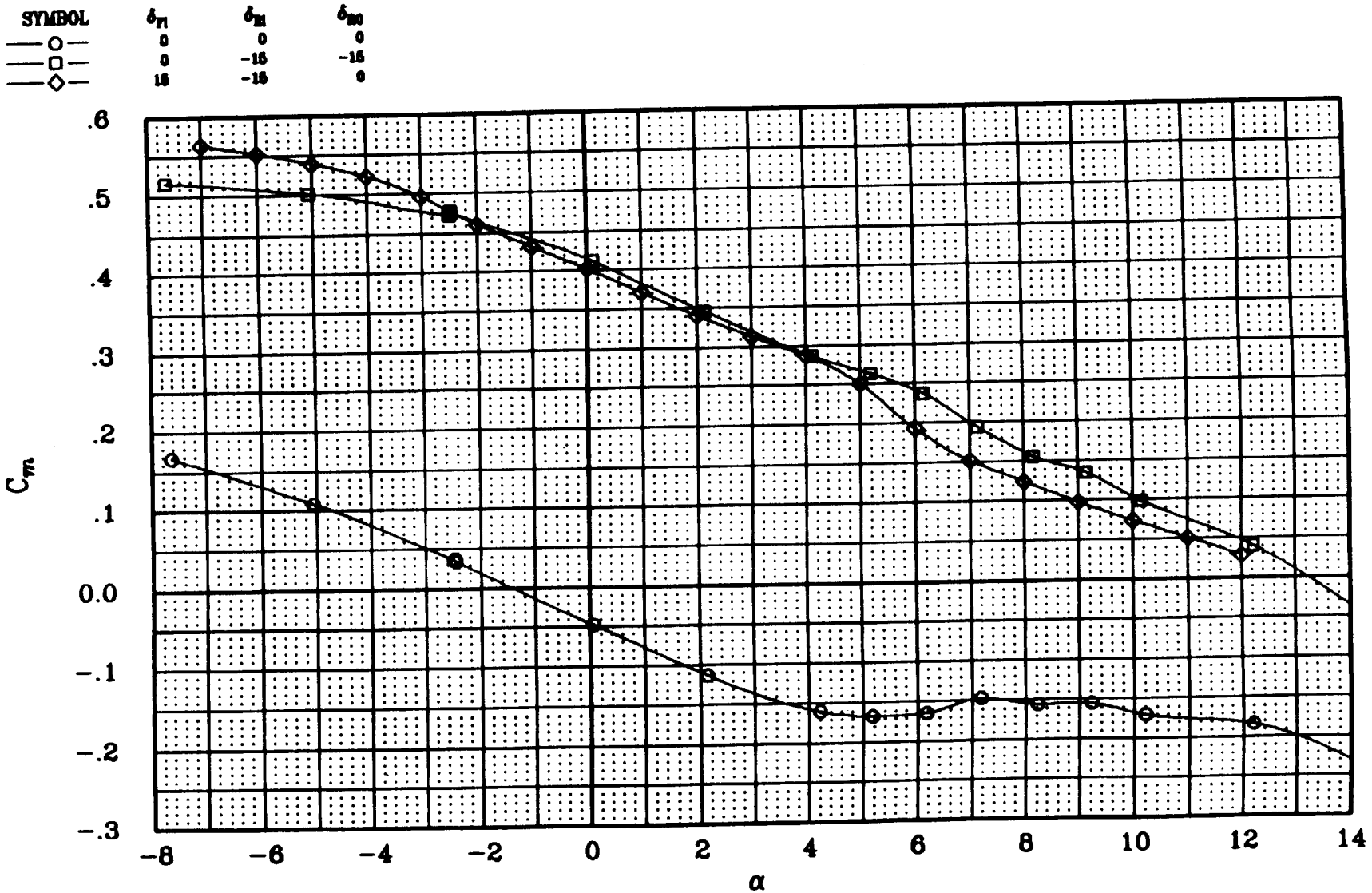

Figure 52. Effectiveness of Various Elevator Configurations on the JW-2: C_m vs. α.

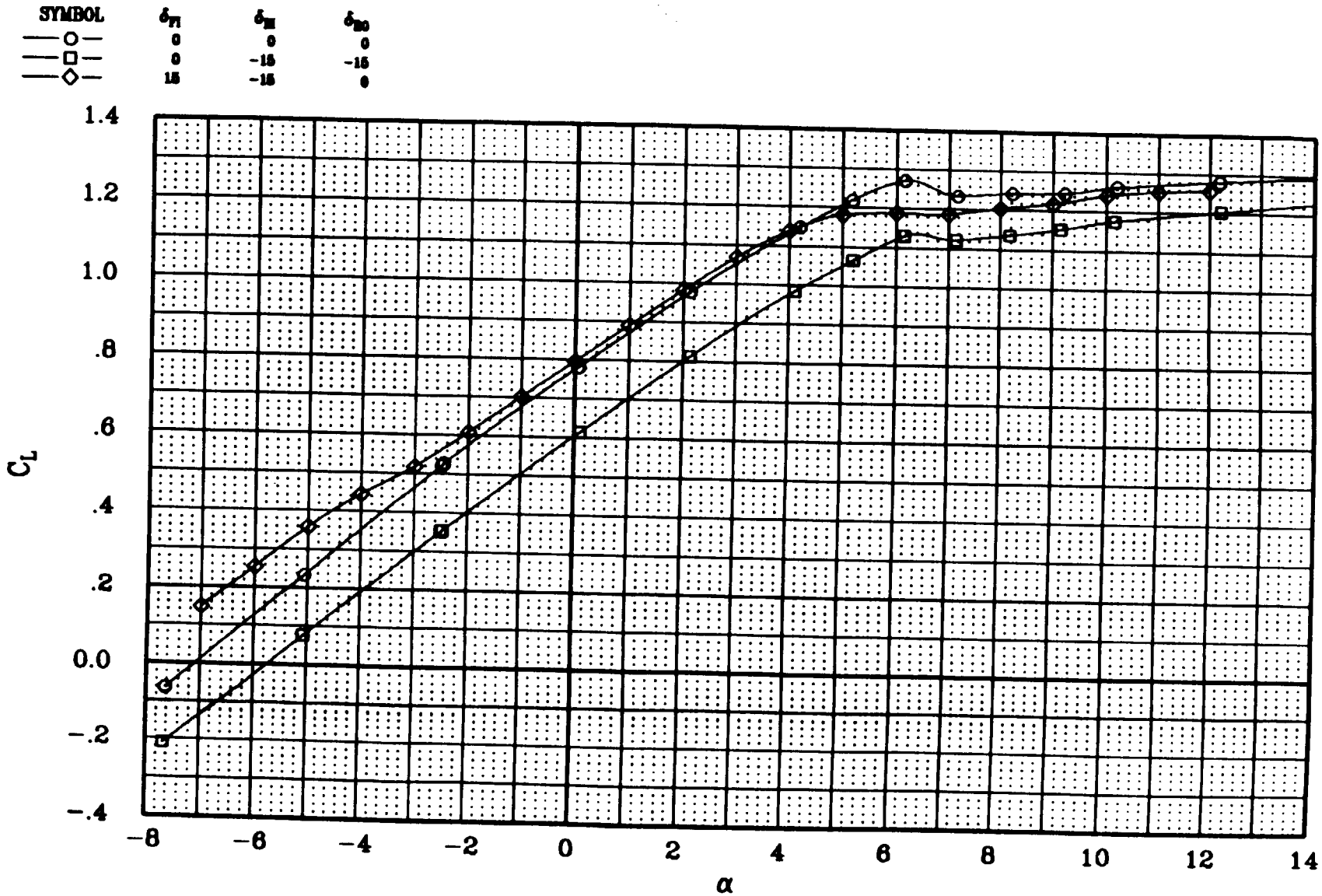

Figure 53. Effect of Various Elevator Configurations on the JW-2: C_L vs. α.

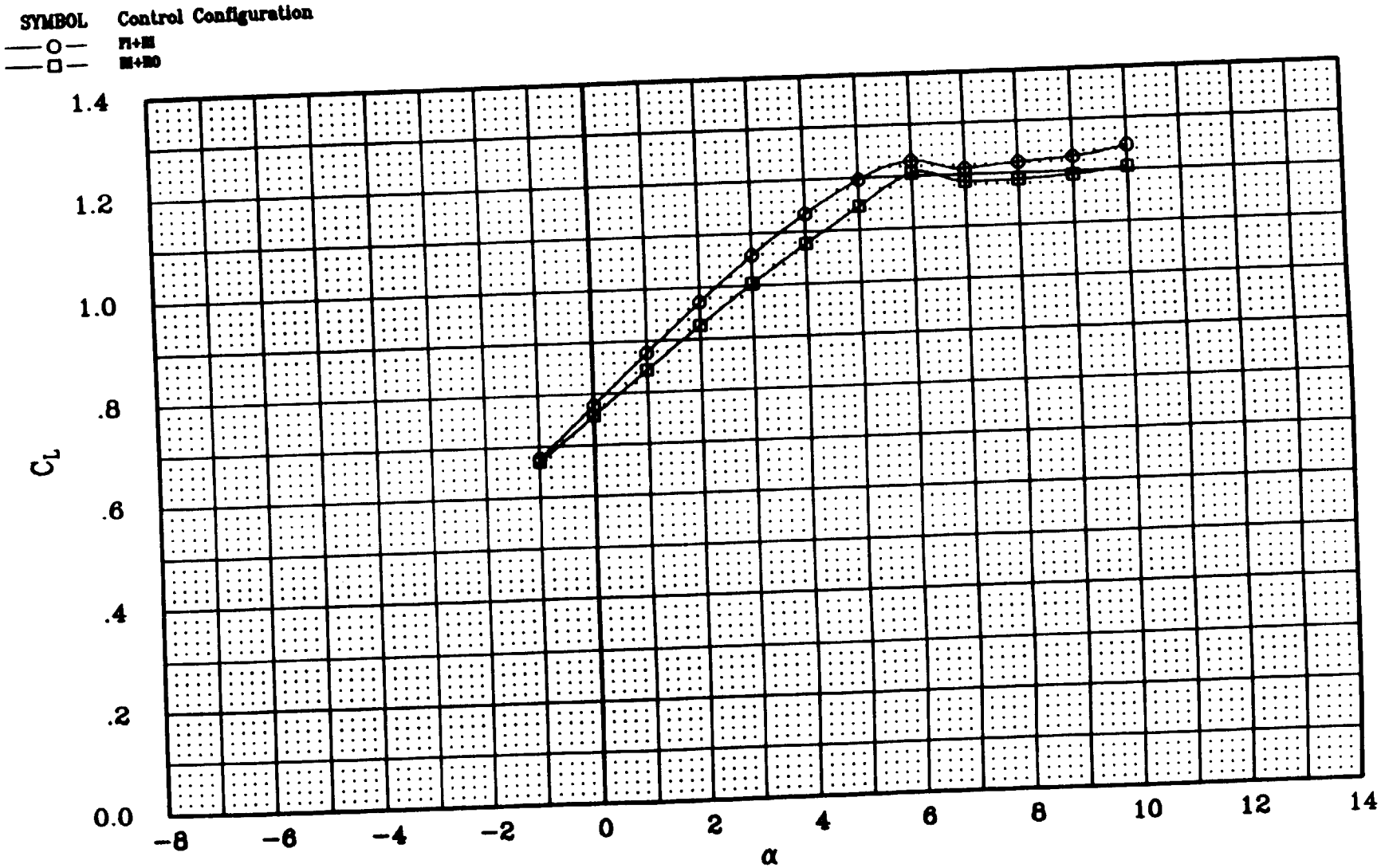

Figure 54. Trimmed Lift Characteristics of the JW-2.

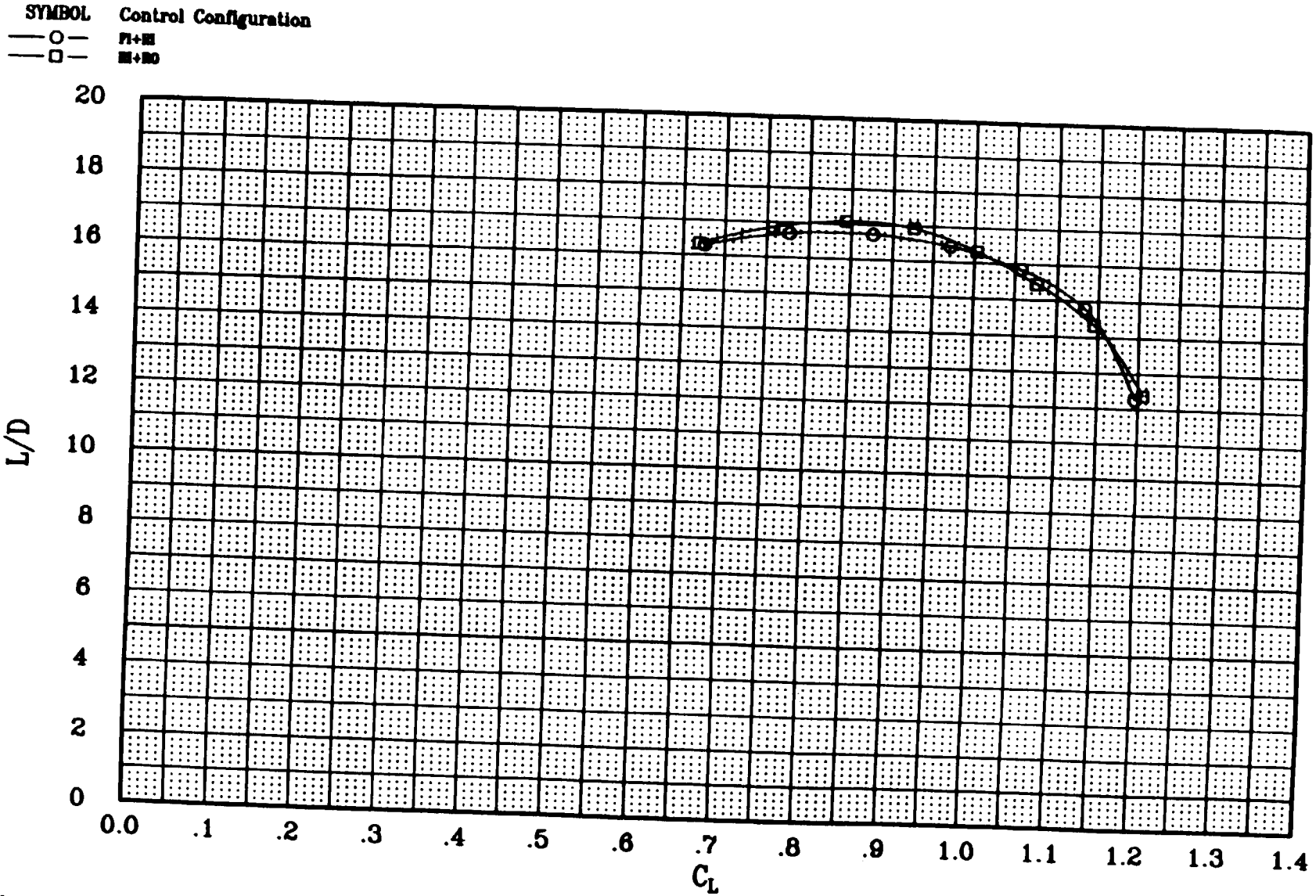

Figure 55. Trimmed Lift-to-Drag Ratio of the JW-2.

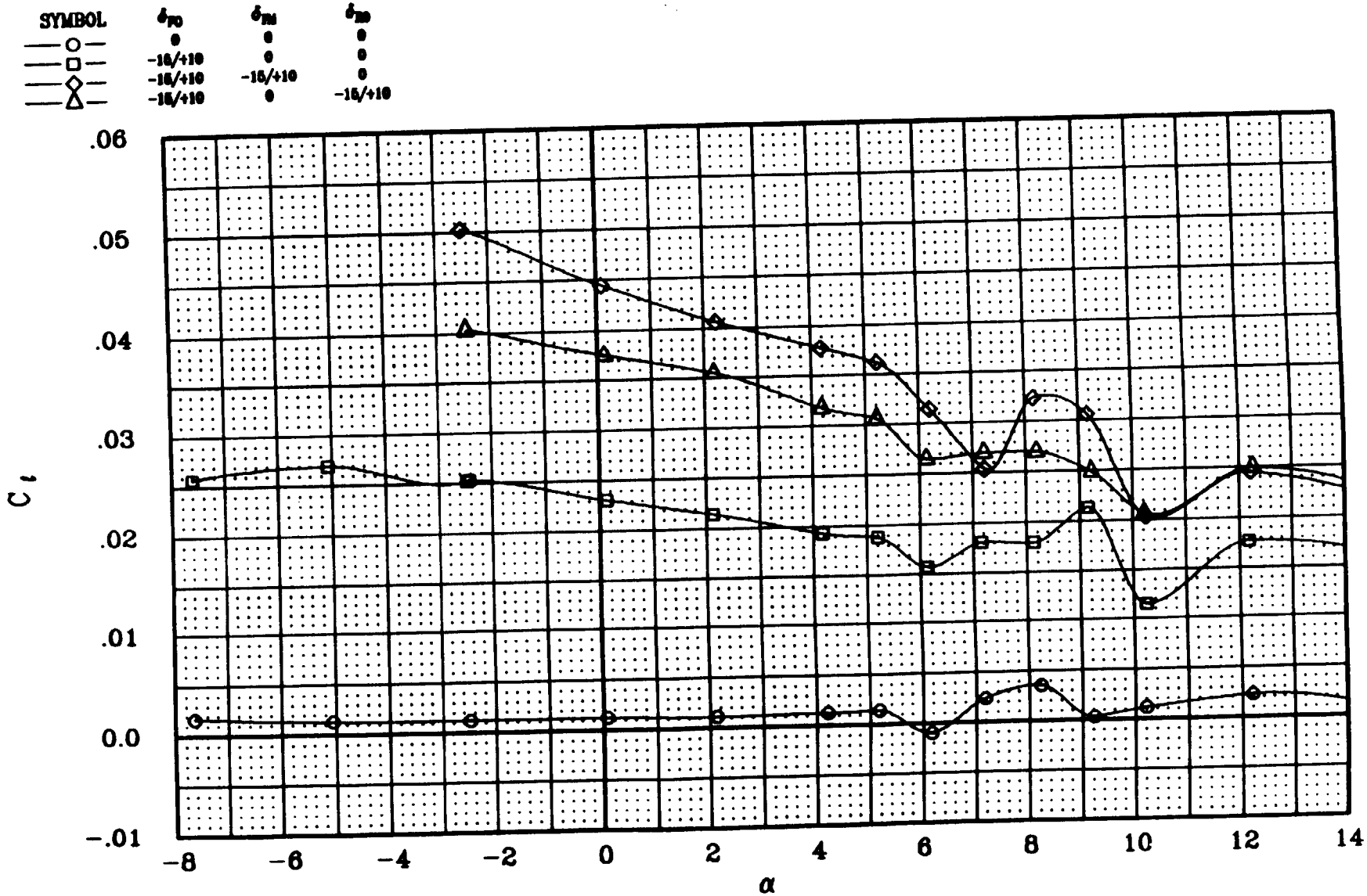

Figure 56. Effectiveness of Various Aileron Configurations on the JW-2: C_l vs. α.

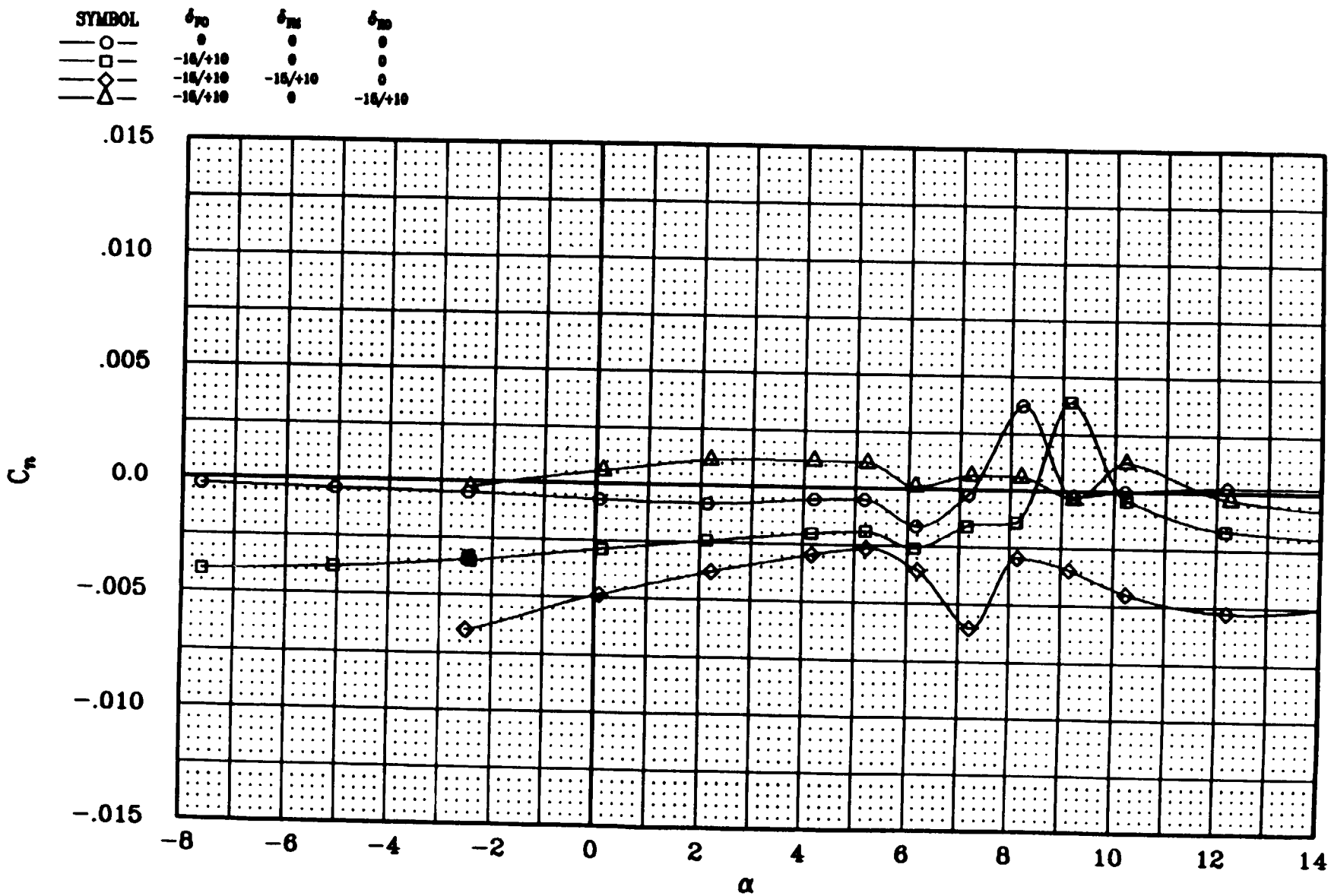

Figure 57. Yawing Moment induced by various Aileron Configurations on the JW-2.

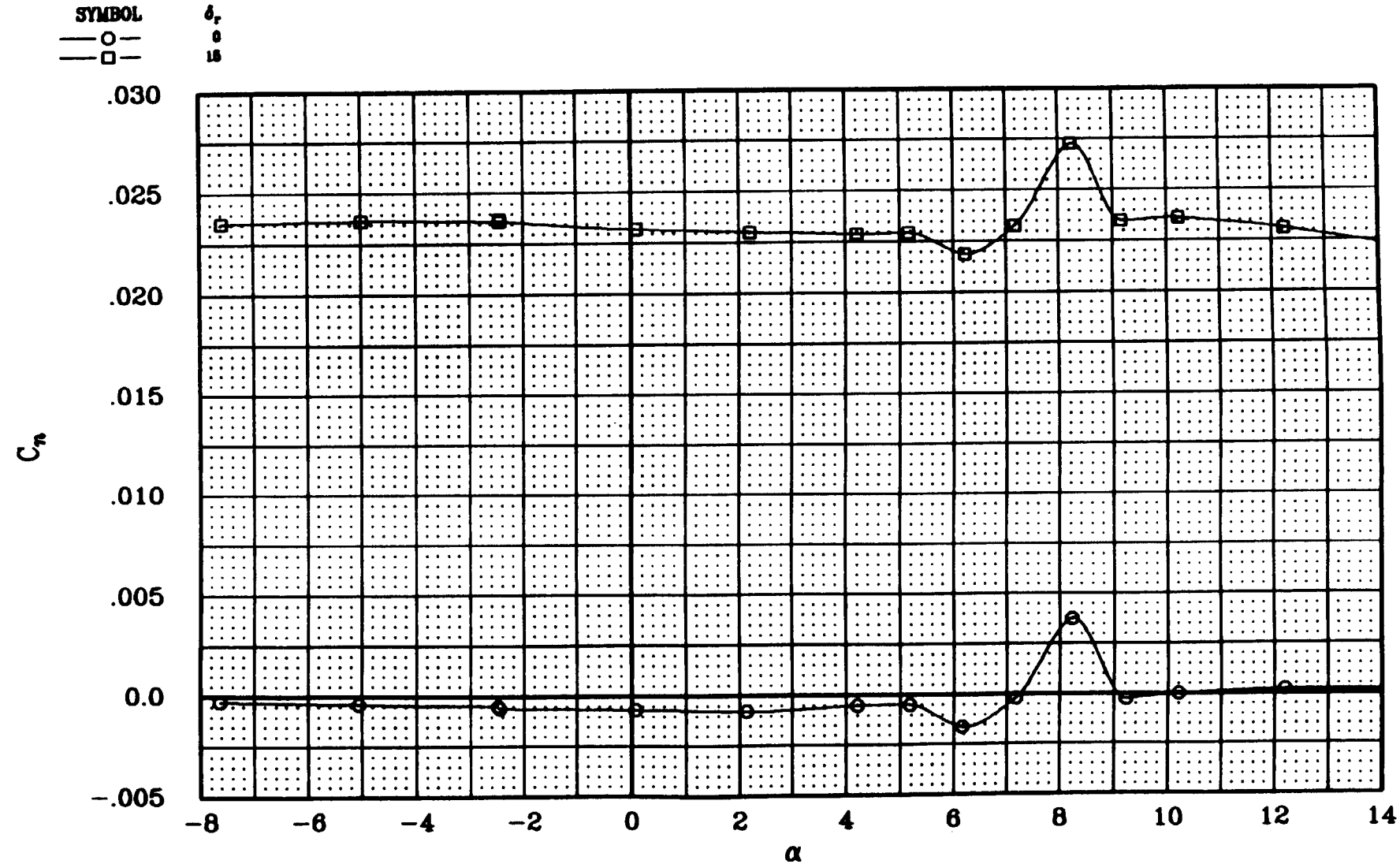

Figure 58. Rudder Effectiveness on the JW−2.

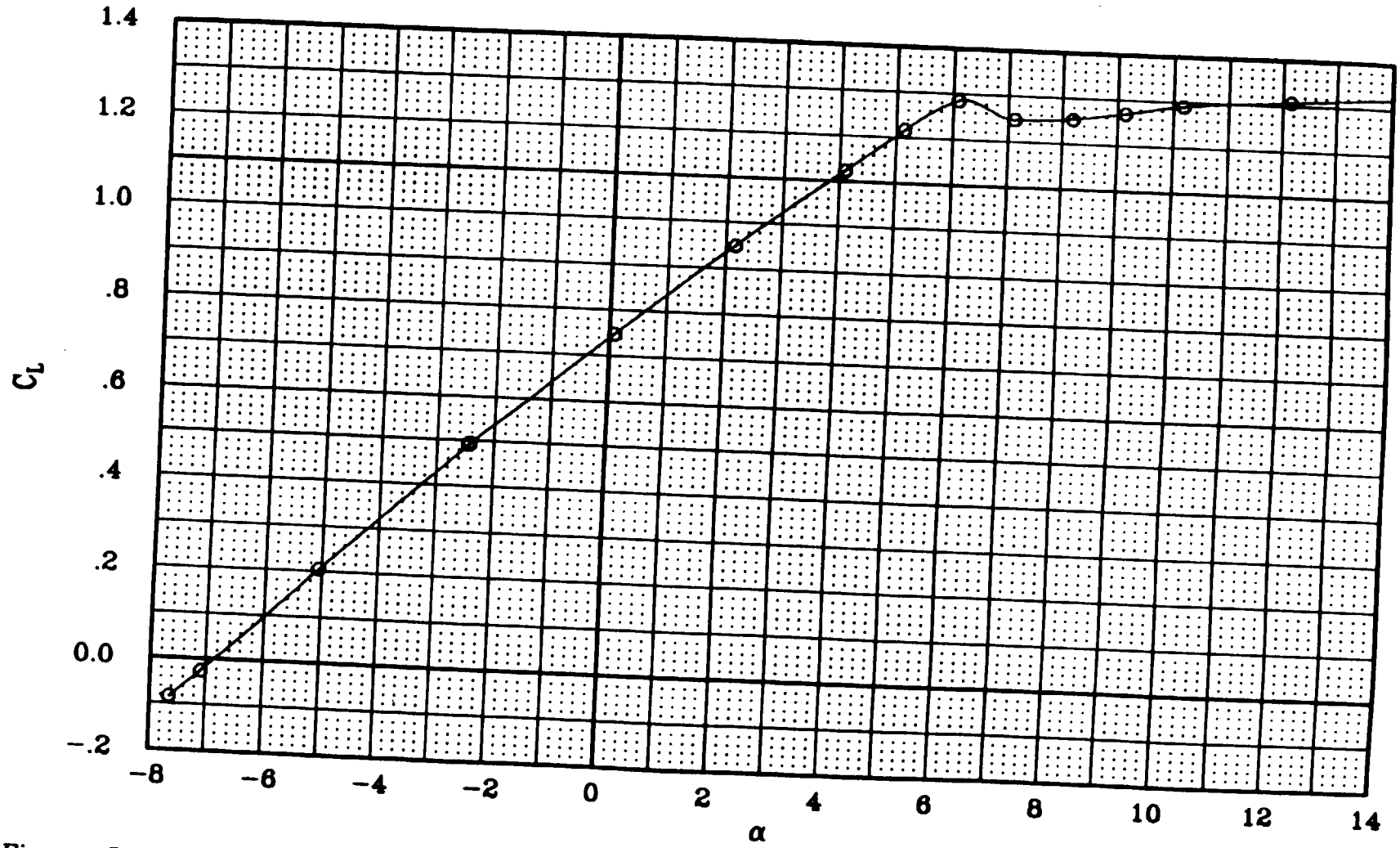

Figure 59. Longitudinal Characteristics of the JW-3 Configuration: C_L vs. α.

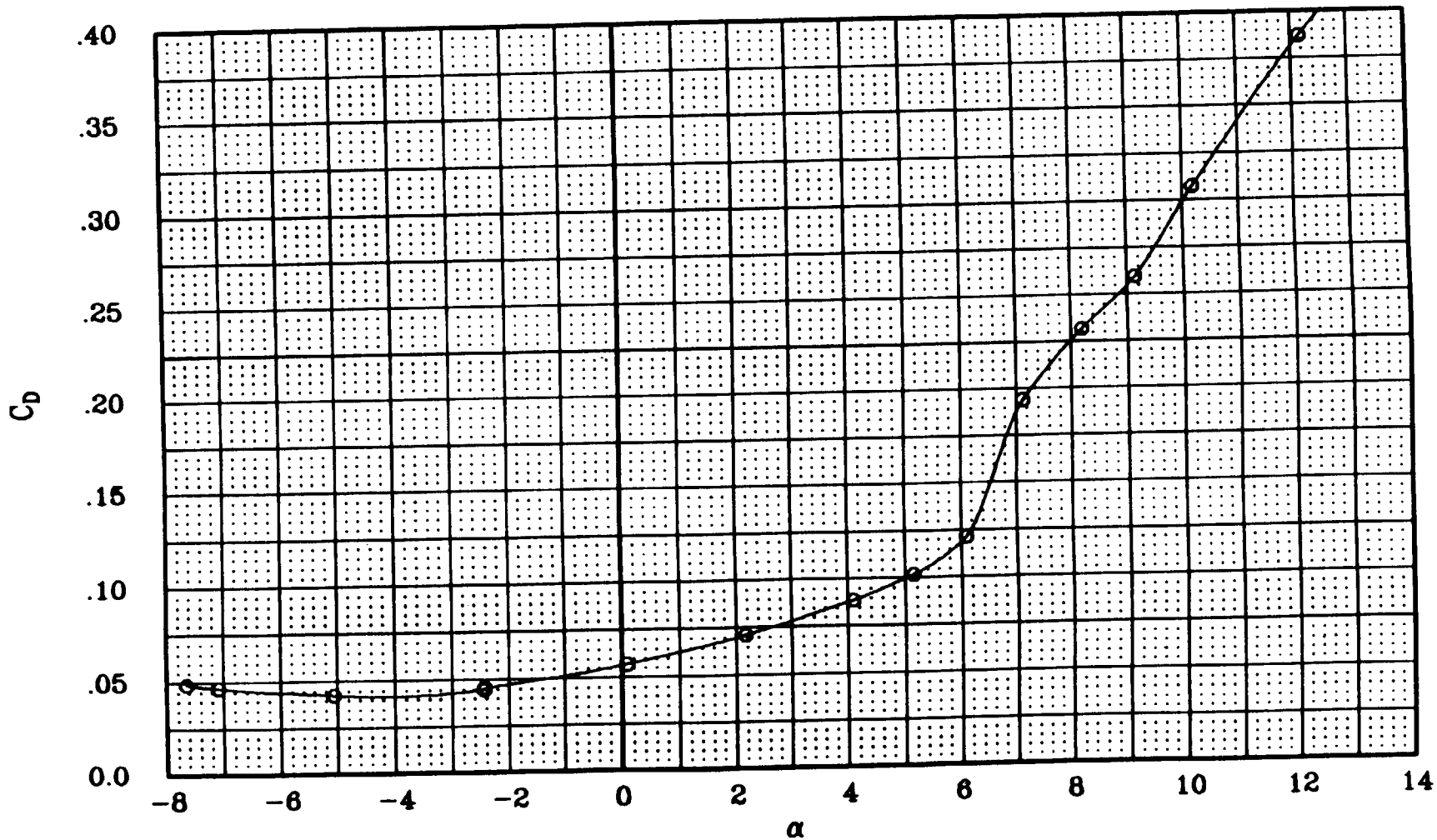

Figure 60. Longitudinal Characteristics of the JW-3 Configuration: C_D vs. α.

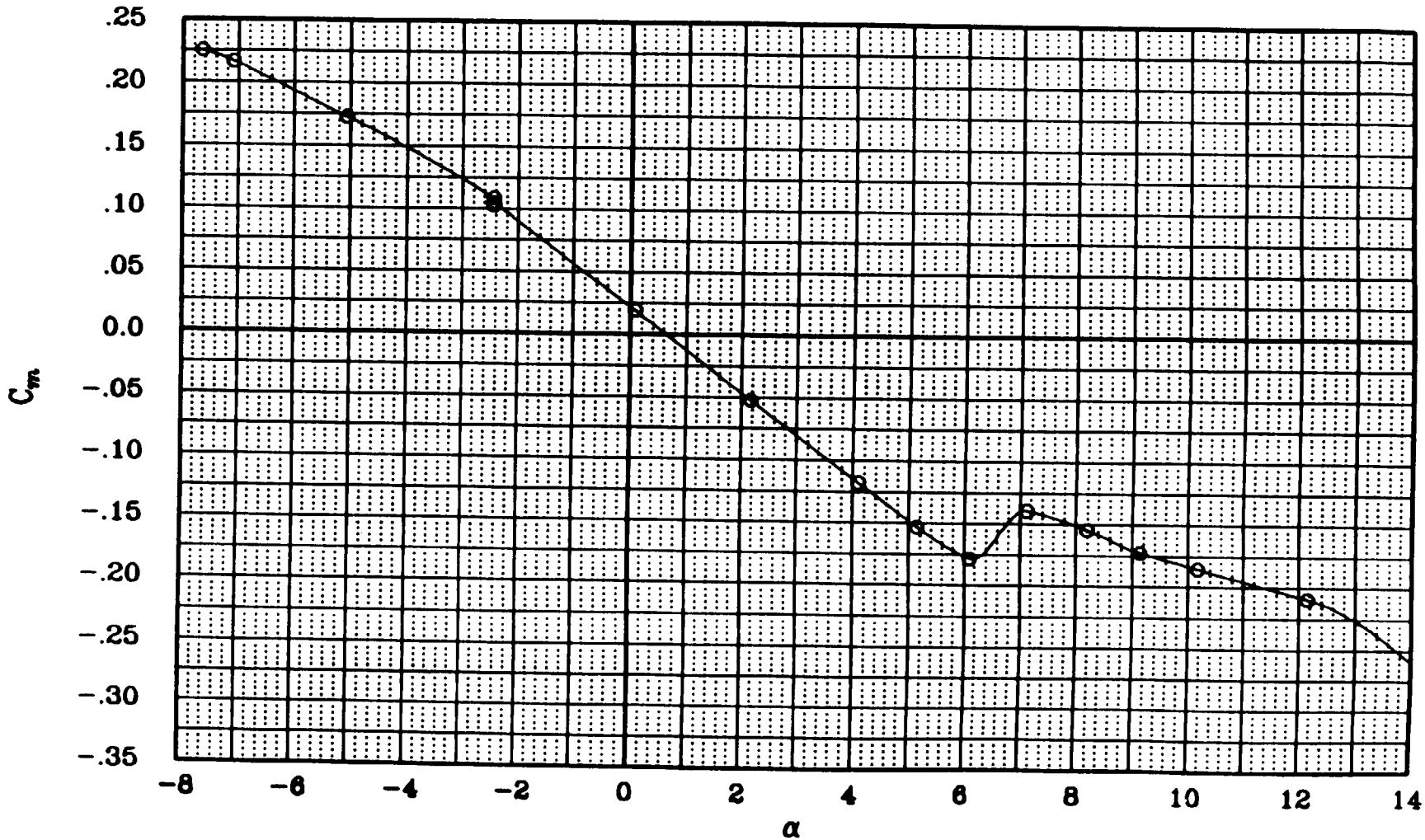

Figure 61. Longitudinal Characteristics of the JW−3 Configuration: C_m vs. α.

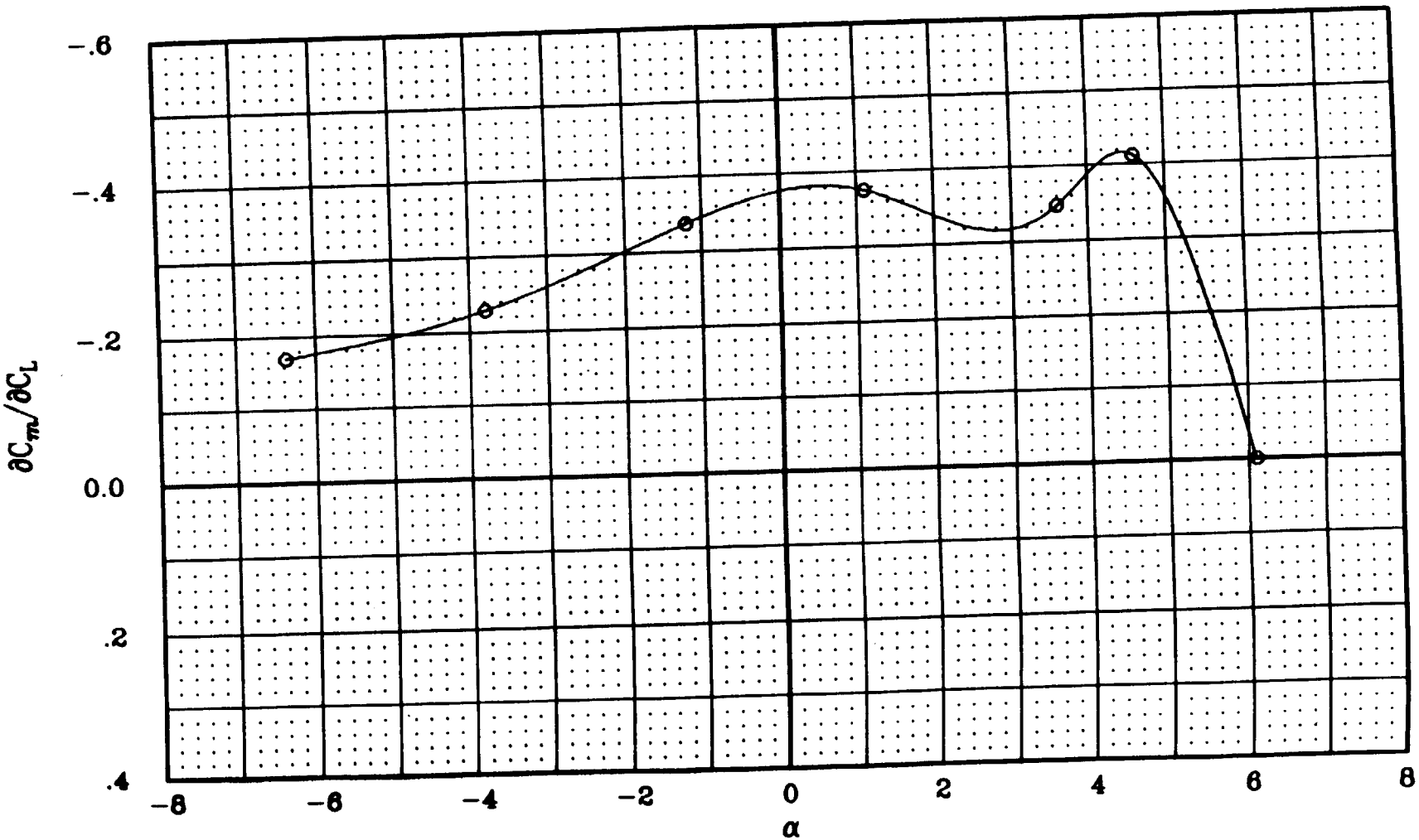

Figure 62. Longitudinal Stability, $\partial C_m/\partial C_L$, of the JW-3 Configuration.

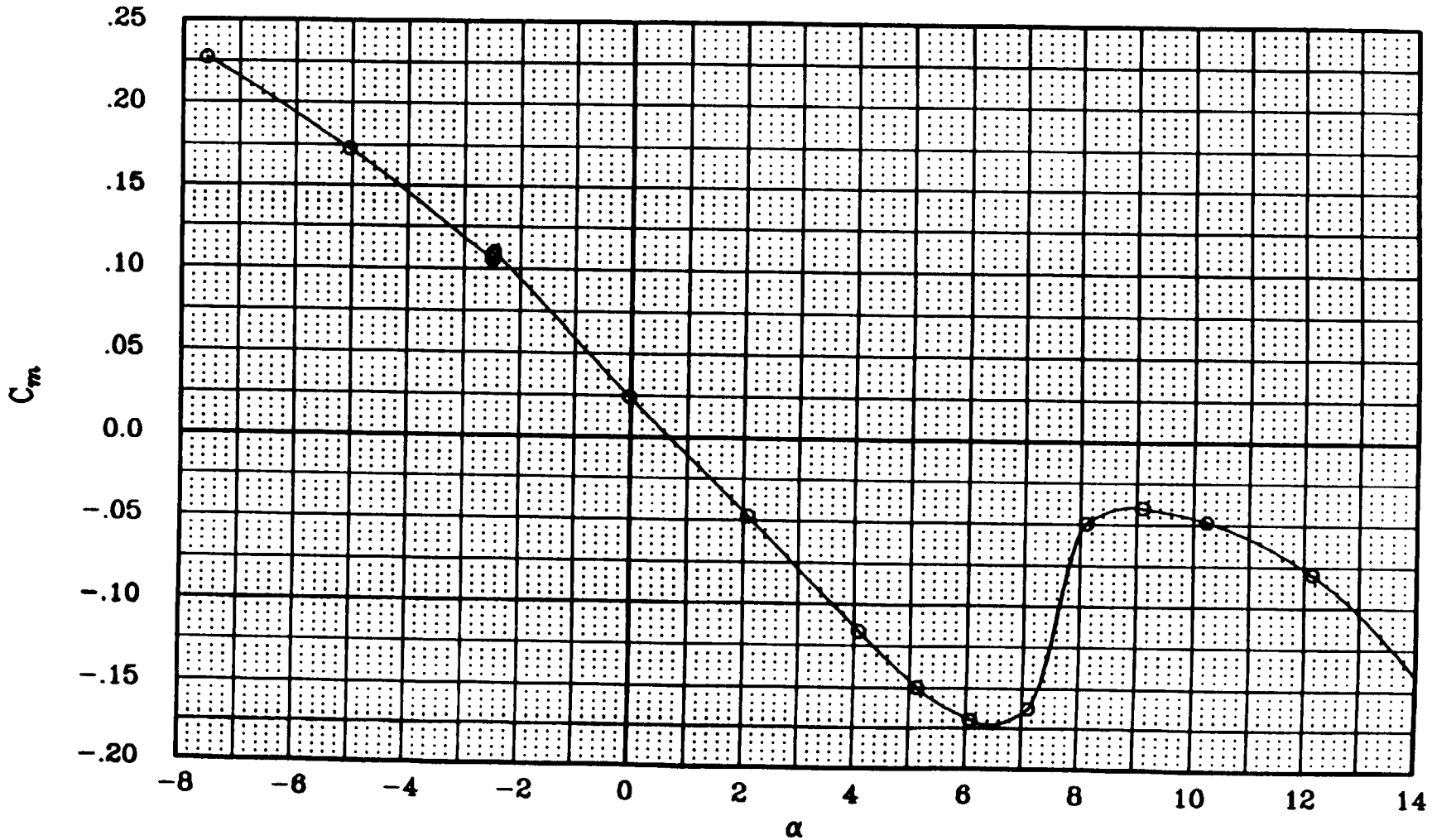

Figure 63. Longitudinal Characteristics of the JW-3 Configuration: C_m vs. α. Vortilon Removed.

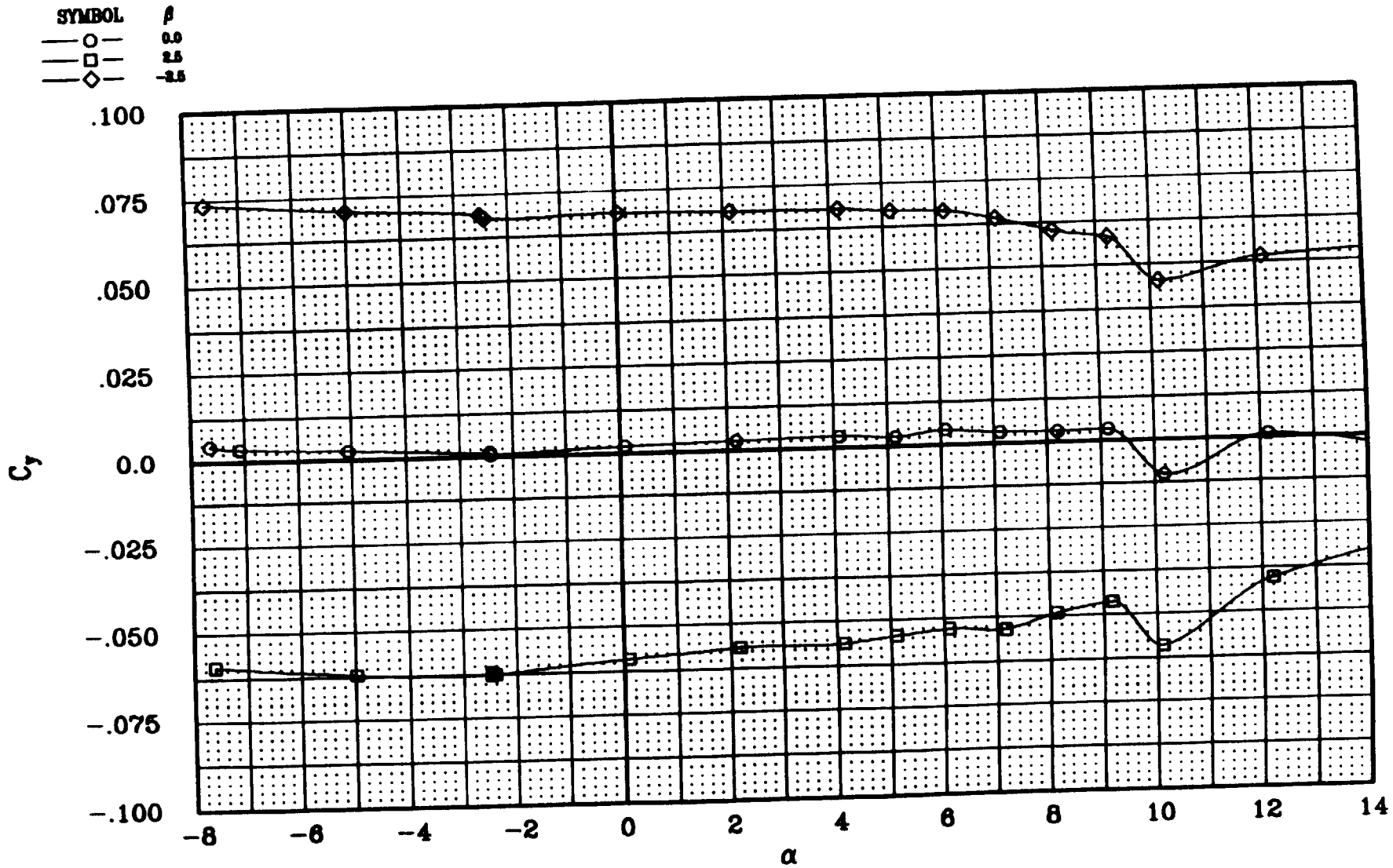

Figure 64. Lateral-Directional Characteristics of the JW-3: C_y vs. α.

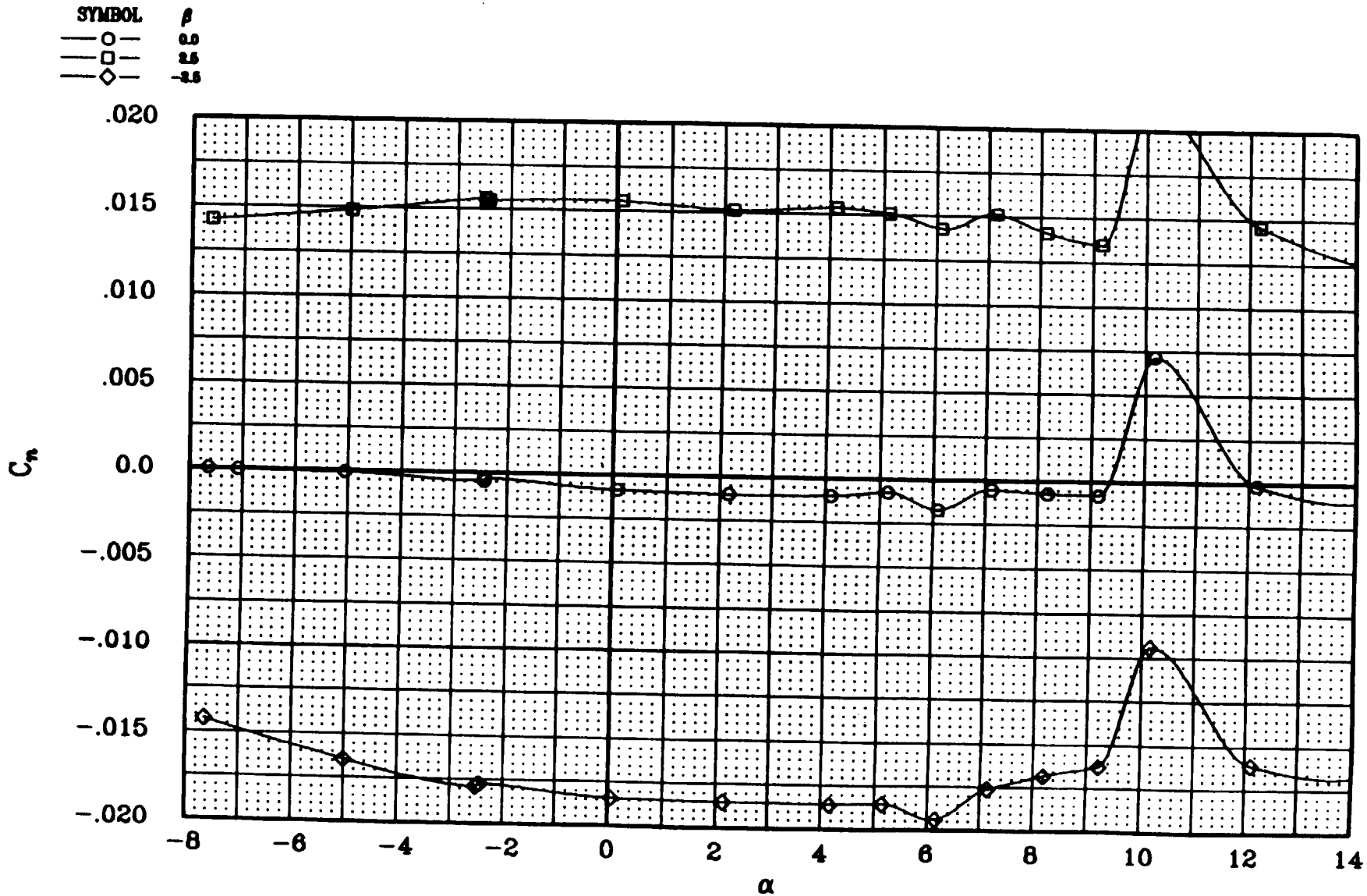

Figure 65. Lateral-Directional Characteristics of the JW-3: C_n vs. α.

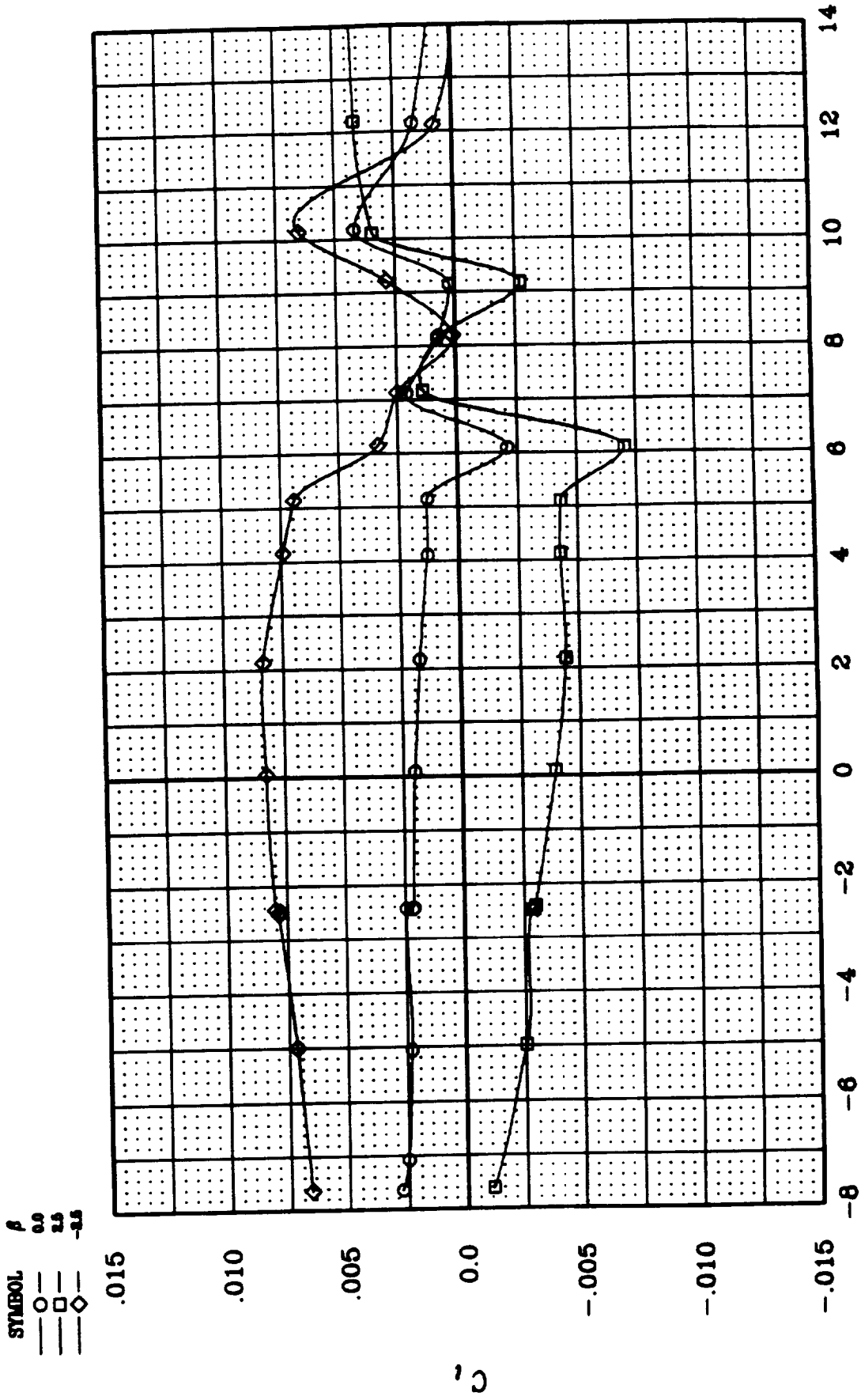

Figure 66. Lateral-Directional Characteristics of the JW-3: C_l vs. α.

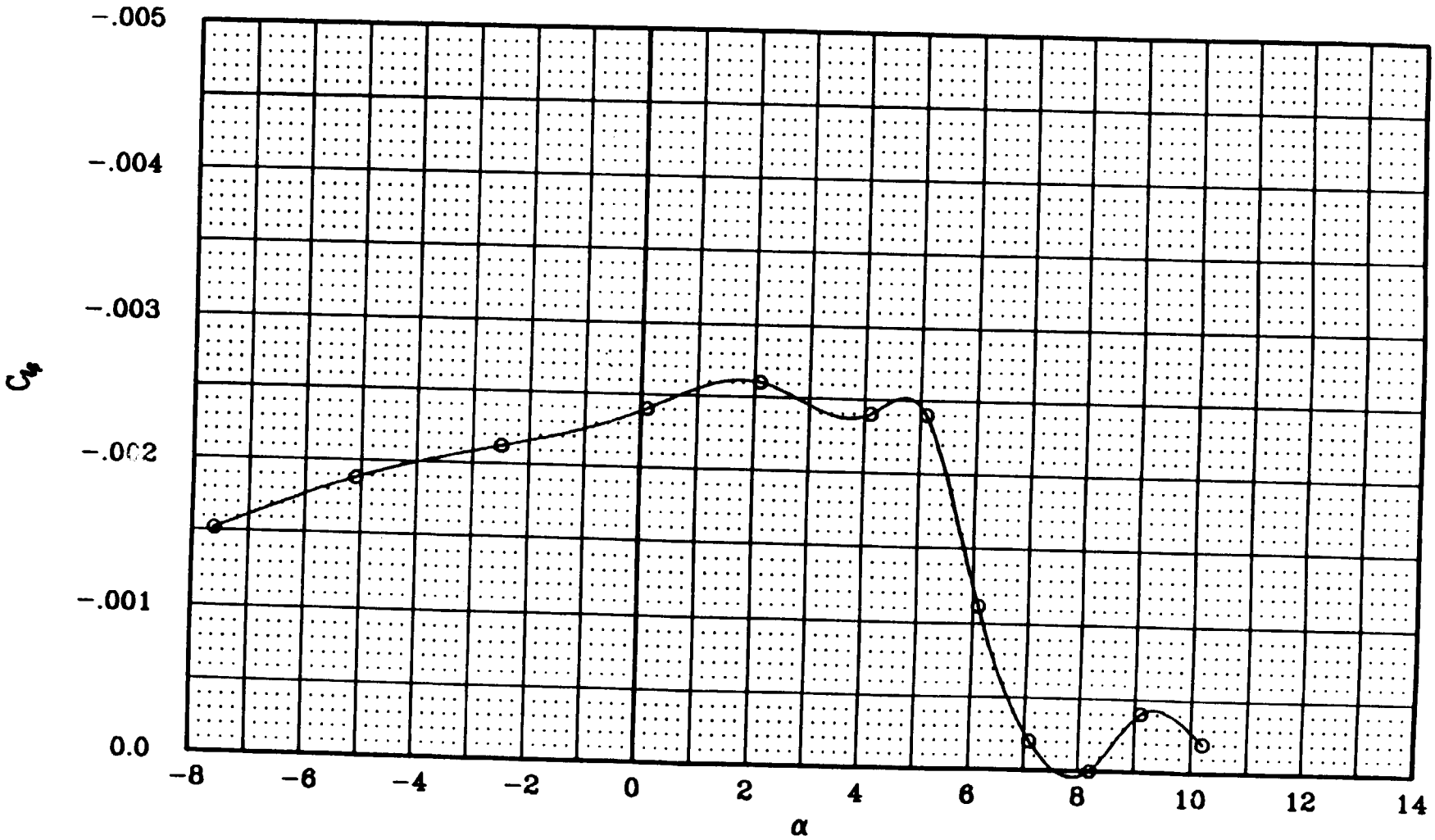

Figure 67. Lateral-Directional Stability of the JW-3 Configuration: C_{l_β} vs. α.

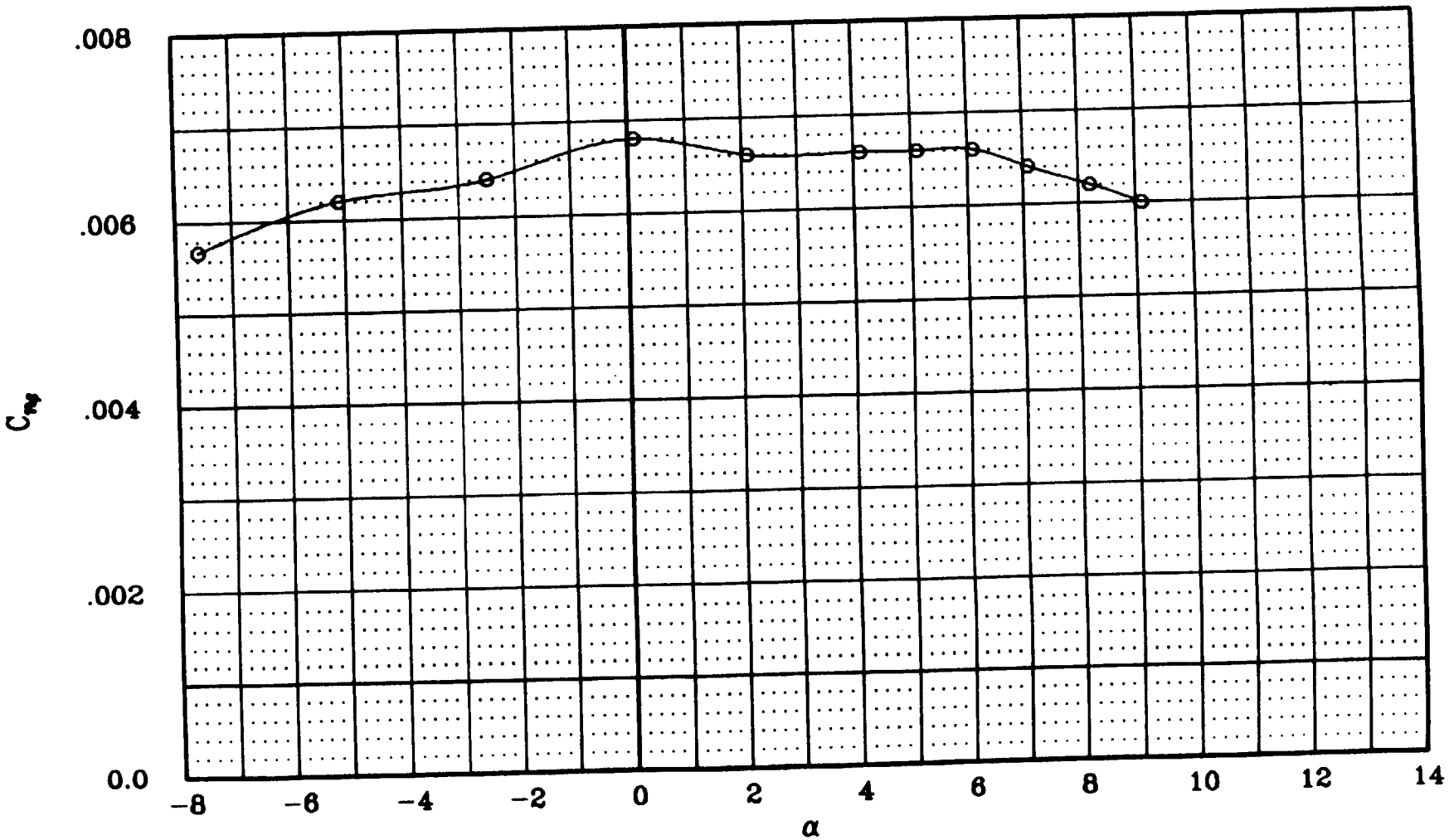

Figure 68. Lateral-Directional Stability of the JW-3 Configuration: C_{n_β} vs. α.

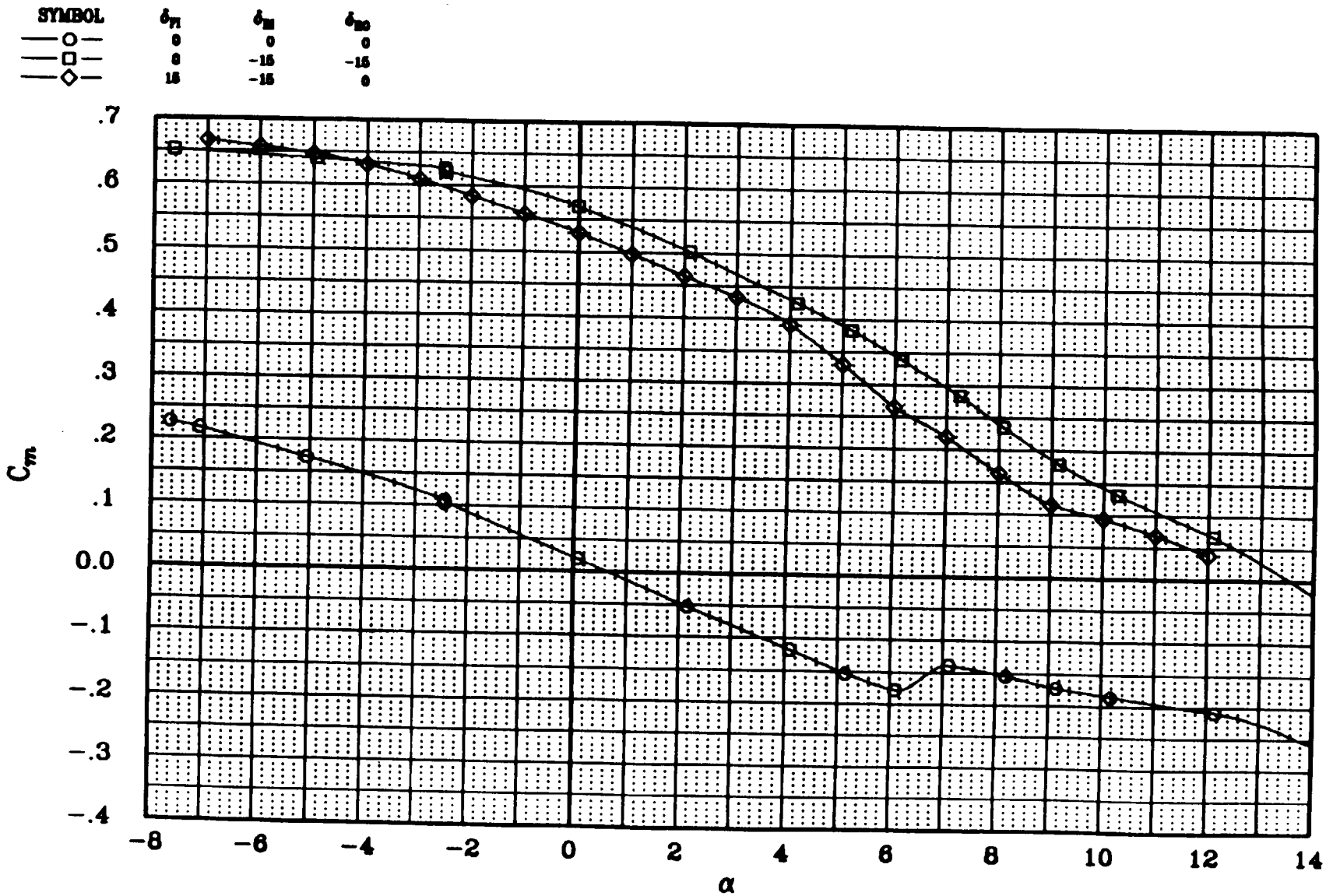

Figure 69. Effectiveness of Various Elevator Configurations on the JW−3: C_m vs. α.

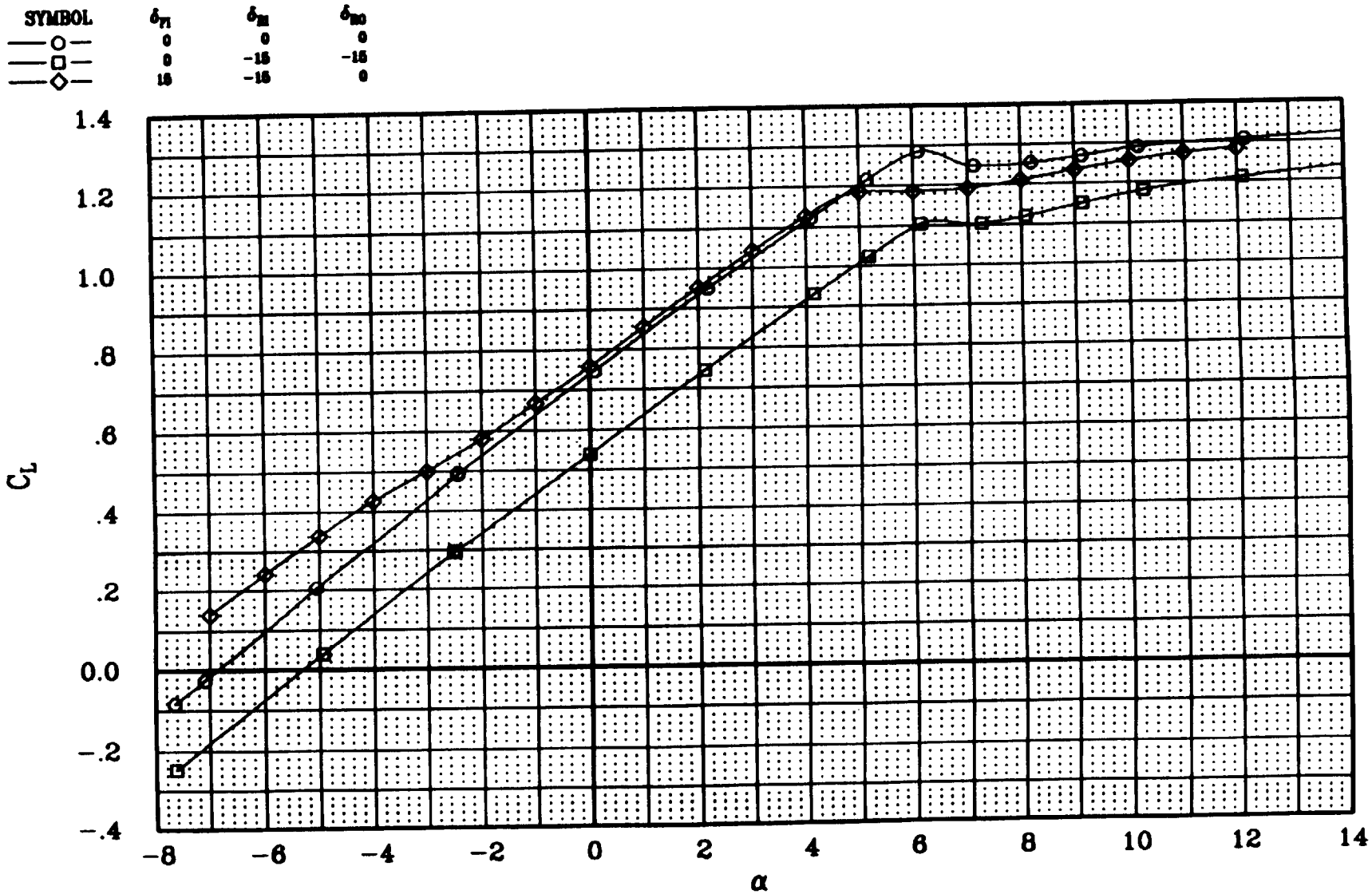

Figure 70. Effect of Various Elevator Configurations on the JW-3: C_L vs. α.

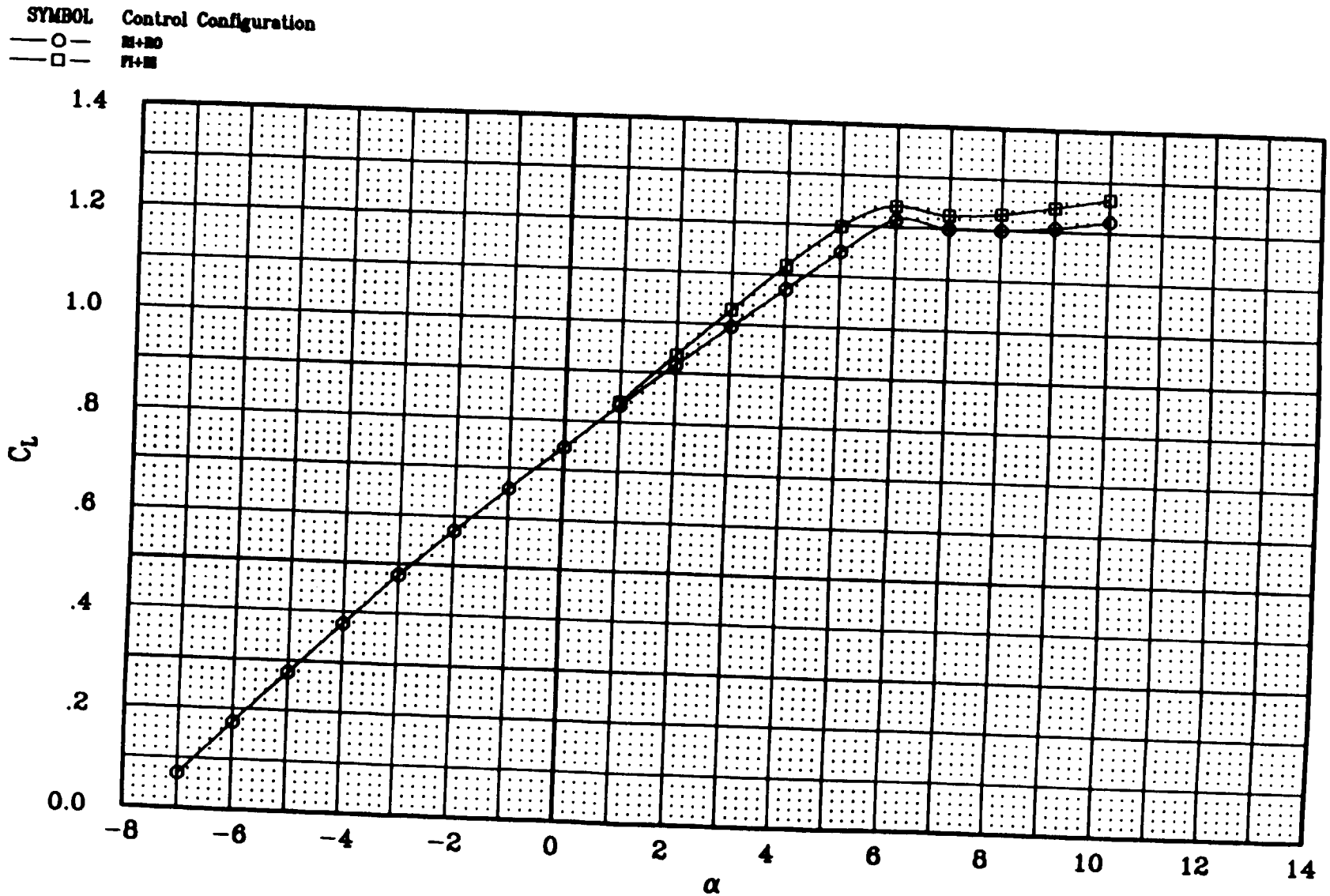

Figure 71. Trimmed Lift Characteristics of the JW-3.

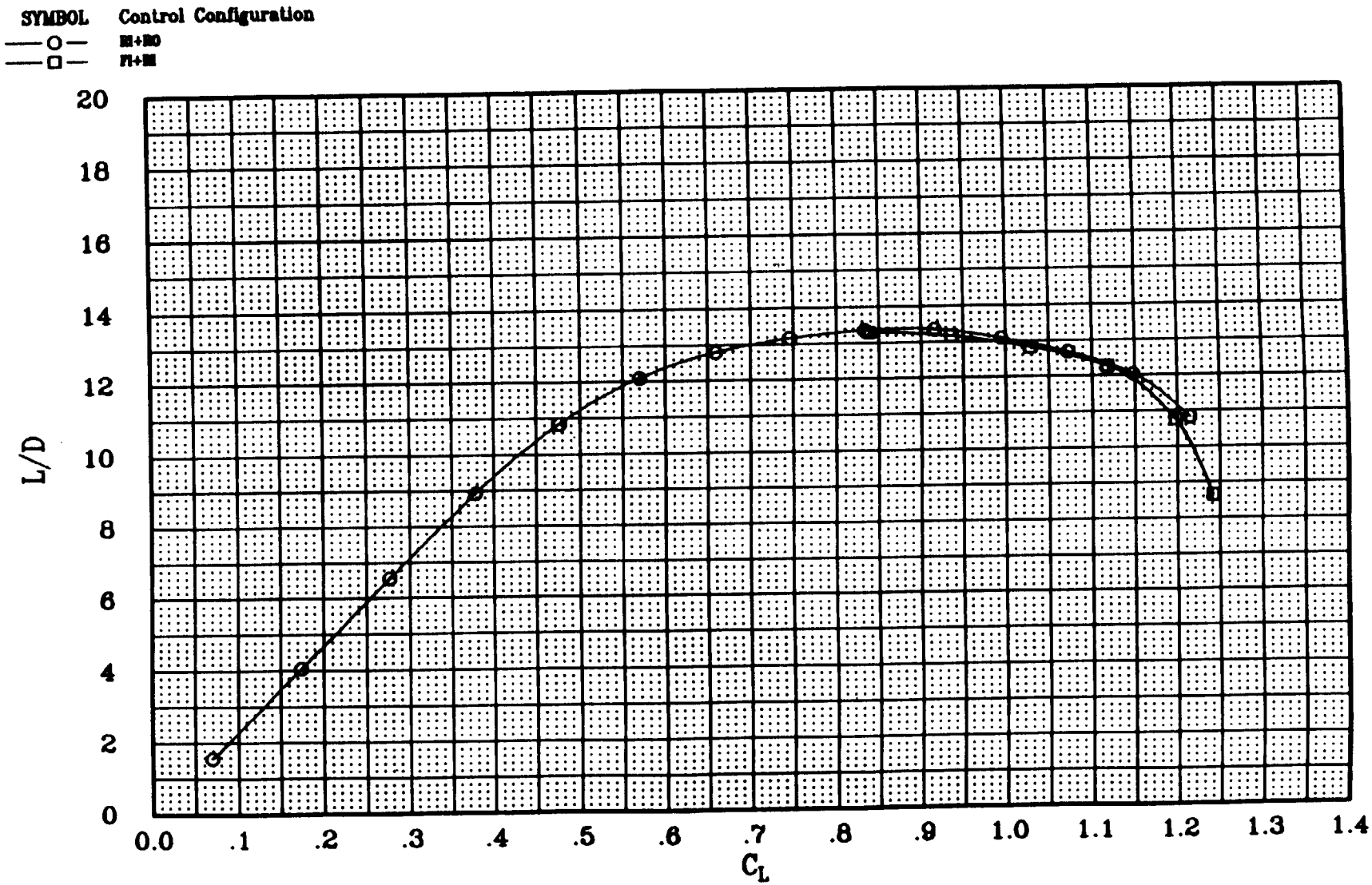

Figure 72. Trimmed Lift-to-Drag Ratio of the JW-3.

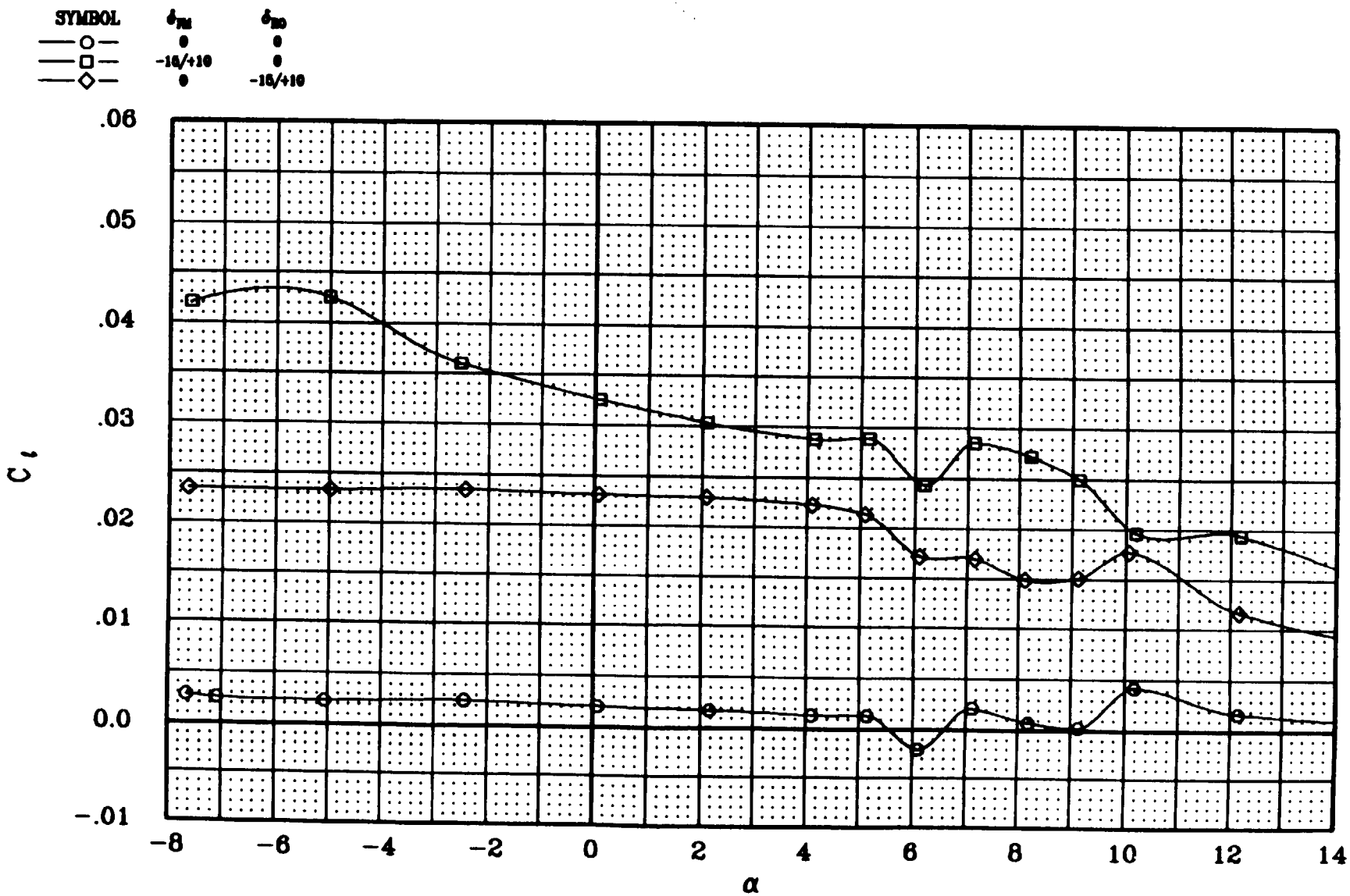

Figure 73. Effectiveness of Various Aileron Configurations on the JW-3: C_l vs. α.

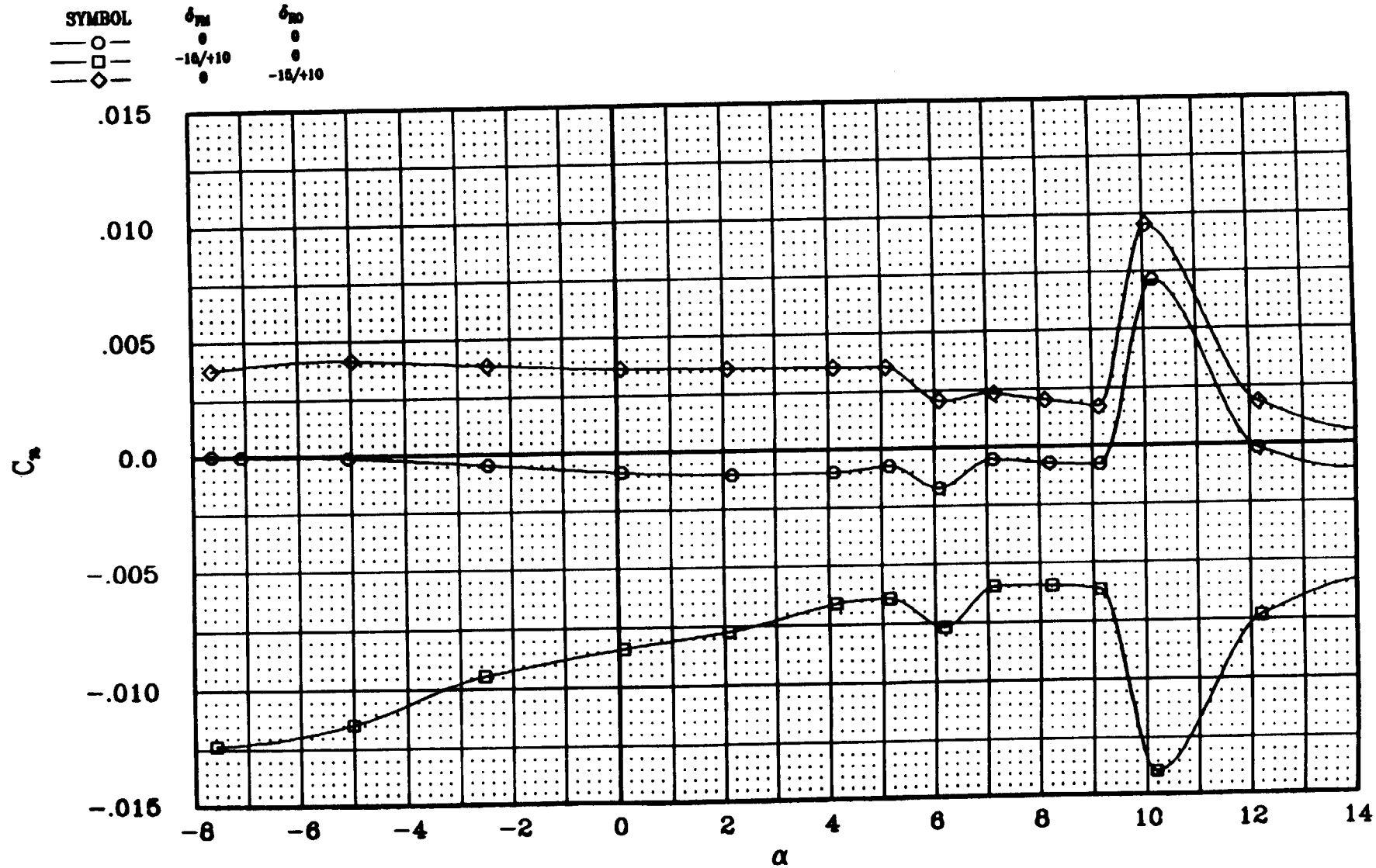

Figure 74. Yawing Moment induced by various Aileron Configurations on the JW-3.

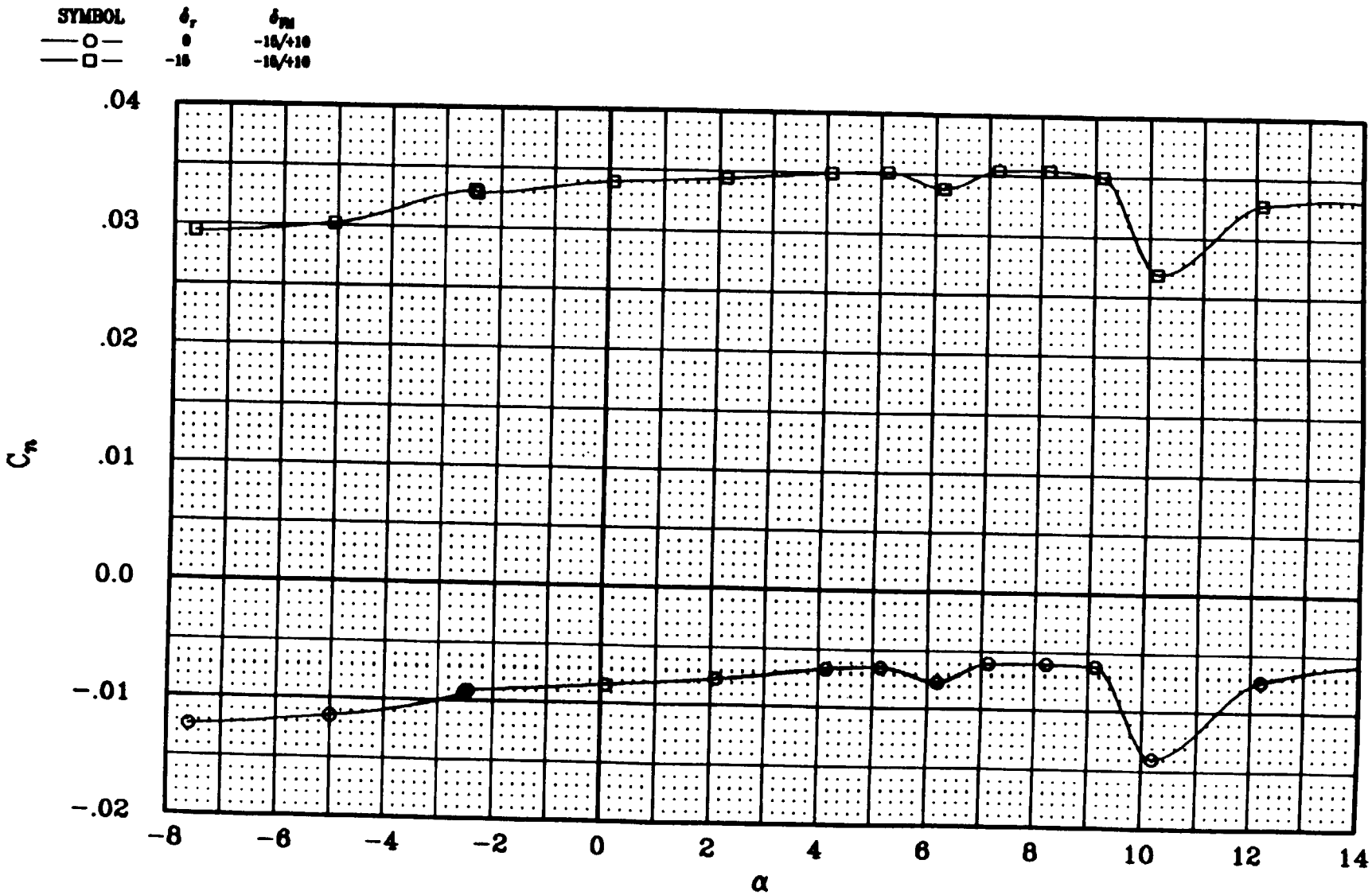

Figure 75. Rudder Effectiveness on the JW-3.

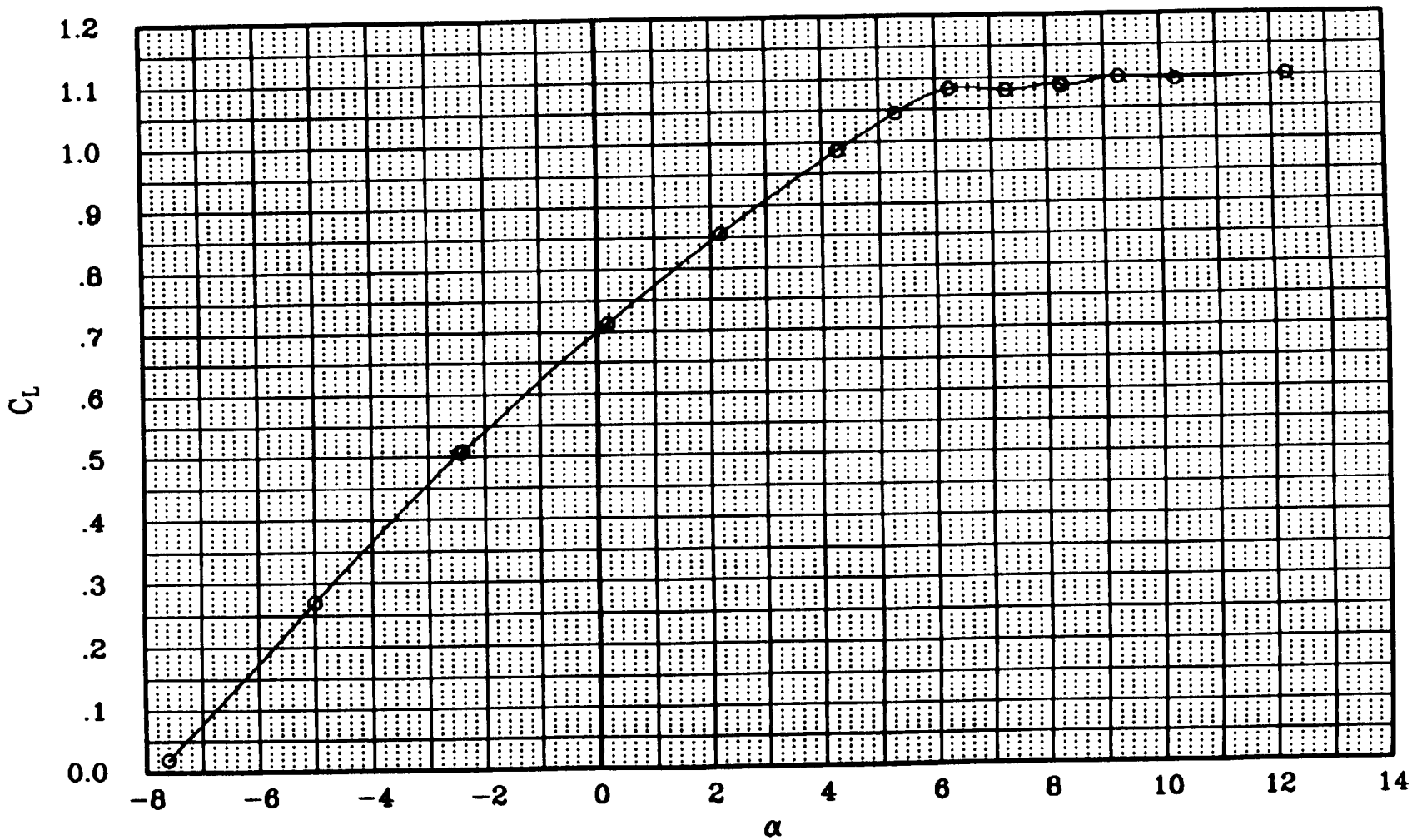

Figure 76. Longitudinal Characteristics of the JW−1 Wing−Body: C_L vs. α.

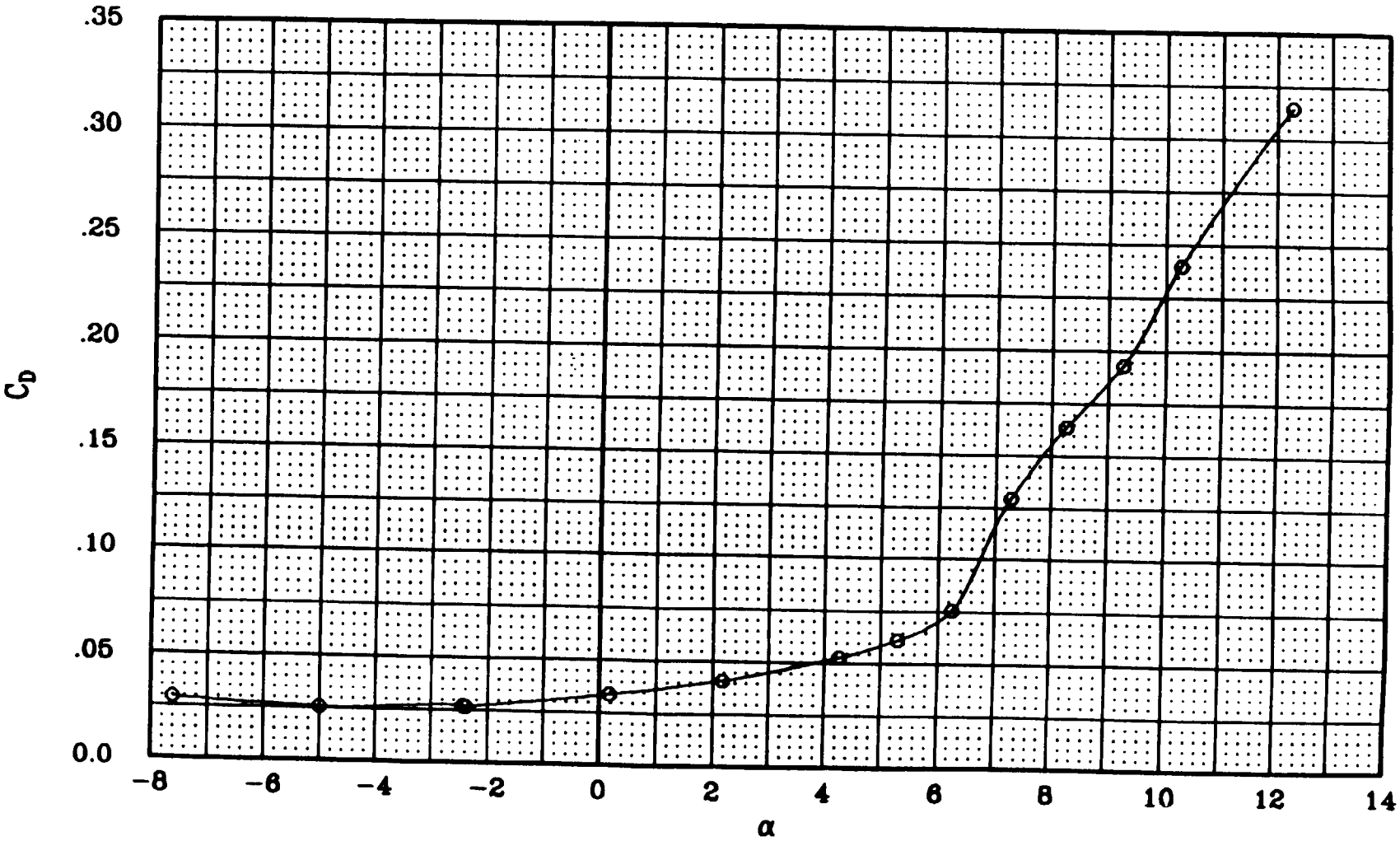

Figure 77. Longitudinal Characteristics of the JW−1 Wing−Body: C_D vs. α.

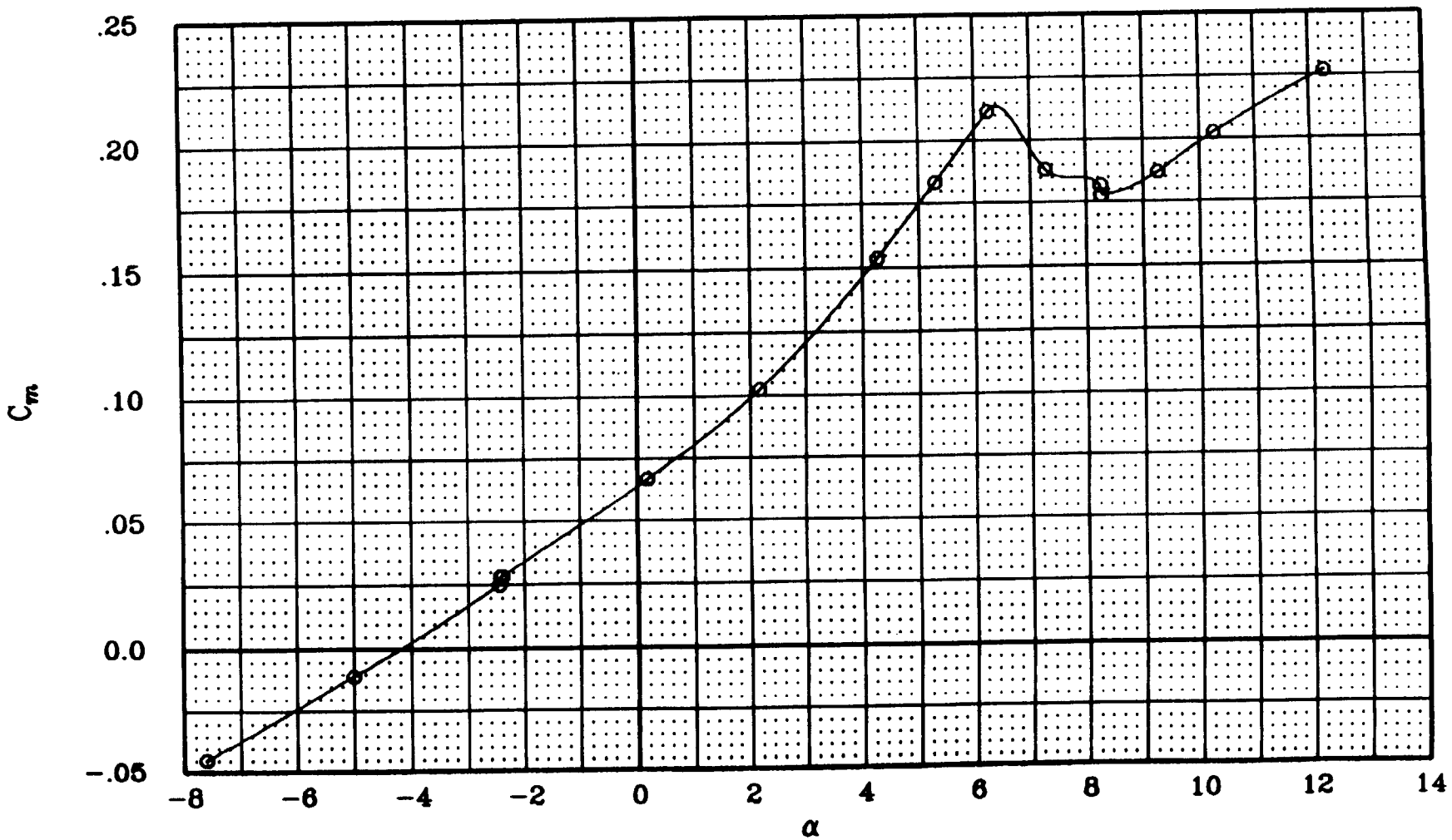

Figure 78. Longitudinal Characteristics of the JW−1 Wing−Body: C_m vs. α.

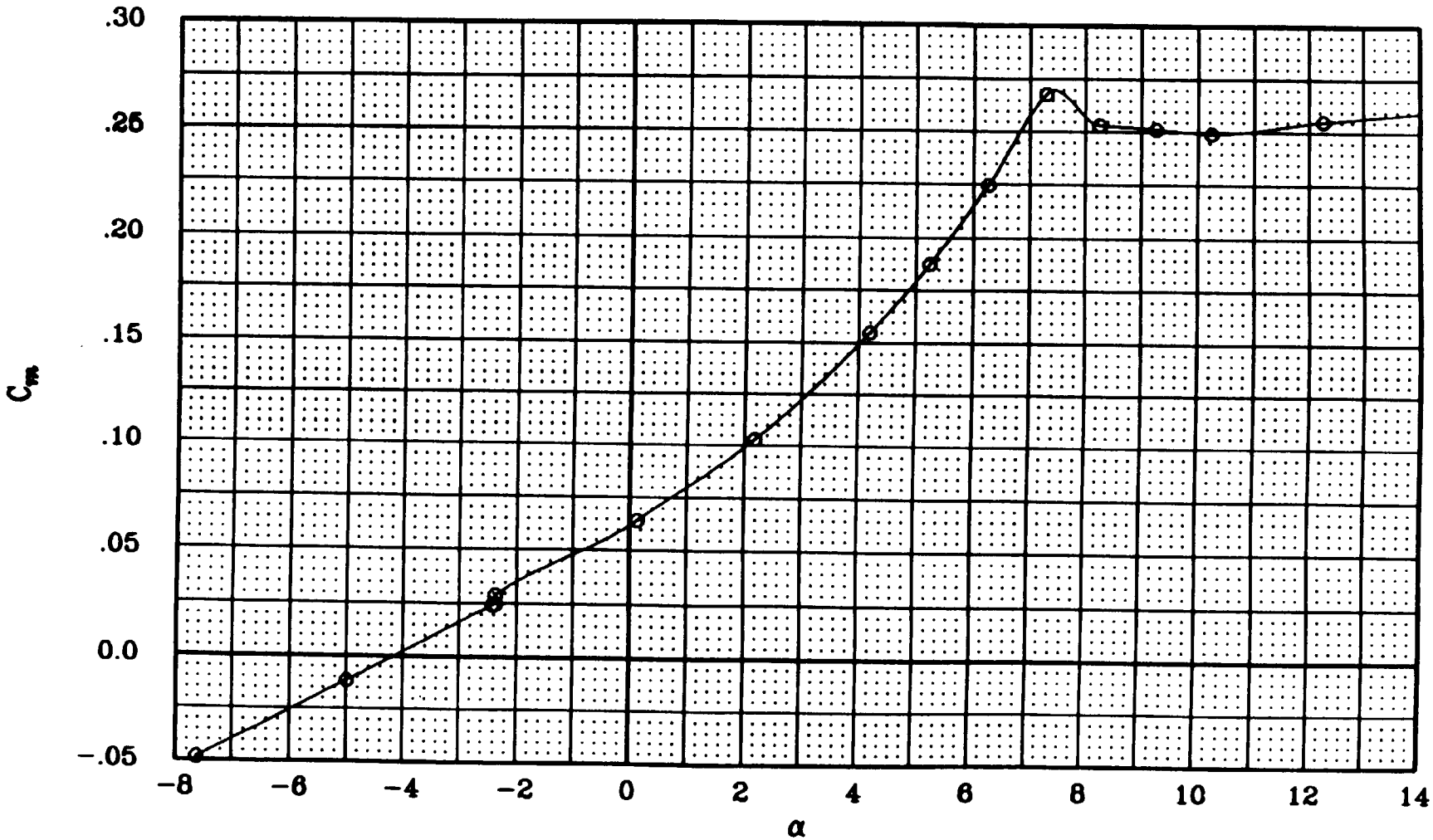

Figure 79. Longitudinal Characteristics of the JW−1 Wing−Body: C_m vs. α; Vortilons Removed.

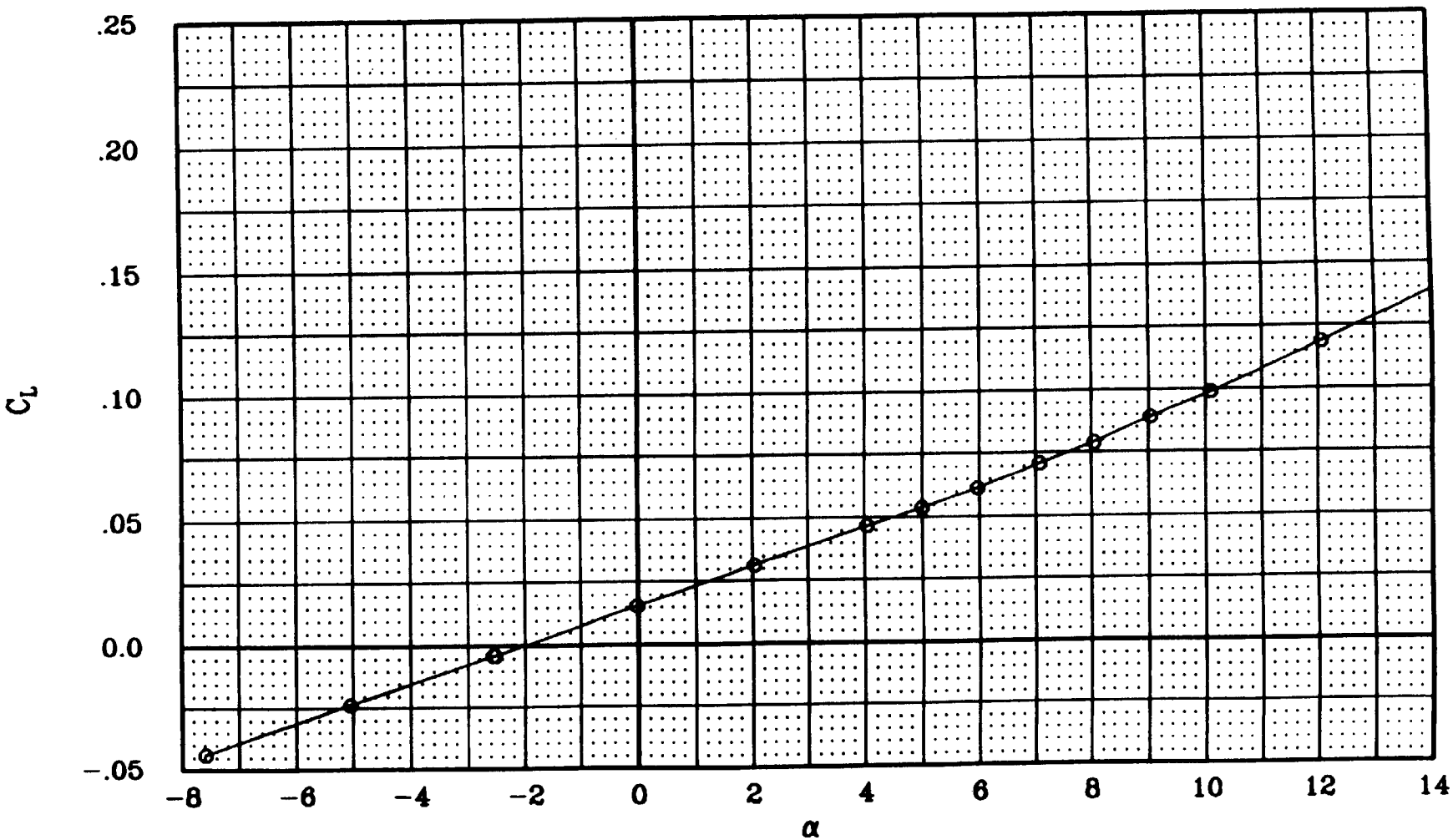

Figure 80. Longitudinal Characteristics of the JW−1 Fuselage: C_L vs. α.

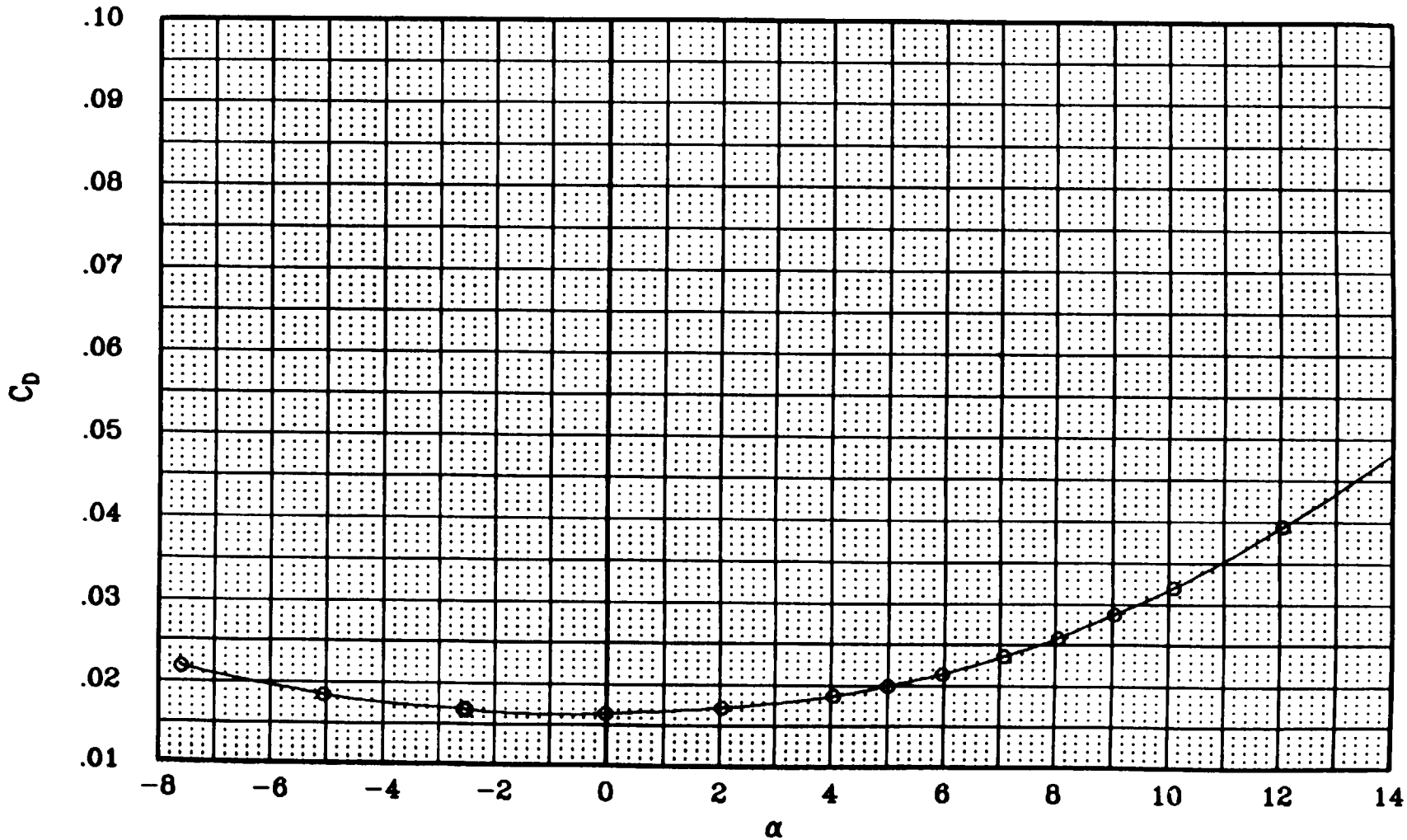

Figure 81. Longitudinal Characteristics of the JW-1 Fuselage: C_D vs. α.

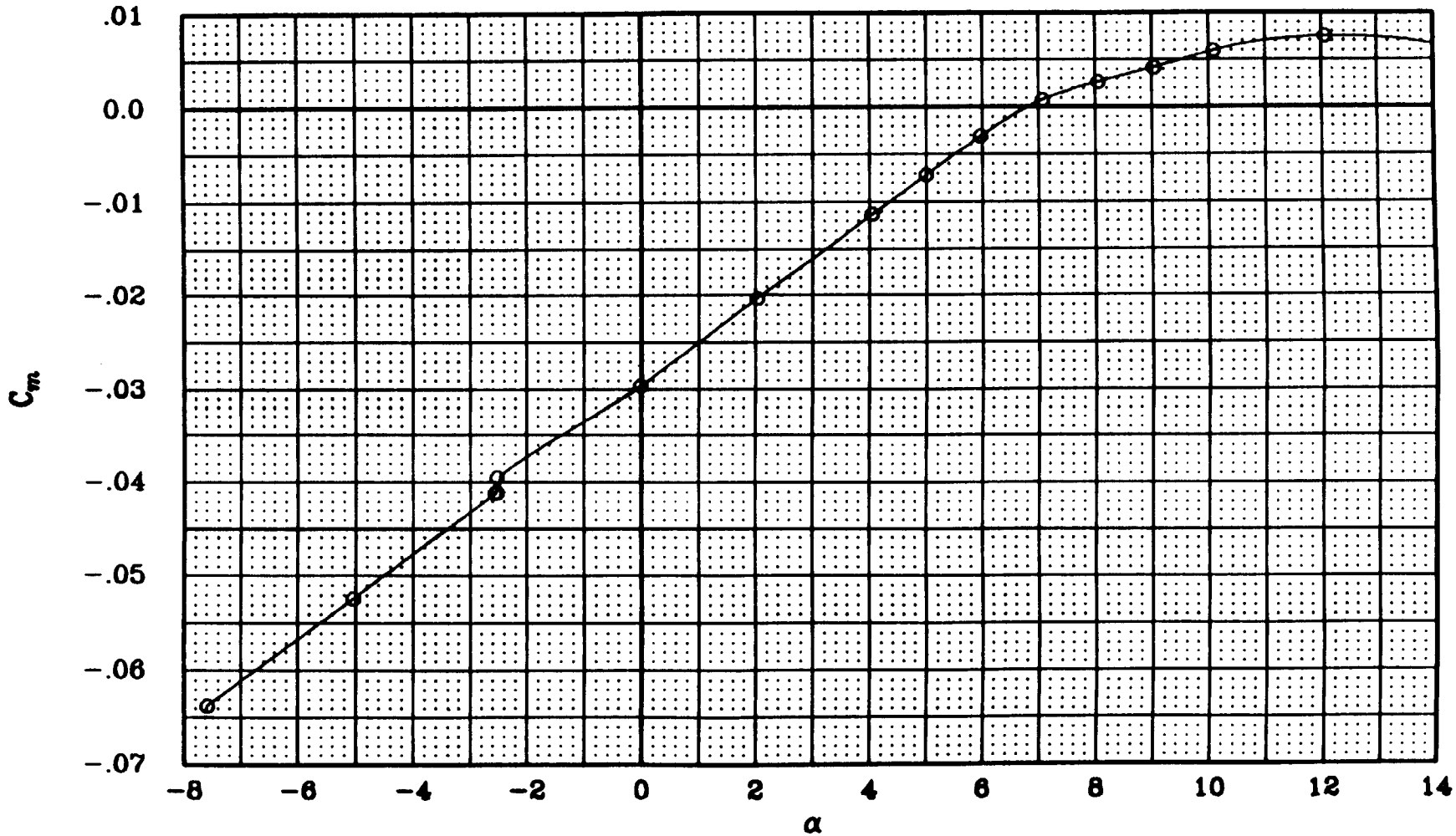

Figure 82. Longitudinal Characteristics of the JW−1 Fuselage: C_m vs. α.

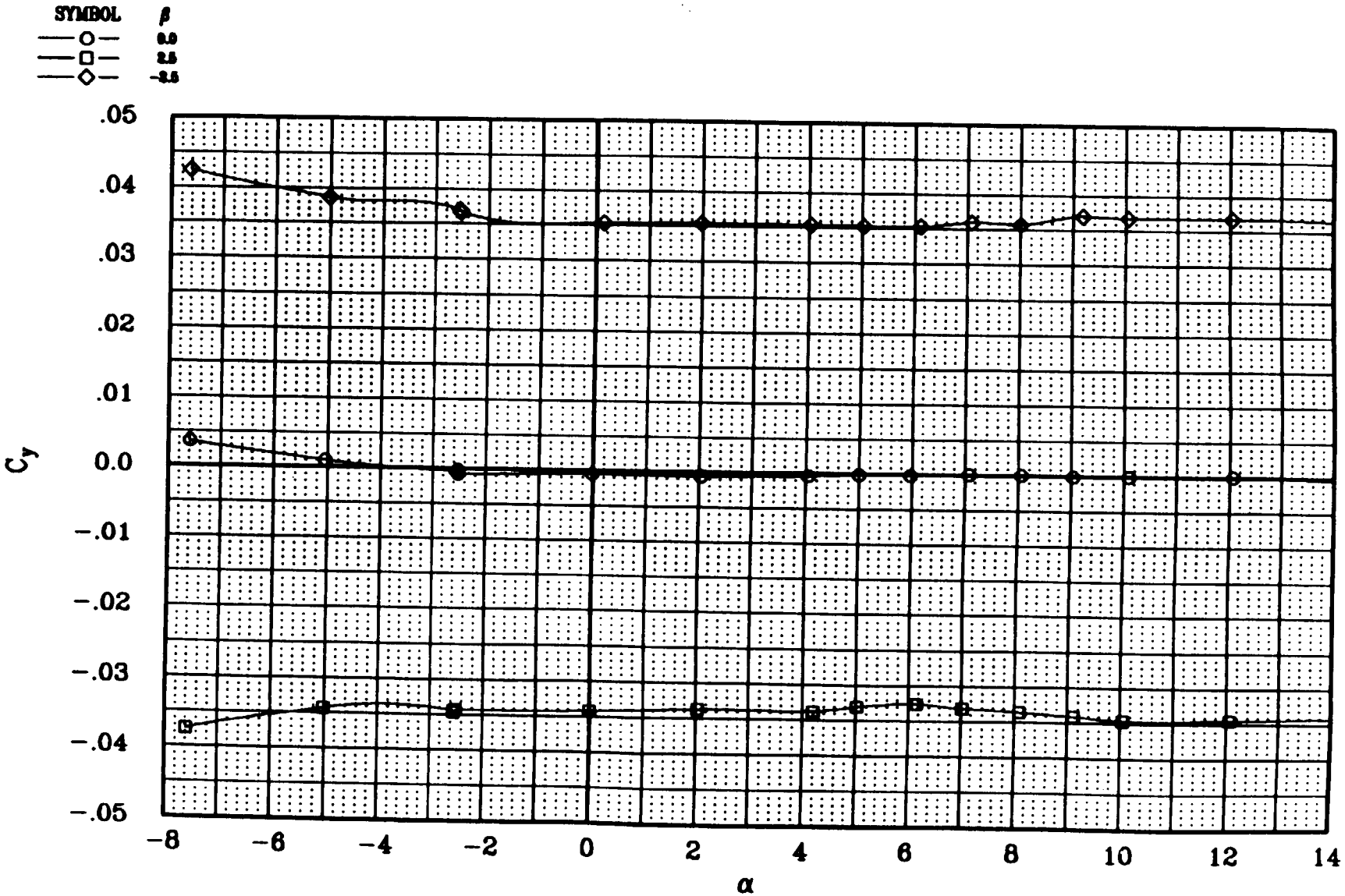

Figure 83. Directional Characteristics of the JW-1 Fuselage: C_y vs. α.

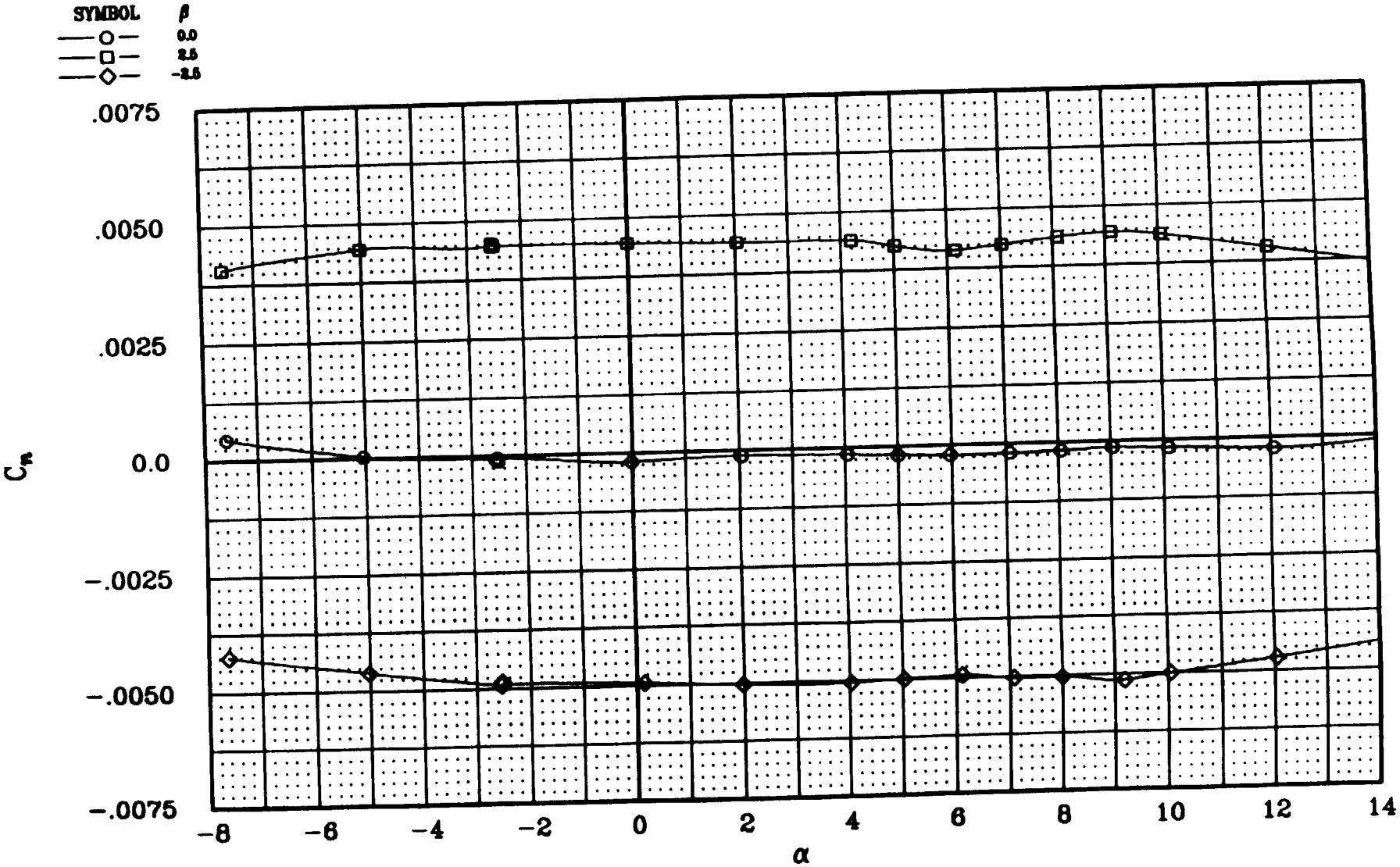

Figure 84. Directional Characteristics of the JW-1 Fuselage: C_n vs. α.

NASA National Aeronautics and Space Administration

Report Documentation Page

1. Report No.	2. Government Accession No.	3. Recipient's Catalog No.
NASA TM-101083		

4. Title and Subtitle

Experimental Aerodynamic Characteristics of a Joined-Wing Research Aircraft

5. Report Date

April 1989

6. Performing Organization Code

7. Author(s)

Stephen C. Smith and Ronald K. Stonum (First Lieutenant, Air Force Systems Command Liaison Office, U.S. Air Force)

8. Performing Organization Report No.

A-89074

10. Work Unit No.

505-61-21

9. Performing Organization Name and Address

Ames Research Center
Moffett Field, CA 94035

11. Contract or Grant No.

12. Sponsoring Agency Name and Address

National Aeronautics and Space Administration
Washington, DC 20546-0001

13. Type of Report and Period Covered

Technical Memorandum

14. Sponsoring Agency Code

15. Supplementary Notes

Point of Contact: Stephen C. Smith, Ames Research Center, MS 227-2, Moffett Field, CA 94035
(415) 694-5856 or FTF 464-5856

16. Abstract

A wind-tunnel test was conducted at Ames Research Center to measure the aerodynamic characteristics of a joined-wing research aircraft (JWRA). This aircraft was designed to utilize the fuselage and engines of the existing NASA AD-1 aircraft. The JWRA was designed to have removable outer wing panels to represent three different configurations with the interwing joint at different fractions of the wing span. A one-sixth-scale wind-tunnel model of all three configurations of the JWRA was tested in the Ames 12-Foot Pressure Wind Tunnel to measure aerodynamic performance, stability, and control characteristics.

This report presents the results of these tests. Longitudinal and lateral-directional characteristics were measured over an angle of attack range of −7° to 14° and over an angle of sideslip range of −5° to +2.5° at a Mach number of 0.35 and a Reynolds number of 2.2×10^6/ft. Various combinations of deflected control surfaces were tested to measure the effectiveness and impact on stability of several control surface arrangements. In addition, the effects on stall and post-stall aerodynamic characteristics from small leading-edge devices called vortilons were measured.

The results of these tests indicate that the JWRA had very good aerodynamic performance and acceptable stability and control throughout its flight envelope. The vortilons produced a profound improvement in the stall and post-stall characteristics with no measurable effects on cruise performance.

17. Key Words (Suggested by Author(s))	18. Distribution Statement
Joined wing Vortilons Experimental aerodynamics	Unclassified – Unlimited Subject category – 02

19. Security Classif. (of this report)	20. Security Classif. (of this page)	21. No. of pages	22. Price
Unclassified	Unclassified	98	A05

NASA FORM 1626 OCT 86

For sale by the National Technical Information Service, Springfield, Virginia 22161